PB-234 171

TURBULENT DIFFUSION IN LIQUID JETS

Strong C. Chaung, et al

Purdue University

Prepared for:

Pacific Northwest Environmental Research Laboratory
Office of Water Resources

March 1974

DISTRIBUTED BY:

NTIS

National Technical Information Service
U. S. DEPARTMENT OF COMMERCE
5285 Port Royal Road, Springfield Va. 22151

RESEARCH REPORTING SERIES

Research reports of the Office of Research and Monitoring, Environmental Protection Agency, have been grouped into five series. These five broad categories were established to facilitate further development and application of environmental technology. Elimination of traditional grouping was consciously planned to foster technology transfer and a maximum interface in related fields. The five series are:

1. Environmental Health Effects Research
2. Environmental Protection Technology
3. Ecological Research
4. Environmental Monitoring
5. Socioeconomic Environmental Studies

This report has been assigned to the ECOLOGICAL RESEARCH series. This series describes research on the effects of pollution on humans, plant and animal species, and materials. Problems are assessed for their long- and short-term influences. Investigations include formation, transport, and pathway studies to determine the fate of pollutants and their effects. This work provides the technical basis for setting standards to minimize undesirable changes in living organisms in the aquatic, terrestrial and atmospheric environments.

ib

EPA 660/3-74-004b
March 1974

TURBULENT DIFFUSION IN LIQUID JETS: FINAL REPORT

by

Strong C. Chaung and Victor W. Goldschmidt
Engineering Experiment Station
School of Mechanical Engineering
Purdue University
Lafayette, Indiana 47907

Project No. 16070 DEP
Program Element 1BA025

Project Officer

George R. Ditsworth
Pacific Northwest Environmental Research Laboratory
National Environmental Research Center
Corvallis, Oregon 97330

Prepared for
OFFICE OF RESEARCH AND DEVELOPMENT
U.S. ENVIRONMENTAL PROTECTION AGENCY
WASHINGTON, D.C. 20460

For sale by the Superintendent of Documents, U.S. Government Printing Office Washington, D.C. 20402 - Price $1.70

ia

EPA Review Notice

This report has been reviewed by the Environmental Protection Agency, and approved for publication. Approval does not signify that the contents necessarily reflect the views and policies of The Environmental Protection Agency, nor does mention of trade names or commercial products constitute endorsement or recommendation for use.

SELECTED WATER RESOURCES ABSTRACTS
INPUT TRANSACTION FORM

PB 234 171
W 74-10195

4. Title
TURBULENT DIFFUSION IN LIQUID JETS: FINAL REPORT,

7. Author(s)
S~~trong~~ C. Chaung and V~~ictor~~ W. Goldschmidt

9. Organization
Engineering Experiment Station,
School of Mechanical Engineering.
Purdue University,
Lafayette, ~~IN 47907~~ Indiana,

10. Project
16070 DEP

11. Contract/Grant No
~~16070-DEP~~

15. Supplementary Notes
Environmental Protection Agency, Ecological Research Series, Report ~~Number~~, EPA-660/3-74-004b, March 1974.
126p, 45 fig, 5 tab, 91 ref.

16. Abstract

Laboratory studies were conducted on the dispersion of gas droplets of different sizes in turbulent water jets. The main purpose was to determine the turbulent transport coefficient of contaminants suspended in turbulent flows.

The experimental results were compared to measurements of diffusion of liquid droplets in air jets as well as to a numerical analysis based on the equations of the particles themselves.

The results confirm that small particles in turbulent flows have an increasing turbulent transport coefficient with size. The collated experimental results exhibit when Reynolds analogy (in the transport of mass and momentum) can be validly employed. ~~(EPA)~~ (Ditsworth - EPA)

(See also W74-10196)

17a. Descriptors
Bubble, *Diffusion, Dispersion, Equations, Instrumentation, *Turbulence, *Turbulent Flow, *Jets

17b. Identifiers
Bubble Sampling, Bubble Sizing, Concentration of Contaminants, Hot Film Anemometer, Jet Flow, Liquid Jets, *Turbulent Diffusion, *Turbulent Transport.

Copy Available from GPO Sup Doc as EP1.23: 660/3-74-004b $ 1.20 ;
microfiche from NTIS as PB
$1.45

17c. COWRR Field & Group 05B 08 B

18. Availability

Send To:
WATER RESOURCES SCIENTIFIC INFORMATION CENTER
U.S. DEPARTMENT OF THE INTERIOR
WASHINGTON, D. C. 20240

Abstractor G. R. Ditsworth
Institution Environmental Protection Agency

Reproduced by
NATIONAL TECHNICAL
INFORMATION SERVICE
U S Department of Commerce
Springfield VA 22151

ABSTRACT

Laboratory studies were conducted on the dispersion of gas droplets of different sizes in turbulent water jets. The main purpose was to determine the turbulent transport coefficient of contaminants suspended in turbulent flows.

The experimental results were compared to measurements of diffusion of liquid droplets in air jets as well as to a numerical analysis based on the equations of motion of the particles themselves.

The results confirm that small particles in turbulent flows have an increasing turbulent transport coefficient with size. The collated experimental results exhibit when Reynolds analogy (in the transport of mass and momentum) can be validly employed.

This report was submitted in (partial) fulfillment of Contract 16070 DEP under the (partial) sponsorship of the U.S. Environmental Protection Agency.

CONTENTS

Section		Page
I	Conclusions	1
II	Recommendations	3
III	Introduction	5
IV	Statement of The Problem	7
V	Literature Review	9
VI	Theoretical Background	15
VII	Experimental Set-up and Measurement Principles	21
VIII	Experimental Results	35
IX	Turbulent Diffusivities	71
X	Turbulent Diffusion Characteristics	87
XI	Significance of Results	95
XII	Acknowledgements	97
XIII	References	99
XIV	Publications	107
XV	Glossary of Symbols	109
XVI	Appendices	115

FIGURES

No. Page

1 Schematic Diagram of Experimental Equipment 22

2 Constant Head Tank, Water Filter, Deionizer 23

3 Photograph of Jet Tank. 24

4 Energy Distribution of Bubble Signal. 28

5 Filtered vs. Unfiltered Peak Voltage. 30

6 Filtered and Unfiltered Signals 31

7 Block Diagram of Electronic Instrumentation 32

8 Electronic Instrumentation. 33

9 Normalized Velocity Profile (With Syringe Tube) 36

10 Velocity Half Width (With Syringe Tube) 38

11 Velocity Distribution Along Jet Axis (With Syringe Tube) 39

12 Normalized Velocity Profile (Without Syringe Tube). . . 42

13 Velocity Half Width (Without Syringe Tube). 43

14 Velocity Distribution Along Jet Axis (Without Syringe Tube) 44

15 Distribution of Eddy Viscosity Based on Different Models. 46

16 Sensor Calibration Curve. 47

17 Sensor Sensitivity Curve. 48

18 Transverse Distribution of Turbulence Intensities . . . 49

19 Energy Spectrum Along Center Line of the Jet. 51

No. Page

20 Longitudinal Macro Scale Along the Turbulent Jet Axis 53

21 Variation of the Integrated Concentration Flux Along the Axial Direction. 56

22 Concentration Flux Profile 57

23 Concentration Flux Profile 58

24 Concentration Flux Profile 59

25 Concentration Flux Profile 60

26 Half Width Spreading of the Concentration Flux . . . 62

27 Center Line Concentration Flux Decay 63

28 Normalized Velocity Profile (With & Without Contamination) 66

29 Velocity Half Width (With and Without Bubble Contamination) 67

30 Velocity Distribution Along Jet Axis (With & Without Bubble Contamination). 68

31 Transverse Fluctuation Level (With and Without Bubble Contamination 69

32 Concentration Profile. 74

33 Concentration Profile. 75

34 Concentration Profile. 76

35 Concentration Profile. 77

36 Concentration Profile. 79

37 Concentration Profile. 80

No.		Page
38	Concentration Profile (With Bubble Rising Vel. Corr.)	81
39	Concentration Profile (With Bubble Rising Vel. Corr.)	82
40	Concentration Profile (With Bubble Rising Vel. Corr.)	83
41	Concentration Profile (With Bubble Rising Vel. Corr.)	84
42	Concentration Profile (With Bubble Rising Vel. Corr.)	85
43	Concentration Profile (With Bubble Rising Vel. Corr.)	86
44	Dependence of S_t^{-1} on Particle Paramenter ψ_T.	89
45	Dependence of S_t^{-1} on Particle Parameter ψ_T'	94

TABLES

No.		Page
1	Comparison of Various Axi-symmetric Turbulent Jet Measurements	41
2	Total Bubble Concentration of the Experiments	55
3	Rising Bubble Velocity	71
4	Turbulent Schmidt Number	72
5	Calculation of S_t^{-1} versus ψ_T'	93

SECTION I

CONCLUSIONS

1. Turbulent diffusion measurements of four different bubble sizes i.e., 343, 527, 780, and 970 microns were made. The measured concentration profiles of the bubbles in the axisymmetric water jet revealed that similarity at successive sections was preserved and that the profiles had the same virtual origin as the momentum diffusion. This result supported the original postualte that the contaminant is diffused in a manner similar to that of momentum.

2. The particle diffusivities and the corresponding turbulent Schmidt numbers were obtained by matching the measured data with different models. Three models based on phenomenological theories of turbulence were used to analyze the diffusion. The first one, which assumed constant eddy viscosity and constant particle eddy diffusivity, gave the best agreement with the measured data. The results showed that in general the contaminant diffuses faster than the momentum and that the rate of diffusion increases with an increase of particle size.

3. In order to compare the measured results with others, a particle parameter, ψ_T, originally presented by Householder and Goldschmidt (1968) and later modified by Ahmadi (1970), was adopted as a characterizing parameter. The present data suggest that the particle parameter ψ_T is suitable for describing the particle motion only within the Stokesian range. When the particle Reynolds number is outside this range another modified parameter ψ_T' is defined in which the particle response time is correctly predicted from the simplified B.B.O. Equation in the corresponding Reynolds number range.

4. The relationship between the turbulent Schmidt number and the characteristic parameter, ψ_T', is constant at low ψ_T' values. When ψ_T' is large, there seem to be different trends according to the geometry of the flow fields.

SECTION II

RECOMMENDATIONS

This study was limited to the measure of the turbulent transport coefficient of small contaminants of spherical shape in free turbulent jet flows. The results give a direct measure of the eddy diffusivity coefficient necessary to predict the dispersion of contaminants when released in such conditions.

To make the study complete it should be extended to consider the following cases:

1. Dispersion in stratified and disturbed (crossed, deflected, etc) flows.
2. Dispersion of non-spherical contaminants.
3. Optimization of dispersion by control of particle size and shape.
4. Dispersion in flow fields of different geometries.

Preceding page blank

SECTION III

INTRODUCTION

A prediction of the concentration distribution of scalar contaminants (such as heat, dye, particles or bubbles) introduced in a turbulent flow field requires a knowledge of the corresponding turbulent transport coefficients. This work concerns itself with the transport of discrete contaminants suspended in turbulent flows. The specific questions being answered are: Is the coefficient describing the turbulent transport of suspended particles equal to that of momentum? And if it is not, how does it depend on the size of the particle-contaminant?

The specific set of experiments reported herein are for the dispersion of gas bubbles in a turbulent water jet. They were performed simultaneously with a separately funded study on the dispersion of liquid droplets in air jets. In sections IX and X the results are compared and generalized. It is shown that for contaminants with a certain size and specific gravity range it is not possible to assume equality of the turbulent fluid and particle transport coefficients. The results correlate sufficiently well to permint an estimate of the actual turbulent transport coefficient for a given contaminant to carrier stream density ratio, contaminant size, and characteristics of the turbulent flow.

The stated objectives of this work were twofold. One to establish an effective method of tracking contaminants in a liquid jet, including the use of a laser system. Two to determine the diffusion due to turbulence of contaminants of different size and density. The second objective was fully met. This report deals directly with it. On the other hand the first objective was only partly met. It will be reported on in a separate report. The second objective was met through the research of Dr. Strong C. Chuang. His doctoral thesis was completed on August 1970. The research into the use of a laser as a sampling device was conducted by Mr. Charles H. Tinsley as part of his M. S. studies at Purdue University. His Master's Thesis is currently (May 1971) in the final write-up stages. Mr. Tinsley's research and study program is presently being financed through university funds.

SECTION IV

STATEMENT OF THE PROBLEM

It is well known that a turbulent flow field will not only transport but also rapidly disperse any material injected in it. This is of basic importance in problems related to pollution and dispersion of contaminants in oceans, lakes, and rivers as well as the atmosphere and in the transport of slurries and sediments.

Success of attempts at predicting the extent of dispersion of injected contaminants so far has been very limited due to the lack of a simple and yet all-encompassing mathematical model. Consequently most of the research to date has consisted of experimental measurement and empirical formulation. Among these, Householder (1968) (references are alphabetically listed in Section XIII) measured the diffusion of liquid particles in a two dimensional air jet. In his experiment the contaminant particles were much heavier than the carrier stream. The present study is essentially a continuation of Householder's work where now the diffusion characteristics of gas bubbles in an axi-symmetric water jet are treated. In this case the contaminants are much lighter than the carrier stream. The major purpose is to determine the effect of contaminant particle size on the diffusion characteristics, be they heavier or lighter than the carrier stream.

The extension of Householder's measurements was in part suggested by Ahmadi (1970). In his thesis Ahmadi considered Householder's data and proposed different methods of predicting the dependence of the turbulent transport on particle size, as well as on particle specific gravity. The measurements reported in this work will then fill a lack of information on the dispersion of particles whose specific gravity is less than one. The work is then not only a needed extension to Householder's review but also an added input to a bank of data to substantiate analytical predictions such as Ahmadi's.

In this work a series of constant size Nitrogen bubbles were generated at the center of a submerged turbulent axi-symmetric water jet. A hot film anemometer sensor was modified to measure the concentration flux of the bubbles by counting the number of impactions on the sensor per unit time. The corresponding concentration distributions were compared to predictions of three different analytical models, based on the phenomenological theories describing the turbulent flow. The three models are respectively based on Prandtl's mixing length theory, Taylor's vorticity transport theory and Reichardt's Inductive theory. Finally the corresponding eddy viscosity, eddy diffusivity and turbulent Schmidt number of the bubbles are obtained.

Preceding page blank

SECTION V

LITERATURE REVIEW

The turbulent diffusion of a marked fluid particle (a particle of infinitesimal volume) in a homogeneous turbulent flow field was first described by Taylor (1921) and then by Batchelor (1949), Frenkiel (1953), Roberts (1957), Lin (1960a) and Corrsin (1962). The relative dispersion of two marked fluid particles was studied by Batchelor (1952), Roberts (1960), Corrsin (1962) and Kraichnan (1966).

The complications encountered when considering diffusion in a nonuniform turbulent shear flow have been partly overcome by Batchelor and Townsend (1956), Lin (1960b) and Cermak (1963).

A general description of turbulent diffusion of a marked fluid particle requires a knowledge of the Lagrangian correlation coefficient of such a marked fluid particle. When the particles under consideration are distinguishable in their dimensions or density from the main stream, the analysis will then depend on the Lagrangian velocity correlations for these particles (Friedlander (1957)). So far, such a velocity correlation has only been either qualitatively discussed or quantitatively calculated. Such calculations have been through very simplified models with questionable applicability (see for instance Tchen (1947), Shirazi et al (1967) and Ahmadi (1970)).

ANALYTICAL STUDIES

Tchen (1947) first studied the motion of a spherical particle in a homogeneous turbulent flow field. He extended the B.B.O. equation (Basset, Boussinesq and Oseen Equation, see Hinze (1959) for the general equation and the significance of each one of its terms) to the case of a particle in a fluid with variable velocity. Corrsin and Lumley (1956) made further modifications in order to make the equation applicable to the motion of a small spherical particle in a turbulent fluid.

Hinze (1959) assumed that the particle is very small so that the non-linear term in the B.B.O. equation and the viscous drag due to the pressure gradient are negligible. Thus, it was possible to relate the power spectrum of the particle to the power spectrum of the Lagrangian velocity field. Levich and Kuchanov (1967) made a similar approximation. In addition they neglected the unsteady Basset term (which accounts for the effect of the previous history of the particle motion from some original time) and solved the equation for the relative velocity between the particle and the carrier fluid. They concluded that the mean square of the relative velocity is always much smaller than the mean square velocity of the fluid.

Preceding page blank

Shirazi et al (1967) applied a conditional averaging to reduce the B.B.O. equation to a stochastic integro-differential equation with zero mean. By assuming that the particle velocity and the turbulent velocity vectors are uncorrelated, they obtained specific relationships between the statistical properties of the particle velocity and the fluid velocity. Their published results include relationships for the Lagrangian micro scale, autocorrelation function, and diffusivity of the particles.

Ahmadi (1970) studied the dynamic behavior of a small spherical particle in a numerically generated two dimensional turbulent flow field and calculated the particle diffusivity as a function of particle size and density. He found that the particle diffusivity increases with particle size and decreases with particle density.

EXPERIMENTAL STUDIES

Rouse (1938) performed a basic study in particle diffusion by measuring the concentration in the vertical direction of sand particles in which the turbulence was generated in repeating patterns by mechanical agitation in a cylindrical tank. He found that for any particle size, the particle diffusivity ε_γ is directly proportional to the frequency of agitation; at low frequencies, ε_γ is independent of the particle size; and at high frequencies ε_γ increases with an increase in particle size.

Kampe de Feriet (1938) reported diffusion experiments by Dupuit in a wind tunnel, where soap bubbles about 3 mm in diameter were used and introduced at a point in the wind tunnel stream. The concentration of the bubbles passing a plane perpendicular to the mean flow showed a Gaussian distribution.

Kalinske and Pien (1944) performed diffusion experiments in water flowing through a channel at a certain distance from the bottom and side walls, the turbulent flow there being nearly isotropic. Small drops were formed by injecting a mixture of carbon tetrachloride and benzene of the same density as the water. The value of the variance of the displacement was determined from photographic records. The concentration distribution of the droplets passing a plane perpendicular to the flow at a distance from the point of injection was found to be very close to Gaussian. The rough shape of the Lagrangian correlation coefficient could be well approximated by an empirical function.

Vanoni (1946) used sand of geometric mean sieve sizes of 0.147 mm, 0.12 mm and 0.091 mm and found that for coarse sediment ε_γ is less than the momentum diffusivity ε_m and for fine sediment ε_γ is greater than ε_m. The difference in the two eddy diffusivities is due to differences in the possible combinations of u and v as compared to the combinations of v and γ , thus leading to a difference between momentum transfer and sediment transfer (u and v are respectively the longitudinal and lateral velocity fluctuations and γ is the fluctuation of the sediment concentration). Vanoni argued that during acceleration the relative velocity between the sediment and the fluid must be greater than the fall velocity in the quiescent fluid and thus the sediment is carried a shorter distance than assumed. This tends to make ε_γ less than ε_m.

Carstens (1952) solved the equation of motion of a sphere in an oscillating fluid, omitting the gravitational force. For a motion of the oscillating fluid specified by $x=x_o \sin \omega t$, he showed that the motion of the sphere may be described by $x_s=x_{so} \sin (\omega t+\phi)$, in which ϕ is a phase difference. By assuming such an oscillation to be prevailing in a sediment-laden flow field, he concluded that for sediment particles in water $\varepsilon_\gamma/\varepsilon_m$ can never be greater than 1. He developed a mathematical expression for the ratio $\varepsilon_\gamma/\varepsilon_m$ for an oscillating spherical particle in a liquid flow field. It reads:

$$\frac{\varepsilon_\gamma}{\varepsilon_m} = \frac{(1+3N/2)^2 + [(3N/2)(1+N)]^2}{(\frac{2}{3}\frac{\rho_s}{\rho_f} + \frac{1}{3} + \frac{2N}{3})^2 + [(3N/2)(1+N)]^2} \qquad \text{(II-1)}$$

where $N = \sqrt{8\nu/(\omega/d)}$, an oscillation parameter and ω is circular frequency.

Ismail (1952) performed experiments with suspended sediment in a closed channel. He obtained $\varepsilon_\gamma/\varepsilon_m=1.5$ for 0.1 mm sand and 1.3 for 0.16 mm sand. Brush et al (1965) applied corrections to the fall velocity term and showed that the values would be reduced to 1 and 0.6, respectively.

Longwell and Weiss (1953) assumed the velocity fluctuations to be sinusoidal functions of time, and by solving the equation of motion with certain simplifications they showed that the eddy diffusivity of liquid drops in a turbulent gas stream should be less than the eddy diffusivity of the marked gas particles.

Laursen (1958) measured the velocity distribution and the sediment concentration distribution for 0.04 mm and 0.1 mm sands. Without correcting the concentration by accounting for the actual fall velocity, and assuming Karman's K to be a constant and that the turbulence characteristics were unchanged by the particles, he concluded that $\varepsilon_\gamma/\varepsilon_m>1$.

Smith (1959) investigated the expansion of a falling cluster of particles in an isotropic homogeneous turbulent flow field. He showed that the rate of expansion of the cluster decreases as the terminal fall velocity increases.

Brush (1962) studied the diffusion of glass beads in a submerged axi-symmetric jet in order to compare the characteristics of the diffusion of sediment with those of momentum in free turbulent shear flow. The efflux velocity was maintained at 20 feet per second to lessen the relative importance of the fall velocity of the individual particles. He obtained the corresponding particle turbulent Schmidt number for different particle sizes. The following results were obtained:

Particle mean diameter (mm)	$\varepsilon_\gamma/\varepsilon_m$
0.55	0.15
0.32	0.50
0.19	1.00

Ho (1964) found that the fall velocity in an oscillating fluid was significantly lower than in a still fluid. Reasonable values of the settling velocity in an oscillating fluid were found to be predictable from numerical solutions of the equation of motion.

Goldschmidt and Eskinazi (1966) measured the concentration distribution of aerosol droplets in a plane jet of air by means of a hot wire anemometer. It was found that the turbulent diffusivity of the contaminant particles ε_γ varies with the location in the flow field and that an average value for the turbulent diffusivity of the droplets (with an average size of 3.3 microns) in a plane jet of air is $0.03U_m b_u$, where U_m is the maximum velocity and b_u is the half width of the two dimensional jet. A comparison of the velocity and concentration profiles at various sections of the flow field shows that although the concentration profiles have spread more than the velocity profiles, their rate of diffusion is lower. The average ratio of $\varepsilon_\gamma/\varepsilon_m$ (inverse of the particle turbulent Schmidt number) was found to be 0.91.

Baker and Chao (1965) measured the relative velocity of bubbles in a vertical turbulent conduit. The size of the bubbles used ranged from 760 to 7,000 microns. They concluded that the bubble relative velocity in a turbulent water stream is similar to the rise velocity of single bubbles through a quiescent liquid.

Kennedy (1965) measured the dispersion of 1,250 micron soap bubbles, and 700 and 900 micron polystyrene beads in a grid generated turbulent air flow. The following results were obtained:

Particles	$\varepsilon_\gamma/\varepsilon_m$	Particle-carrier stream density ratio
1250μ soap bubbles	1.52	1.41
700μ polystyrene beads	1.42	39
900μ polystyrene beads	1.10	39

Singamsetti (1966) used sand with a geometric mean sieve diameter of 0.068, 0.115, 0.23, 0.32 and 0.46 mm for measurement of diffusion in a circular jet of water and obtained the following:

Particle diameter (mm)	Particle Reynolds number	$\varepsilon_\gamma/\varepsilon_m$
0.068	0.4	1.23
0.115	1.2	1.20
0.23	7.2	1.24
0.32	18.0	1.35-1.39
0.46	33.0	1.43-1.45

The particle Reynolds number is based on the fall velocity of the particle in a quiescent infinite fluid. Singamsetti concluded from his measurements that (1) the linear oscillation model for simulating the turbulent flow field is invalid for three dimensional turbulence, (2) $\varepsilon_\gamma/\varepsilon_{\gamma_o}$ approaches unity within the Stokes range. $\varepsilon_{\gamma o}$ is the diffusivity of the marked fluid particle and the Stokes range is understood to be that for which the viscous drag on the spherical particle is given by Stokes law. (3) $\varepsilon_\gamma/\varepsilon_{\gamma o}$ is greater than unity for particle Reynolds number beyond the Stokes range provided that the fall velocity is less than the rms value of the turbulent fluctuation in the direction of fall.

Jones et al (1966) developed a linearized theory based on the particle displacement rather than the particle velocity to describe the motion of small particles in a turbulent flow. They found that most of the energy of the particle fluctuation was contained at lower frequencies (less than 3 cps) than that of the carrier fluid (less than 10 cps). Moreover, the heavier particles contained more tubulent energy than the lighter one.

Majumdar and Carstens (1967) used nearly neutrally buoyant particles in an apparatus restricting the particle motion to a horizontal plane in a supposedly homogeneous isotropic turbulent flow field. The particle diffusion occurs without mean motion. The motion of individual particles was recorded on motion picture film, which was subsequently projected for displacement measurements. The particle displacement data were analyzed, using the diffusion theory of continuous movement. The values of the particle diffusivity, ε_γ, and particle mixing length, ℓ_c, were plotted as a function of particle diameter, d. They concluded that

(1) if $d < \ell_c, \varepsilon_\gamma = \varepsilon_{\gamma o}$:
(2) if $d > 3\ell_c$, $\varepsilon_\gamma = 0$; and
(3) $\varepsilon_\gamma/\varepsilon_{\gamma_o}$ continuously decreases in the range $1 < d/\ell_c < 3$.

Sayre and Chang (1968) investigated the dispersion process in a turbulent open channel flow. They found that the longitudinal dispersion process for suspended silt-size sediment particles differs from the process for a dissolved dispersant in that the particles tend to settle toward the slower moving flow near the bed and eventually deposit on the bed. The lateral dispersion of floating particles (released from an intermittent point source at the water surface) can be represented as a Fickian diffusion process. However, the dispersion pattern is somewhat distorted by the effects of secondary circulation.

Householder (1968) performed an experiment similar to that of Goldschmidt and Eskinazi, and found the following dependence of the particle turbulent Schmidt number on the particle size:

Particle size (microns)	$\varepsilon_\gamma/\varepsilon_m$
6.4	2.38
13.1	7.70
16.7	3.33

Householder and Goldschmidt (1969) made an extensive review and unified the available data on dispersion of contaminants in open channels and circular pipes. They related the turbulent Schmidt number to a particle parameter, ψ, proportional to the Stokesian particle response and defined as

$$\psi = R_e\left(\frac{d}{a}\right)^2 \left(\frac{2\rho_p}{\rho_f} + 1\right) \qquad \text{(II-2)}$$

where R_e is the Reynolds number,(based on the mean flow velocity and a characteristic width of the conduit),d is the particle diameter, a is the characteristic dimension of the flow field and ρ_p and ρ_f are the density of the particle and carrier fluid respectively. They concluded that there is a general trend towards an increase of particle diffusion with ψ, and hence particle size.

SECTION VI

THEORETICAL BACKGROUND

MOMENTUM TRANSPORT IN AN AXI-SYMMETRIC JET

Based on the assumptions that (1) the mean motion is steady, (2) the flow field is axi-symmetric, and (3) the turbulent region is narrow in the radial direction when compared with the axial direction, the equation of motion of an axi-symmetric turbulent jet in the axial direction, (Appendix I), reads:

$$U \frac{\partial U}{\partial x} + V \frac{\partial U}{\partial r} = \frac{1}{\rho} \frac{1}{r} \frac{\partial}{\partial r} (r\sigma_{xr}) \qquad \text{(VI-1)}$$

where x and r are respectively the coordinates in the axial and radial directions, U and V are respectively the mean values of the x and r components of velocity, σ_{xr} is the Reynolds stress, and ρ is the fluid density. The corresponding boundary conditions are:

$$\left.\begin{array}{l} r = 0 : \quad V = 0 ; \quad \frac{\partial U}{\partial r} = 0 \\ r = \infty : \quad U = 0 \\ \text{conservation of momentum} \end{array}\right\} \qquad \text{(VI-2)}$$

Equation (VI-1) together with the equation of mass conservation and the boundary conditions (VI-2) can be integrated to give (Appendix II)

$$\frac{\sigma_{xr}}{\rho U_m^2} = - \frac{1}{\eta} \frac{U}{U_m} \int_0^{\eta} d\eta \; \eta \left(\frac{U}{U_m}\right) \qquad \text{(VI-3)}$$

where $\eta = r/(x+a)$. With η so defined the immediate consequences of the similarity of the flow field will give (Appendix II)

$$\frac{b_u}{D} = k_b \left(\frac{x}{D} + \frac{a}{D}\right) \qquad \text{(VI-4)}$$

$$\frac{U_o}{U_m} = k_u \left(\frac{x}{D} + \frac{a}{D}\right) \qquad \text{(VI-5)}$$

where a is the distance from the virtual origin to the jet nozzle plane, U_o is the jet efflux velocity, U_m is the maximum velocity at the section of consideration, b_u and k_b are respectively the values of r and η where the velocity is half the maximum at the section of consideration, and k_u is the slope of the linear relationship as given in Equation (VI-5). The Reynolds stress σ_{xr} is expressed as $\sigma_{xr} = -\rho uv$, where u and v are respectively the fluctuation velocity components in the x and r directions. In this derivation the "kinematic" and "dynamic" virtual origins have been assumed to be equivalent. The experimental results for the particular jet will confirm this. In general (see Flora & Goldschmidt (1969)) this need not be true. In analogy with the coefficient of viscosity in Stokes' law for laminar flows, Boussinesq introduced the kinematic eddy viscosity, ε_m, for the Reynolds stress in turbulent flows by putting

$$\sigma_{xr} = \rho\varepsilon_m \frac{\partial U}{\partial r} \tag{VI-6}$$

Note that ε_m accounts only for the turbulent transport. The molecular transport is neglected since it is approximately three orders of magnitude smaller than the transport due to turbulence. Substituting Equation (VI-6) into Equation (VI-3), the relation between ε_m and U/U_m reads:

$$\frac{\varepsilon_m}{U_m(x+a)} = - \frac{\frac{U}{U_m}\int_o^\eta d\eta\ \eta\ (\frac{U}{U_m})}{\eta \frac{d}{d\eta}\ (\frac{U}{U_m})} \tag{VI-7}$$

An assumption concerning ε_m has to be made in order to calculate the velocity distribution.

First Model: (Constant Eddy Viscosity)

Prandtl's mixing length hypothesis leads to a simplified expression for the eddy viscosity (Schlichting (1960)) as follows:

$$\varepsilon_m = \ell^2 \left|\frac{\partial U}{\partial r}\right|$$

In the above ℓ is the mixing length, a length scale related to the size of the fluid lump in the turbulent flow field. If it is further assumed that the dimensions of the lumps of fluid which move in a transverse direction during turbulent mixing are of the same order of magnitude as the width of the mixing zone and that the mixing length is proportional to the half width, b_u, of the mixing zone then

$$\varepsilon_m = \chi b_u\ U_m \tag{VI-8}$$

Here χ denotes a dimensionless constant to be determined experimentally. From conversation of momentum, Schlichting (1960) showed that for a turbulent circular jet

$$b_u \sim x \tag{VI-9}$$

and

$$U_m \sim x^{-1}$$

Thus from Equations (VI-8), (VI-9) and (VI-10), the kinematic eddy viscosity (employing Prandtl's mixing length hypothesis) becomes a constant value over the whole flow field of a turbulent jet. Consequently Equation (VI-7) can be solved for U/U_m. One useful form of the solution (Appendix III) reads:

$$\frac{U}{U_m} = 1 + \frac{U_m(x+a)}{8\varepsilon_m}\eta^2 \quad {}^{-2} \tag{VI-11}$$

Second Model: (Taylor's Vorticity Transport Theory)

Equation (VI-7) states that if $U_m(x+a)$ is constant then ε_m would be a function of η. Another form of the solution, without adopting the intuitive assumption given in Equation (VI-8), is obtained using Taylor's vorticity transport theory (Schlichting (1960)). Introducing an eddy viscosity based on the mixing length of the vorticity transport, ℓ_ω, such that

$$\varepsilon_m = \frac{\ell_\omega^2}{2}\left|\frac{\partial U}{\partial r}\right| \tag{VI-12}$$

and

$$\ell_\omega = C_\omega(x+a) \tag{VI-13}$$

and substituting then Equation (VI-12) and (VI-13) into Equation (VI-7), Tomotika (1938) obtained the approximate solution

$$\frac{U}{U_m} = 1 - a_1(\eta^*)^{3/2} + a_2\,(\eta^*)^3 - a_3(\eta^*)^{9/2} \tag{VI-14}$$

where

$$\eta^* = \eta\left(\frac{C_\omega^2}{2}\right)^{-1/3}$$

$$a_1 = \frac{2\sqrt{2}}{3\sqrt{3}}$$

$$a_2 = \frac{11}{81} \tag{VI-15}$$

$$a_3 = \frac{1363\sqrt{2}}{6123\sqrt{3}}$$

The corresponding eddy viscosity based on Equation (VI-7) becomes

$$\frac{\varepsilon_m}{U_m(x+a)} = \left(\frac{C_\omega^2}{2}\right)^{2/3}\left|\frac{d}{d\eta^*}\left(\frac{U}{U_m}\right)\right| = \left(\frac{C_\omega^2}{2}\right)^{2/3}\quad -\frac{3}{2}a_1\eta^{*1/2} + 3a_2(\eta^*)^2 - \frac{9}{2}a_3(\eta^*)^{7/2}$$

Third Model: (Reichardt's Inductive Theory)

Another solution is obtained by applying Reichardt's inductive theory and transforming Equation (VI-1) into a diffusion type of equation (Hinze (1959)). The theory yields an exponential solution:

$$\frac{U}{U_m} = e^{-K_u \eta^2} \qquad \text{(VI-17)}$$

Substituting Equation (VI-17) into Equation (VI-7) the corresponding eddy viscosity becomes

$$\frac{\varepsilon_m}{U_m(x+a)} = \frac{1-e^{-K_u \eta^2}}{4K_u^2 \; \eta^2} \qquad \text{(VI-18)}$$

It is worthy to note that the above three models have all been used in the literature, together with other solutions not reported herein. Equations (VI-11), (VI-14) and (VI-17) result from different models used to obtain an expression relating the Reynolds stress to the mean flow properties. Which one of the listed models is more suitable can only be determined by a comparison with accurate measurements of the mean velocity and the Reynolds stress or by an up to now unavailable rigorous formulation for the eddy viscosity itself. For comparison purposes all of the models described will be used in the discussion that follows.

SCALAR QUANTITY TRANSPORT IN AN AXI-SYMMETRIC JET

The equation of transport for a scalar quantity in an axi-symmetric jet (Appendix IV) reads:

$$U\frac{\partial \Gamma}{\partial x} + V\frac{\partial \Gamma}{\partial r} = -\frac{1}{r}\frac{\partial}{\partial r}(r\,\overline{v\gamma}) \qquad \text{(VI-19)}$$

where γ is the fluctuation component of the scalar quantity. The above is limited, again, to (1) steady mean motion, (2) an axi-symmetric flow field, (3) a narrow turbulent region in the radial direction when compared with the axial direction, and (4) neglect of molecular transport.

Assuming that the turbulent transport of Γ can be described by analogy to Fick's law, using a coefficient of diffusivity ε_γ, the following expression is postulated:

$$-\overline{v\gamma} = \varepsilon_\gamma \left| \frac{\partial \Gamma}{\partial r} \right| \qquad \text{(VI-20)}$$

Again, as for ε_m, ε_γ doesn't account for the molecular effects. By substituting Equation (VI-20) into Equation (VI-19) and invoking conservation of Γ, the distribution of the scalar quantity becomes (Appendix IV):

$$\frac{\Gamma}{\Gamma_m} = \exp\left\{ - \int_o^\eta \frac{(x+a)U_m}{\varepsilon\gamma\eta}\left[\int_o^\eta \eta\left(\frac{U}{U_m}\right) d\eta\right] d\eta\right\} \tag{VI-21}$$

Again, the above expression implies the similarity of the Γ -distribution. The immediate consequences of the similarity give (Appendix IV)

$$\frac{b_\gamma}{D} = k_h \left(\frac{x}{D} + \frac{a}{D}\right) \tag{VI-22}$$

$$\frac{\Gamma_o}{\Gamma_m} = k_\gamma\left(\frac{x}{D} + \frac{a}{D}\right) \tag{VI-23}$$

Where a is the distance from the virtual source of the concentration to the jet nozzle plane and is assumed to be equal to that to the virtual origin of the velocity distribution. This need not be the case, it is now assumed so strictly for convenience. Γ_o is the efflux concentration at the jet nozzle, Γ_m is the maximum concentration at the section of consideration, b_γ and k_h are respectively the values of r and η where the concentration is half the maximum at the section of consideration, and k_γ is the slope of the linear relation between the inverted centerline concentration and the axial distance as given in Equation (VI-23).

If ε_m and ε_γ as well as the velocity distribution are known, then the Γ distribution can be obtained from Equation (VI-21). Conversely, in the absence of a proper model for ε_γ, but provided ε_m and U/U_m are given and Γ/Γ_m is measured, then ε_γ can be determined. In the first part of this section different models relating the eddy viscosity to the mean flow properties were discussed. These in turn gave relationships for U/U_m. In a very similar manner if different models were defined for ε_γ, then a relationship for Γ/Γ_m would result. A basic assumption is now made. Irrespective of how ε_γ or ε_m might vary through the jet, it is now assumed that the same basis for describing ε_m will apply toward a description of ε_γ. Hence the three models of section A are now employed to obtain alternate formulations for Γ/Γ_m in terms of ε_γ and ε_m.

First Model: (Constant Eddy Viscosity and Eddy Diffusivity)

If the velocity profile is assumed as expressed in Equation (VI-7), substituting it into Equation (VI-21), the concentration distribution becomes:

$$\frac{\Gamma}{\Gamma_m} = \exp \int_o^\eta d\,\eta \,\frac{\varepsilon_m}{\varepsilon_\gamma}\frac{d}{d\eta} \ln\left(\frac{U}{U_m}\right) \tag{VI-24}$$

Assuming as in section A that ε_m and now ε_γ are constant across the whole flow field then Equation (VI-24) simplifies to

$$\frac{\Gamma}{\Gamma_m} = \left(\frac{U}{U_m}\right)^{\frac{\varepsilon_m}{\varepsilon_\gamma}} = 1 + \frac{U_m(x+a)}{8\,\varepsilon_m}\eta^2 \quad {}^{-2\frac{\varepsilon_m}{\varepsilon_\gamma}} \tag{VI-25}$$

Second Model: (Taylor's Vorticity Transport Theory)

If the velocity profile is calculated according to Taylor's modified vorticity transport theory and the eddy diffusivity is expressed as

$$\frac{\varepsilon_\gamma}{U_m(x+a)} = C_\gamma^2 \left| \frac{d}{d\eta} \left(\frac{U}{U_m}\right) \right| \qquad \text{(VI-26)}$$

then substitution of Equations (VI-14) and (VI-26) into Equation (VI-21) yields a solution of Γ/Γ_m in the form:

$$\frac{\Gamma}{\Gamma_m} = \left\{ \exp\left[\int_o^{\eta^*} d\eta^* \; \frac{1/2\eta^{*1/2} - \frac{2}{7}a_1\eta^{*2} + \frac{a_2}{5}\eta^{*7/2} - \frac{2a_3}{13}\eta^{*5}}{-\frac{3}{2}a_1 + 3a_2\eta^{*3/2} - \frac{9a_3}{2}\eta^{*3}} \right] \right\}^{\frac{\varepsilon_m}{\varepsilon_\gamma}} \qquad \text{(VI-27)}$$

where η^* is as defined in Equation (VI-15).

Third Model: (Reichardt's Inductive Theory)

The velocity profile based on Reichardt's inductive theory is given in Equation (VI-17). Substituting now Equation (VI-17) into Equation (VI-21) and expressing $U_m(x+a)$ in terms of the eddy viscosity as given in Equation (VI-7), the final solution for the concentration profile reads:

$$\frac{\Gamma}{\Gamma_m} = \exp\left\{ -\frac{\varepsilon_m}{\varepsilon_\gamma} K_u \eta^2 \right\} \qquad \text{(VI-28)}$$

Hereafter, Equations (VI-25), (VI-27) and (VI-28) will be referred to as the first, second and third proposed models respectively. To obtain the dependence of the dimensionless parameter $\varepsilon_m/\varepsilon_\gamma$, which is defined as the turbulent Schmidt number, S_t, on the contaminant particle size is the major objective of this work. Its value will be found from measured concentration flux distributions and equations (VI-25), (VI-27) or (VI-28).

SECTION VII

EXPERIMENTAL SETUP AND MEASUREMENT PRINCIPLES

The main purpose of the experimental part of this work is the measurement of the concentration distribution of bubbles in an axi-symmetric jet. The basic setup employs a submerged axi-symmetric water jet as the flow field, a series of constant size bubbles generated through a capillary tube placed at the center of the mouth of the jet as the contaminant, and a hot film sensor as the bubble concentration flux sampler. The experimental equipment and the measurement procedures are described in more detail in the following sections.

JET FLOW FIELD

Axi-symmetric Turbulent Water Jet

A schematic diagram of the experimental setup is shown in Figure 1. The system consists of a constant head tank, a jet tank, a reservoir, a pump and a water filter. The constant head tank has an adjustable elevation permitting changes of the jet efflux velocity. In addition, two interchangeable nozzle contracting sections, of 1/4 and 1/2 inch diameter, permit further variation of the efflux velocity of the submerged jet. The maximum jet velocity reached with the non-metallic 1/4 HP pump and a Cuno Model SS-8 super flow water filter is 20 feet per second. This corresponds to a Reynolds number based on the jet nozzle diameter in the order of $8X10^4$. Figure 2 shows the constant head tank, water filter and pump. A deionizer, also shown in Figure 2, is used to treat the water introduced into the flow system.

The entire flow system is mounted on a level steel frame structure. Figure 3 shows a photograph of the jet tank. It is rectangular in shape to permit optical inspection of the flow field. The top edge of the side wall serves as an overflowing weir so as to maintain a constant water level inside the jet tank. The side gutter which is attached to the outside of the tank wall collects the overflow water and returns it to the reservoir. The overall dimensions of the tank are 18"x18"x25" in height. The jet tank provides a turbulent jet flow field with an axial distance of up to 40 jet diameters when the 1/2 inch nozzle is in use. A traversing mechanism is included to be able to position the measuring probe in the jet. As designed, it allows variations in position in the longitudinal, transverse and vertical directions.

Velocity Measuring System

The mean velocity component of the turbulent water jet was measured with a straight-leg Prandtl-type Pitot-static tube

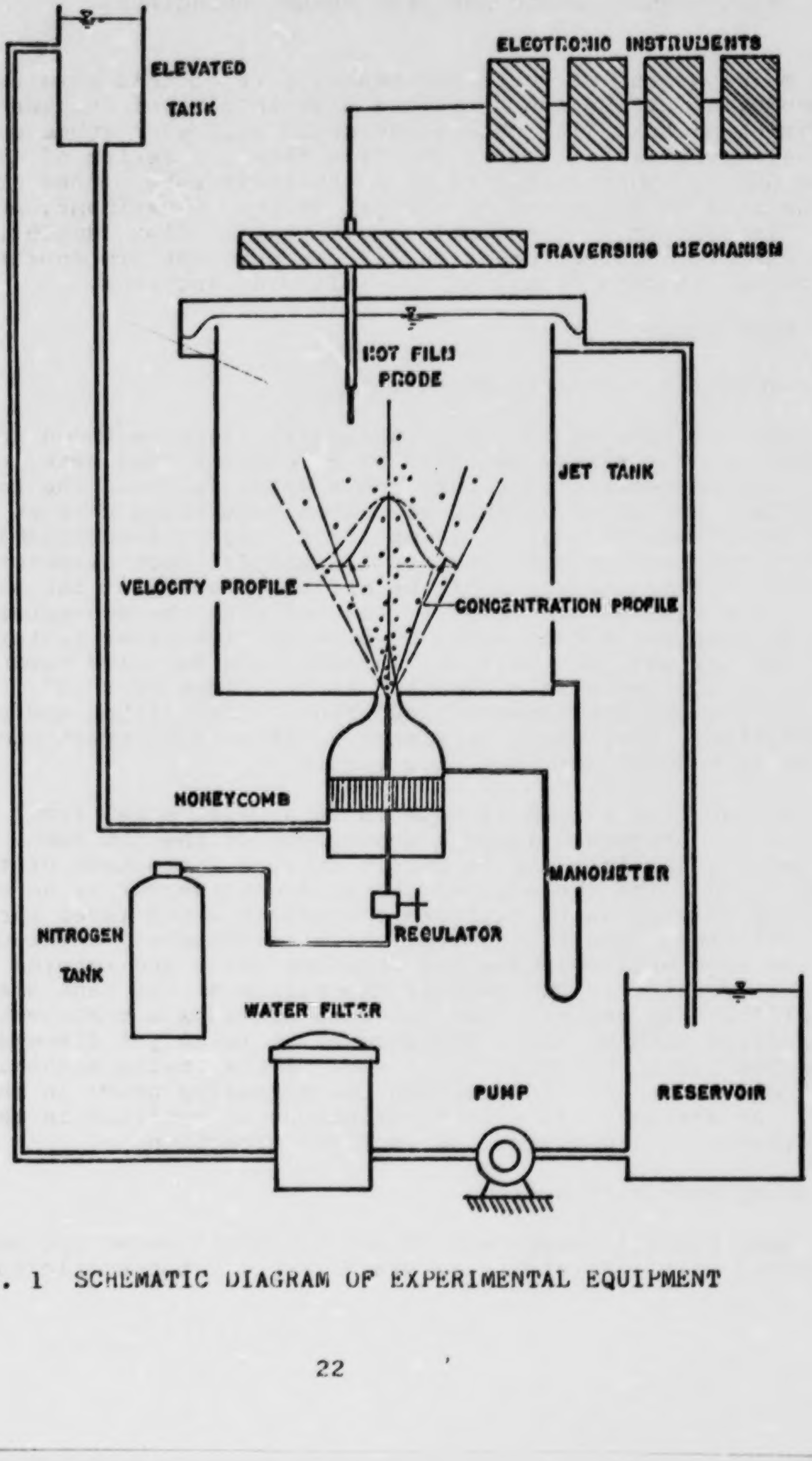
ELEVATED TANK
ELECTRONIC INSTRUMENTS
TRAVERSING MECHANISM
HOT FILM PROBE
JET TANK
VELOCITY PROFILE
CONCENTRATION PROFILE
HONEYCOMB
MANOMETER
NITROGEN TANK
REGULATOR
WATER FILTER
PUMP
RESERVOIR

FIG. 1 SCHEMATIC DIAGRAM OF EXPERIMENTAL EQUIPMENT

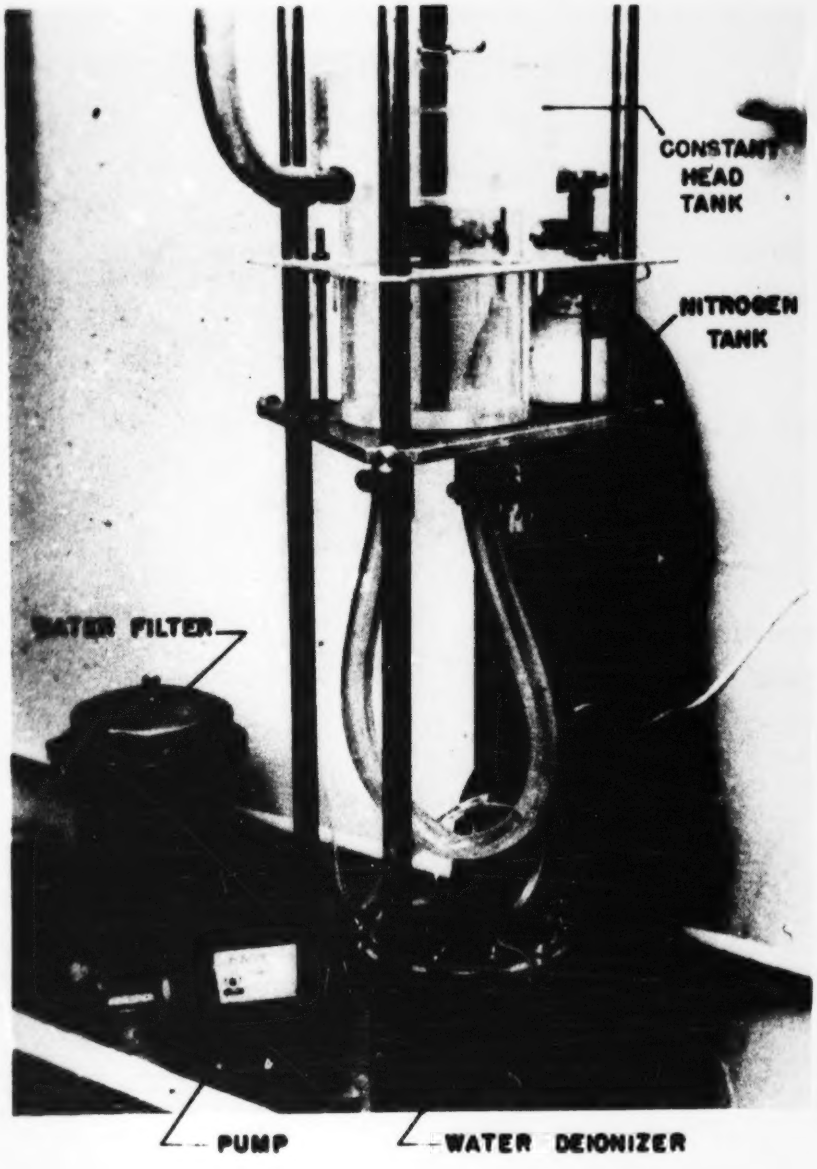
CONSTANT HEAD TANK
NITROGEN TANK
WATER FILTER
PUMP
WATER DEIONIZER

FIG. 2 CONSTANT HEAD TANK, WATER FILTER,DEIONIZER

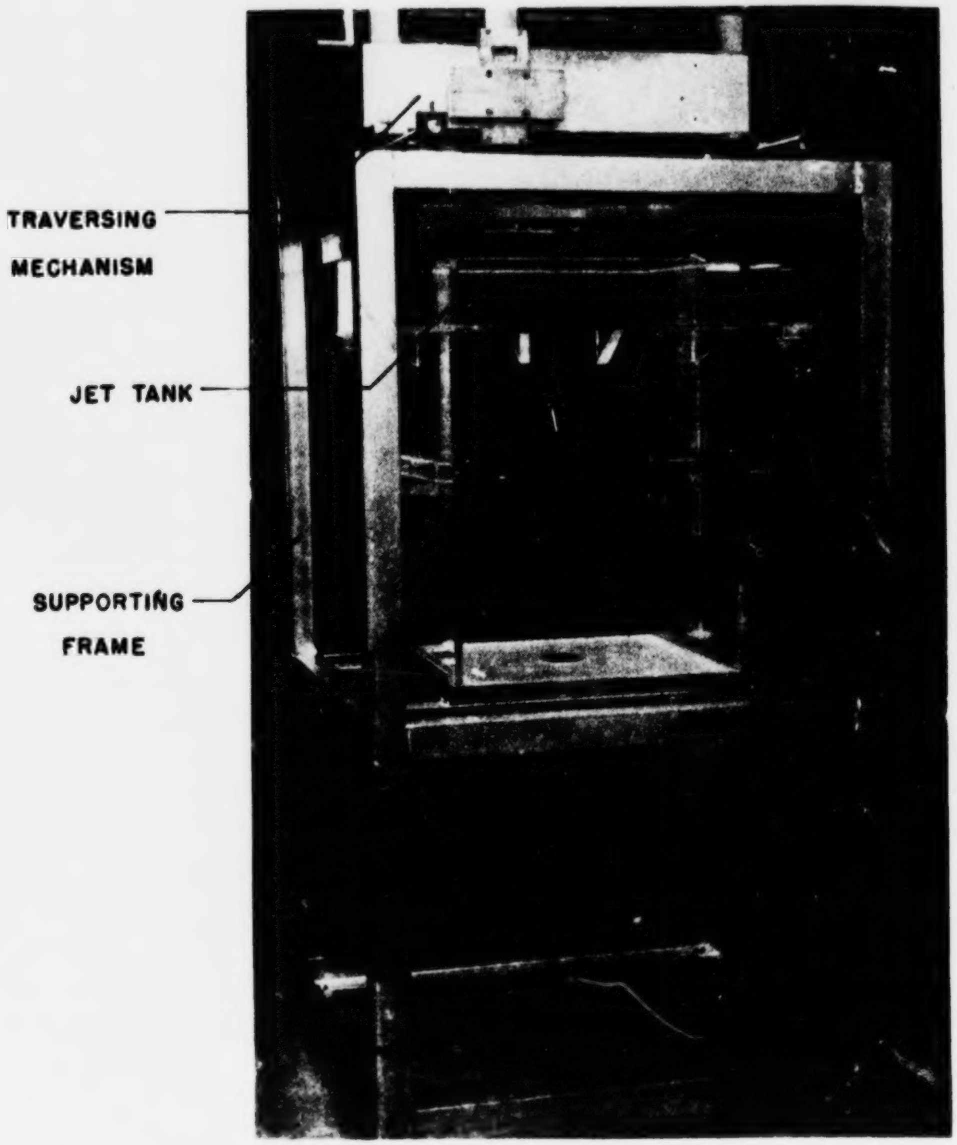
TRAVERSING MECHANISM
JET TANK
SUPPORTING FRAME

FIG 3 PHOTOGRAPH OF JET TANK

and checked with the hot film anemometer. The pitot tube used has an outside diameter of 3/32 inch and a dynamic tap opening of 1/32 inch. Two lines of 4 mm inside diameter tygon tubings were connected from the pitot tube to a differential manometer. The indicating fluid of the manometer was Meriam No. D-8325 fluid with a specific gravity equal to 1.75.

The speed of reading depends on the length and the diameter of the pressure passages inside the probe, the size and the length of the pressure tubes to the manometer, and the displacement volume of the manometer. The time constant in this system was found to be in the order of a few seconds.

The mean velocity measurement was also checked by a TSI 1217-20w, (Thermo Systems Inc., 2500 Cleveland Ave., N. Saint Paul, Minnesota 55113) quartz coated hot film and TSI 1050 anemometer with TSI 1025 Temperature Compensator in series. The axial fluctuation velocity components were also measured with the same hot film sensor.

BUBBLE GENERATION

Generation of a more or less uniform series of air bubbles is possible when supplying a constant air pressure to a small tube submerged in the water. The intent was to generate bubbles and introduce them upstream of the jet mouth in order to permit the study of their undisturbed motion in the turbulent jet. The objective was fulfilled with the system shown in Figure 1. A long glass tube, drawn to a small diameter nozzle at the tip was introduced at the base of the jet tank. Use of a constant pressure nitrogen source (filtered and carefully regulated) resulted in bubbles being generated slightly upstream of the jet mouth.

The sizes of the syringe tubes used were very small when compared with the jet nozzle. The outside diameter of the capillary tubes used was less than 120 microns. (The ratio of the tube cross sectional area to the jet nozzle opening area is correspondingly less than 10^{-4}.) The fragile nature of the glass nozzles caused frequent breakage. The smallest one used had a tip inside diameter of 13.6 microns, and the largest one used had a tip inside diameter of 96 microns.

An analytical and experimental study of bubble formation due to a submerged capillary tube in quiescent and co-flowing streams has been made, and published (Chuang and Goldschmidt (1970)). An abstract is included in the Appendix of Section XVI.

CONCENTRATION FLUX MEASURING SYSTEM

Several techniques for measuring the concentration of the bubbles were considered (such as a laser sampling device, photographic techniques and hot film anemometer sampler). The use of the laser system is discussed in a separate report. The hot film anemometer system was selected in this first phase of the work as the bubble concentration sampler primarily because of its availability. The method described herein was originally developed by Goldschmidt (1965) and then modified by Goldschmidt and Householder (1969) for the diffusion measurement of oil aerosols in a two dimensional air jet.

The applicability of the hot film anemometer for the bubble in water measurement was first described by Hsu et al (1963) and then by Delhaye (1969) and Chuang and Goldschmidt (1969). The principles and the techniques for the application of the hot film sensor to bubble concentration measurement are described in the following.

Principle

The mean concentration of the bubbles at a certain position of an axi-symmetric turbulent jet can be obtained by knowing the mean concentration flux and mean velocity component at that location. The mean concentration flux is measured by counting the number of bubbles impacting on a hot film sensor. The heated sensor of a hot film anemometer when placed in a turbulent water stream contaminated with gas bubbles will suffer unsteady cooling due to the carrier stream velocity fluctuations and the low heat capacity gas bubbles which impact on the sensor. The response of the hot film anemometer to a bubble in a laminar water stream has been extensively discussed and is given in Chuang and Goldschmidt (1969)., (see section XVI).

By discrimination, either through frequency filters or amplitude discriminators, the decrease of the cooling signal due to the impaction of the gas bubbles may be isolated and measured. Since the characteristic frequency of the bubble impaction signal is above 1 KHz and most of the turbulent energy of the carrier stream is below 1 KHz, frequency discrimination was adopted.

The possible errors due to the uncertainty in the impaction coefficient caused by the curving pathlines around the cylindrical sensor are noted in Section VIII.

Frequency Discrimination

In order to use the hot film anemometer as a bubble sampler in a turbulent flow field, it is necessary to frequency discriminate the decrease of the cooling signal from the impacting bubble. The electronics used to accomplish this are shown in Figure 7. The band pass filter was set at the analyzing frequency where the impacting signal has the highest energy density. Discrimination is then possible provided that most of the energy due to the turbulent cooling of the fluid lies at values of frequency below that selected. It is desired, then, to first determine the energy spectrum of the signal for a single bubble impaction.

By harmonic analysis a bubble impaction signal can be transformed from a time-dependent function into a frequency-dependent function, namely the energy density function. Let e(t) be a random time-dependent function such that $e(t)=0$ for $t_1>t$ and $t_2<t$, where t_1 and t_2 represent the times of the bubble hitting and detaching from the sensor. e(t) can then be expressed in a Fourier Integral form:

$$e(t) = \int_0^\infty g(\omega)\, e^{i\omega t} d\omega \tag{VII-1}$$

where

$$g(\omega) = \frac{1}{2\pi} \int_{t_1}^{t_2} e(t)\, e^{-i\omega t}\, dt = \frac{1}{2\pi} \int_{t_1}^{t_2} e(t)\, (\cos \omega t - i \sin \omega t) dt \tag{VII-2}$$

the energy density is then defined as

$$\left| g(\omega) \right|^2 = \frac{1}{4\pi^2} \left\{ \left[\int_{t_1}^{t_2} e(t) \cos\omega t dt \right]^2 + \left[\int_{t_1}^{t_2} e(t) \sin \omega t\ dt \right]^2 \right\} \tag{VII-3}$$

The bubble impaction signal was obtained from the TSI constant temperature anemometer and displayed on a Tektronix Type 564 Storage Oscilloscope. A photograph of the cooling signal was then taken with a polaroid camera. The resulting photograph was digitized and a numerical integration of Equation (VII-3) was performed.

The energy density function of the cooling signal due to a bubble of about 500 microns in diameter approaching the sensor at 3.5 fps is shown in Figure 4. The over heat ratio of the sensor was 1.1, the same as that used in the actual concentration flux measurements. Figure 4 shows that the bubble signal energy is a maximum at 1.8 KHz. This frequency is well above the maximum frequency for the turbulence energy in an axisymmetric turbulent water jet (discussed in the next chapter).

It was then decided to set up a frequeccy band between 1.5 and 2.2 KHz for the concentration flux measurements in such a manner that all frequencies below 1.5 KHz and above 2.2 KHz were cut off.

All of the electronic components are linear in their response to a signal with the exception perhaps of the band pass filter. To ascertain that the band pass filter did not introduce any non-linearity, a calibration of the filtered output e_{pf} compared

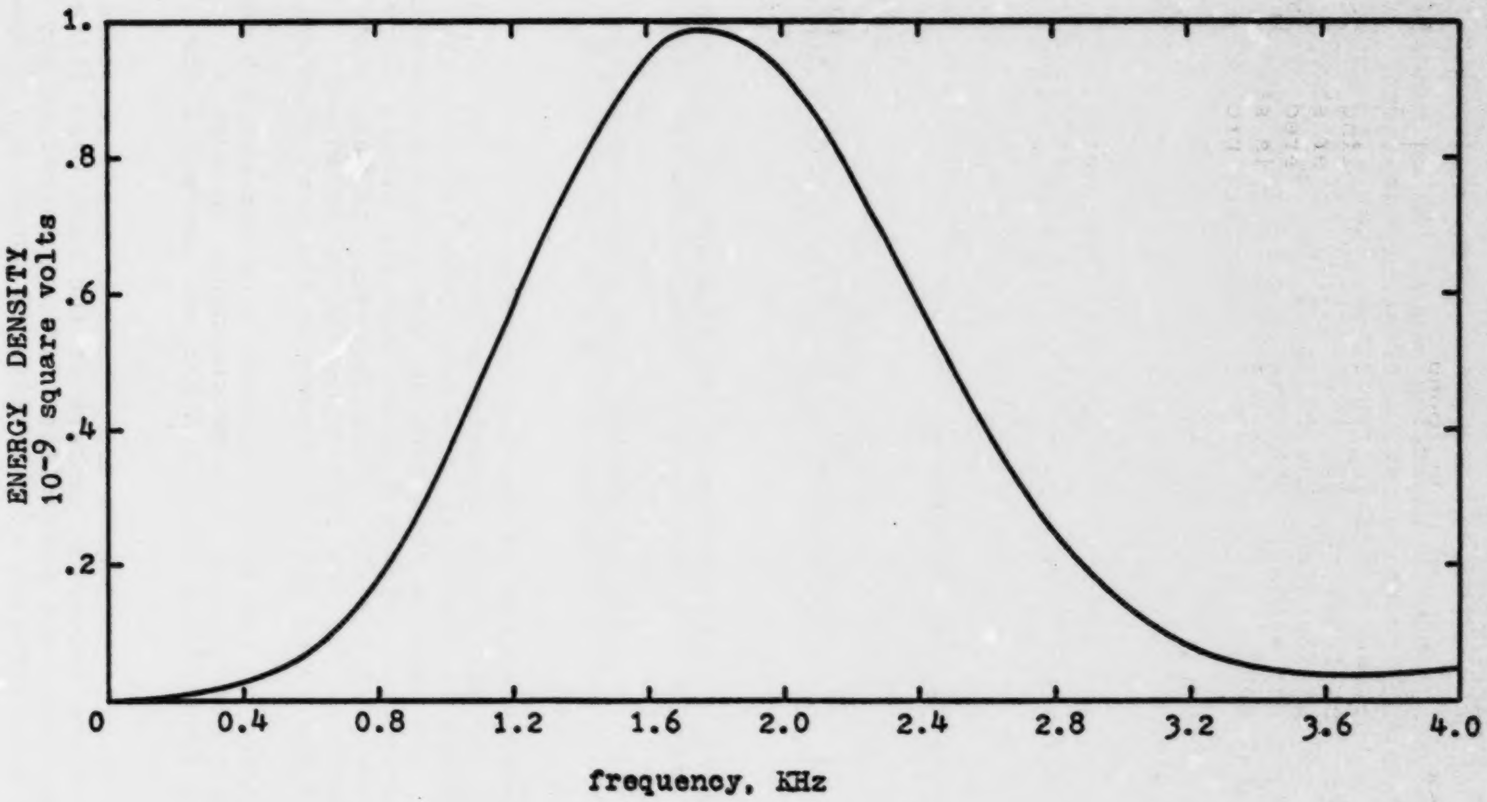

FIG. 4 ENERGY DISTRIBUTION OF BUBBLE SIGNAL

to the unfiltered input e_p was made for this band pass setting. Figure 5 exhibits the expected linearity. Similar results at other band pass settings had been found by Householder (1968) for the same equipment.

The output of the filtered and the un-filtered cooling signal on a sensor in a bubble contaminated turbulent water stream is shown in Figure 6. The upper trace is the filtered signal and the lower trace is the unfiltered signal. It is seen that the low frequency turbulent signals have been properly filtered.

Counting

The components of the system are a hot film anemometer, a tunable band pass filter, an AC amplifier, a Schmitt trigger, and an electronic counter. Due to the active components of the filter, the output is oscillatory as shown in Figure 6. To eliminate erroneous multiple counts from a single bubble impaction, the decaying oscillatory signal was fed to a Schmitt trigger, the output of which was just longer in duration than the oscillatory signal. The trigger, in turn, when provided with an adjustable gate, was used for amplitude sampling. The output from the Schmitt circuit was fed to an electronic counter which recorded the rate of bubbles hitting the sensor and causing a decrease of the cooling signal larger than the trigger level of the Schmitt circuit.

Equipment

The block diagram of the system is shown in Figure 7. The specific components used in this system are shown in Figure 8. Their specifications follow:

- TSI Constant Temperature Anemometer, Type 1050
    - Frequency response: 0-400 KHz
    - Output noise level: corresponding to less than 0.02% turbulent intensity
    - Stability: drift less than 2 microvolts per °F and less than 20 microvolts in 24 hours.
- TSI Model 1217-20w Quartz Coated Cylindrical Hot Film
    - Sensing size: 0.002" diameter, 0.02" long
    - Relative frequency response: 40 KHz
    - Nominal resistance: 4-8 Ohms
- Hewlett Packard Model 450A Amplifier
    - Frequency response: 20+ 1/2 db, 5 Hz to 1 meg. Hz
- Kron-Hite Band Pass Filter, Model 310C
    - Frequency range: 20 Hz to 200 KHz
    - Attenuation slope: 24 db per octave
- Tektronix Oscilloscope, Type 564 Storage Scope with Type 2B67 Time Base
    - Gate width: adjustable from 10 micro sec. to 50 sec.
    - Trigger level: adjustable from 0.002 to 160 volts

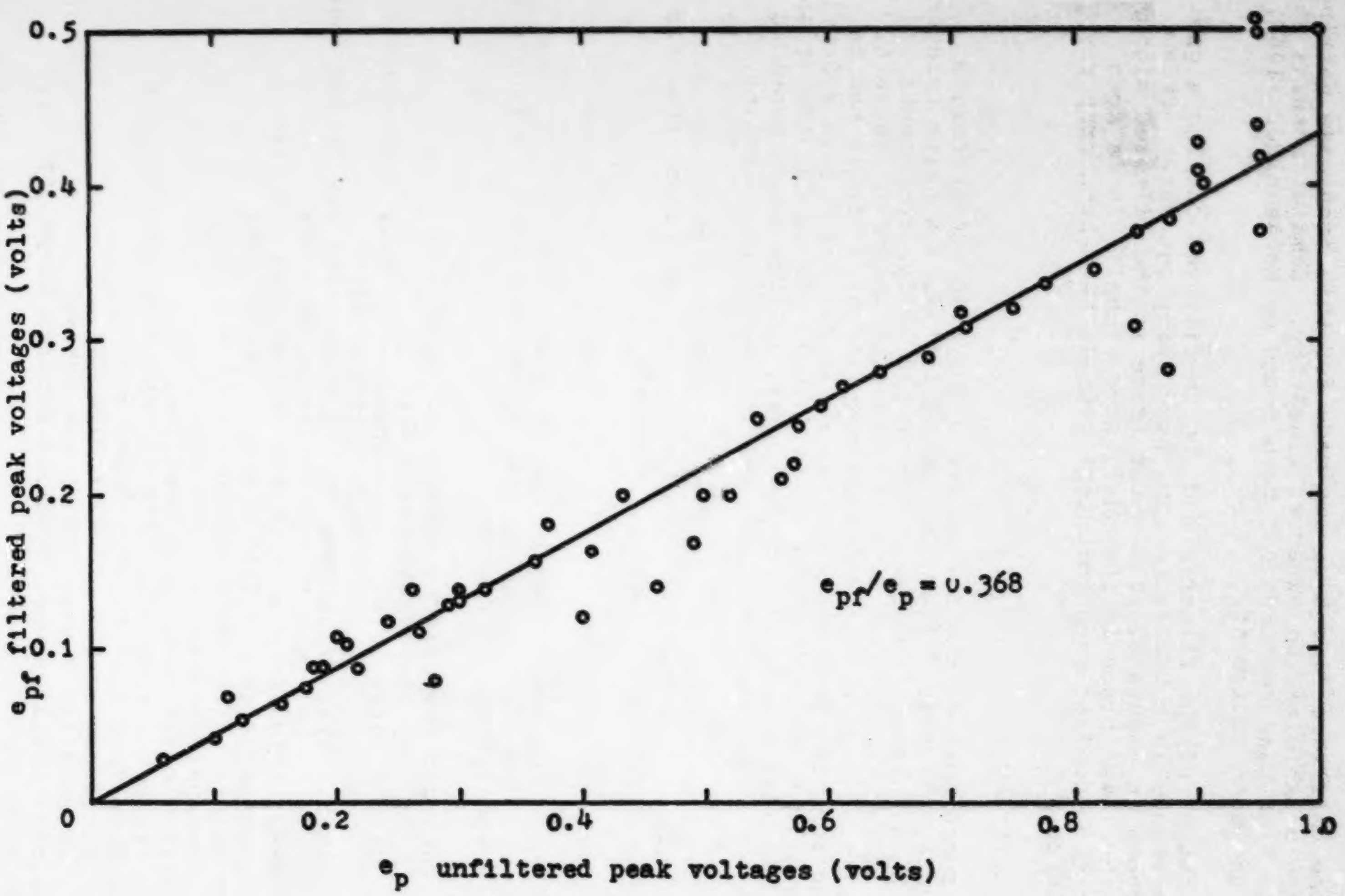

FIG. 5 FILTERED vs UNFILTERED PEAK VOLTAGES

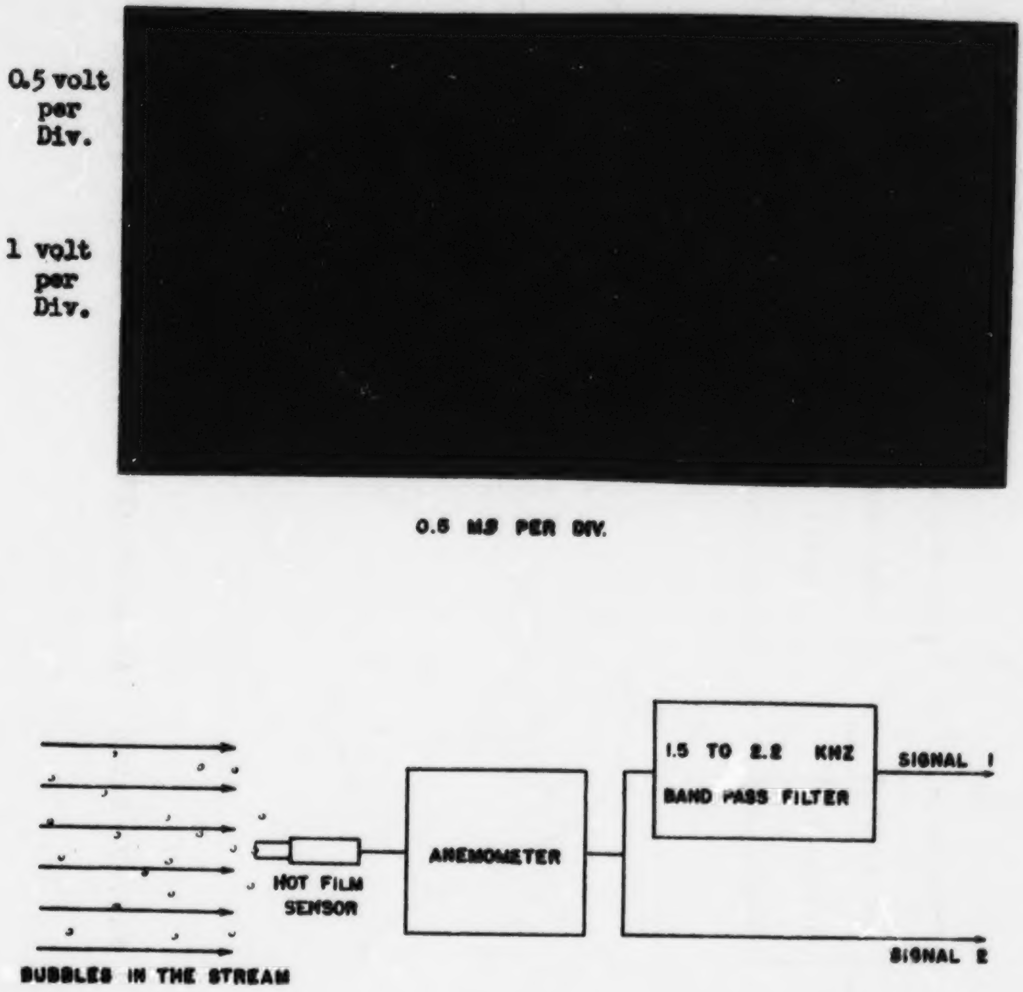
0.5 volt per Div.
1 volt per Div.
0.5 MS PER DIV.
1.5 TO 2.2 KHZ BAND PASS FILTER
SIGNAL 1
HOT FILM SENSOR
ANEMOMETER
SIGNAL 2
BUBBLES IN THE STREAM

FIG. 6 FILTERED AND UNFILTERED SIGNALS

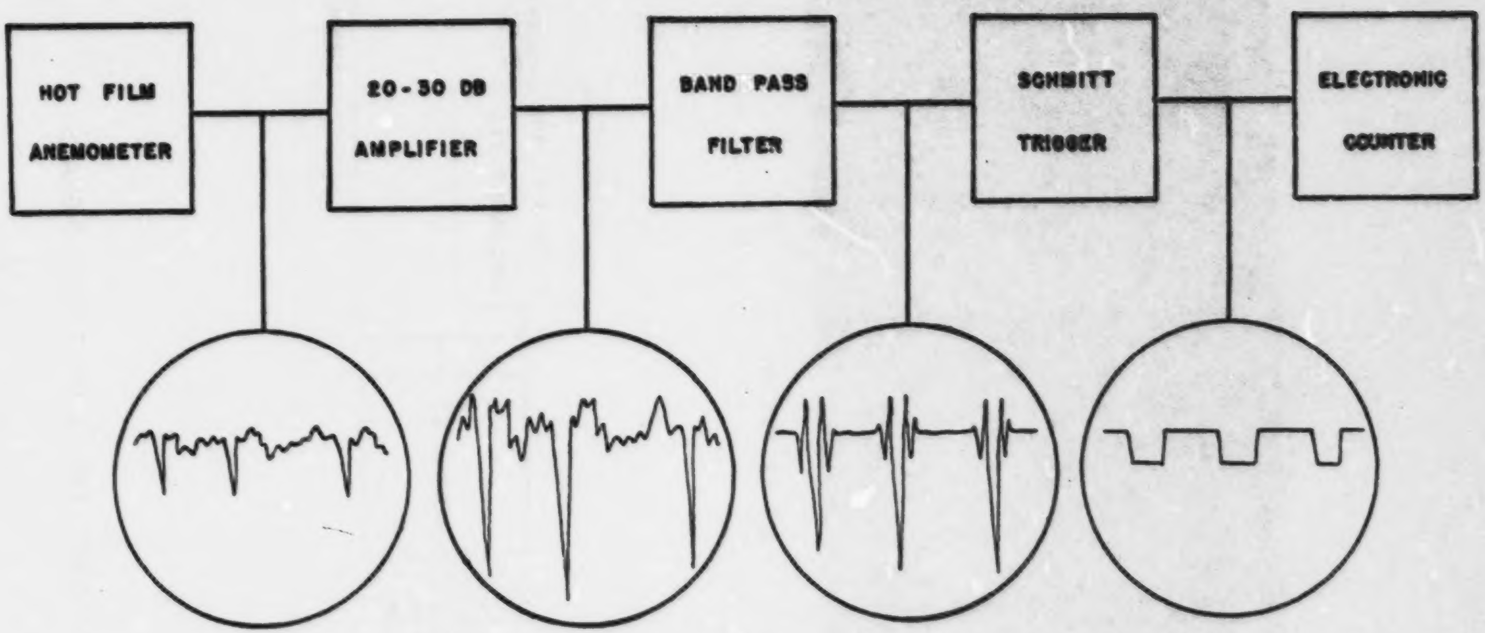
HOT FILM ANEMOMETER
20-30 DB AMPLIFIER
BAND PASS FILTER
SCHMITT TRIGGER
ELECTRONIC COUNTER

FIG. 7 BLOCK DIAGRAM OF ELECTRONIC INSTUMENTATION

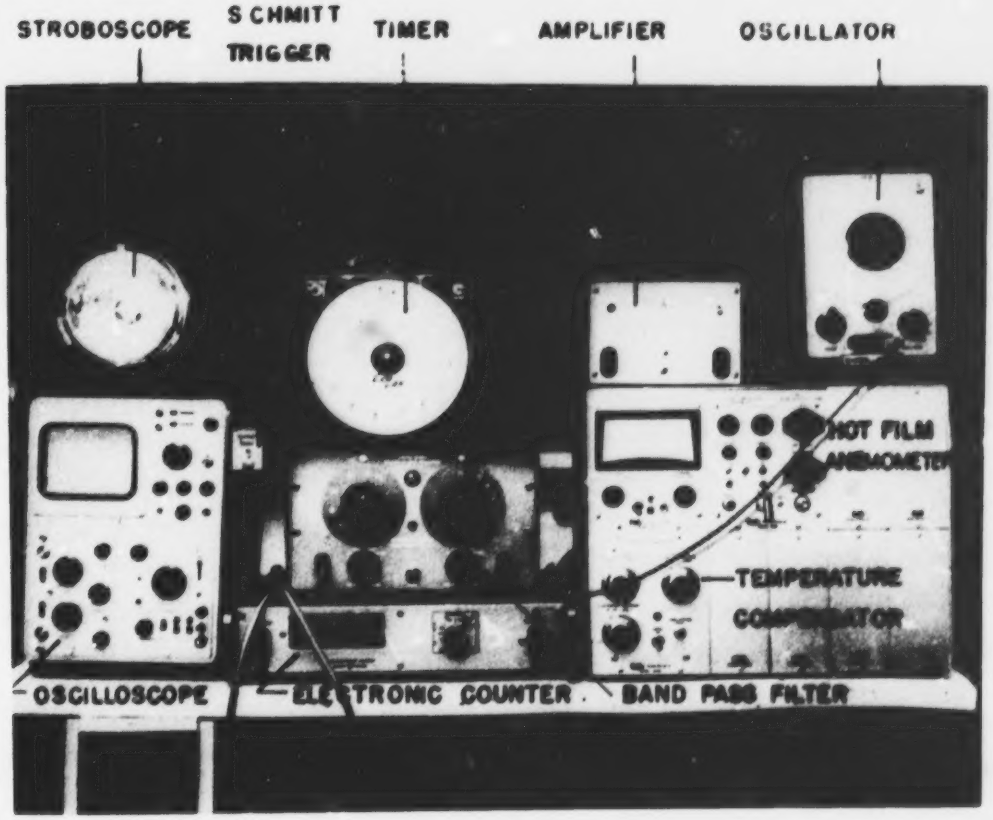
STROBOSCOPE
SCHMITT TRIGGER
TIMER
AMPLIFIER
OSCILLATOR
HOT FILM ANEMOMETER
TEMPERATURE COMPENSATOR
OSCILLOSCOPE
ELECTRONIC COUNTER
BAND PASS FILTER

FIG. 8 ELECTRONIC INSRUMENTATION

Hewlett Packard Electronic Counter, Model H22-5211B
    Maximum counting rate: 300 KHz
    Number of digits: 4
    Time base accuracy: ± 0.1%

Other Instrumentation

Other supplementary instruments were used while measuring the fluctuation components of the velocity field, the energy spectrum, and the frequency of bubble generation. They are itemized in the following:

Bruel & Kjaer Frequency Analyzer, Type 2107
Dana DC Amplifier Model 2000
Hewlett Packard 200 CD Wide Range Oscillator
Hewlett Packard Vacumm Tube Voltmeter, Type 400 AB
Honeywell Accudata 105 Gage Control Unit
Honeywell Accudata 120 DC Amplifier
Honeywell Visicorder Oscillograph Model 2106
TSI Model 1025 Temperature Compensator
TSI Model 1125 Calibrator
General Radio Electronic Stroboscope, Type 1531-A
General Radio Strobolume, Type 1532-B
Dimco-Gray Model 172 Timer
American Optic Model 371734 Long Focusing Distance Microscope
Nikorex 35 mm Camera.

SECTION VIII

EXPERIMENTAL RESULTS

Mean velocity profiles in subsonic axi-symmetric jets have been widely investigated, for instance Kuethe (1935), Corrsin (1943), Squire and Trouncer (1944), Hinze and Van Der Hegge Zijnen (1948), Albertson et al (1948), Keagy and Weller (1949), Corrsin and Uberoi (1949), Trentacoste and Sforza (1967) in air jets and Binnie (1942), Forstall and Gaylord (1955), and Liu (1967) in water jets. In general, there is a satisfactory agreement among the experimental results obtained by the various investigators. For axial coordinate x greater than the length of the potential core x_c (as defined in Appendix II), the following are observed: (1) radial distributions showing good similarity in consecutive sections, (2) a linear spread of the jet, and (3) a hyperbolic decrease of the jet center-line velocity with distance from some apparent source. These three characteristics have been already noted in Section VI.

The jet flow field used in this experiment is somewhat different from the ordinary jet in that there is a bubble generating capillary tube in the center of the jet nozzle. Hence the well known characteristic of the jet mean flow field obtained by the previous workers probably is not applicable to this specific jet flow. An actual flow field measurement becomes a necessity.

MEAN VELOCITY PROFILE MEASUREMENT AND ITS CHARACTERISTICS

Measured Results

The axial velocity profiles were measured with a pitot static tube and checked with a hot film anemometer. The efflux velocity of the jet was 10.83 feet per second. The corresponding Reynolds number was 45,000, based on orifice diameter. The velocity profiles were measured at $x/D = 10, 15, 20, 25$ and 30. Figure 9 shows a plot of U/U_m versus η, where η is the dimensionless variable defined in Appendix II as $r/(x+a)$. The assumed similarity is confirmed. The predicted curves shown in Figure 9 will be further discussed in a later part of this section.

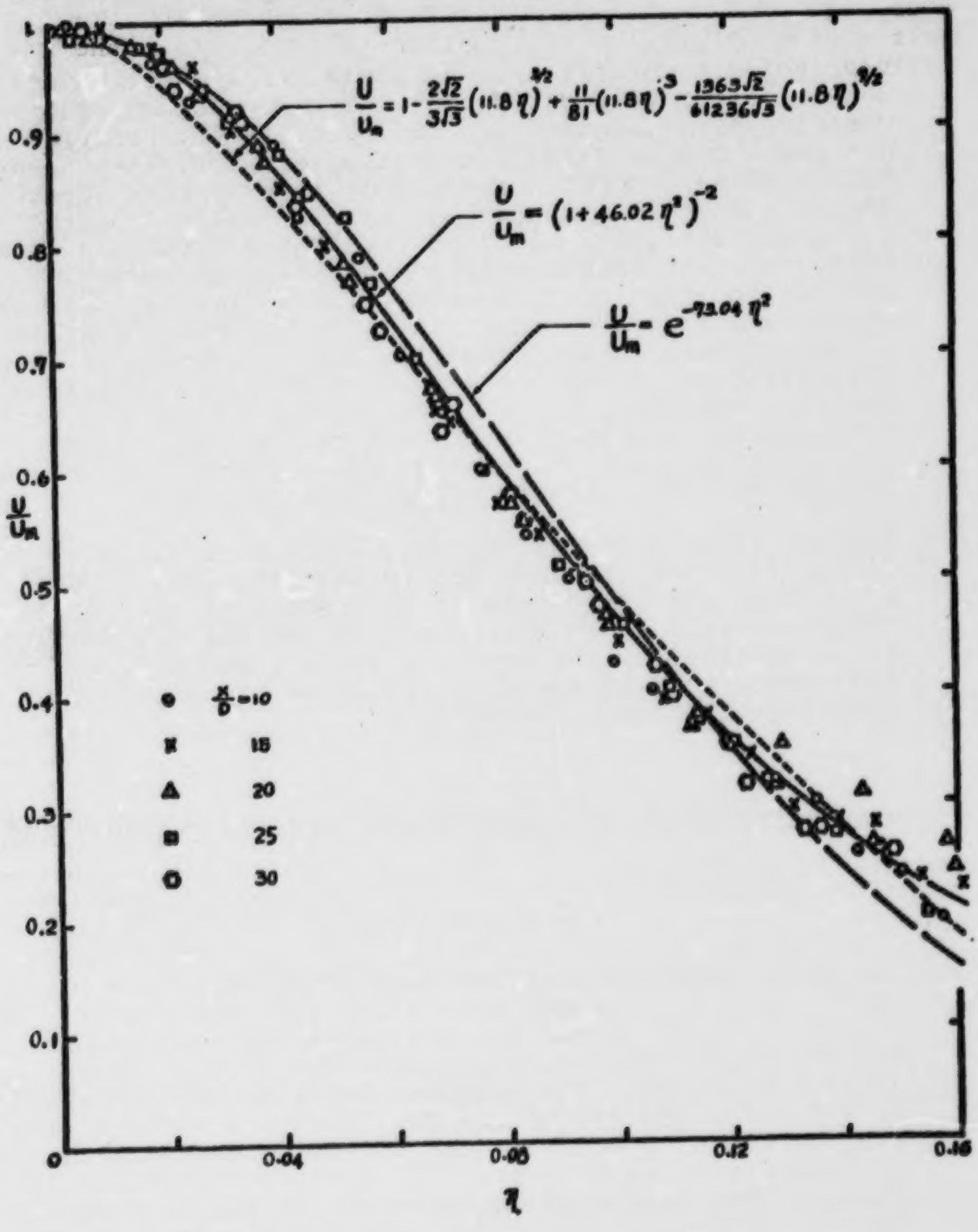

FIG. 9 NORMALIZED VELOCITY PROFILE (WITH SYRINGE TUBE)

The corresponding half width, b_u, and center line velocity decay, $(U_m/U_o)-1$, are shown in Figures 10 and 11. The half width, as defined in Equation (VI-4) follows the relationship

$$\frac{b_u}{D} = 0.0952\ \left(\frac{x}{D} + 0.8\right) \qquad \text{(VIII-1)}$$

for the pitot tube measurement and

$$\frac{b_u}{D} = 0.0978\ \left(\frac{x}{D} + 0.5\right) \qquad \text{(VIII-2)}$$

for the hot film measurement.

The possible error due to the pitot tube as a mean velocity measuring device is found to be negligible. The detailed analysis of the error due to the hot film anemometer as a mean velocity measuring device has not been investigated here. Intuitively, a hot film sensor will sense the total velocity component, $\sqrt{U^2 + V^2}$, instead of only the axial velocity component. At the half width location the ratio of the radial to the axial mean velocity component reaches its maximum of about 3 percent and this will cause a positive error in the axial mean velocity reading. Furthermore, the radial and the tangential fluctuation components will also give a positive error in the axial mean velocity reading (Heskestad (1965)). For these reasons the coefficient of the jet widening rate given in Equation (VIII-2) appears to be larger than the coefficient given in Equation VIII-1). It is felt that Equation (VIII-1) should be the more accurate of the two.

From the principle of momentum conservation, the axial velocity component along the jet axis should decrease hyperbolically. This was noted in Equation (VI-5). Figure 11 shows the linear relationship of $(U_m/U_o)-1$ versus x/D. The best fit linear relationship reads:

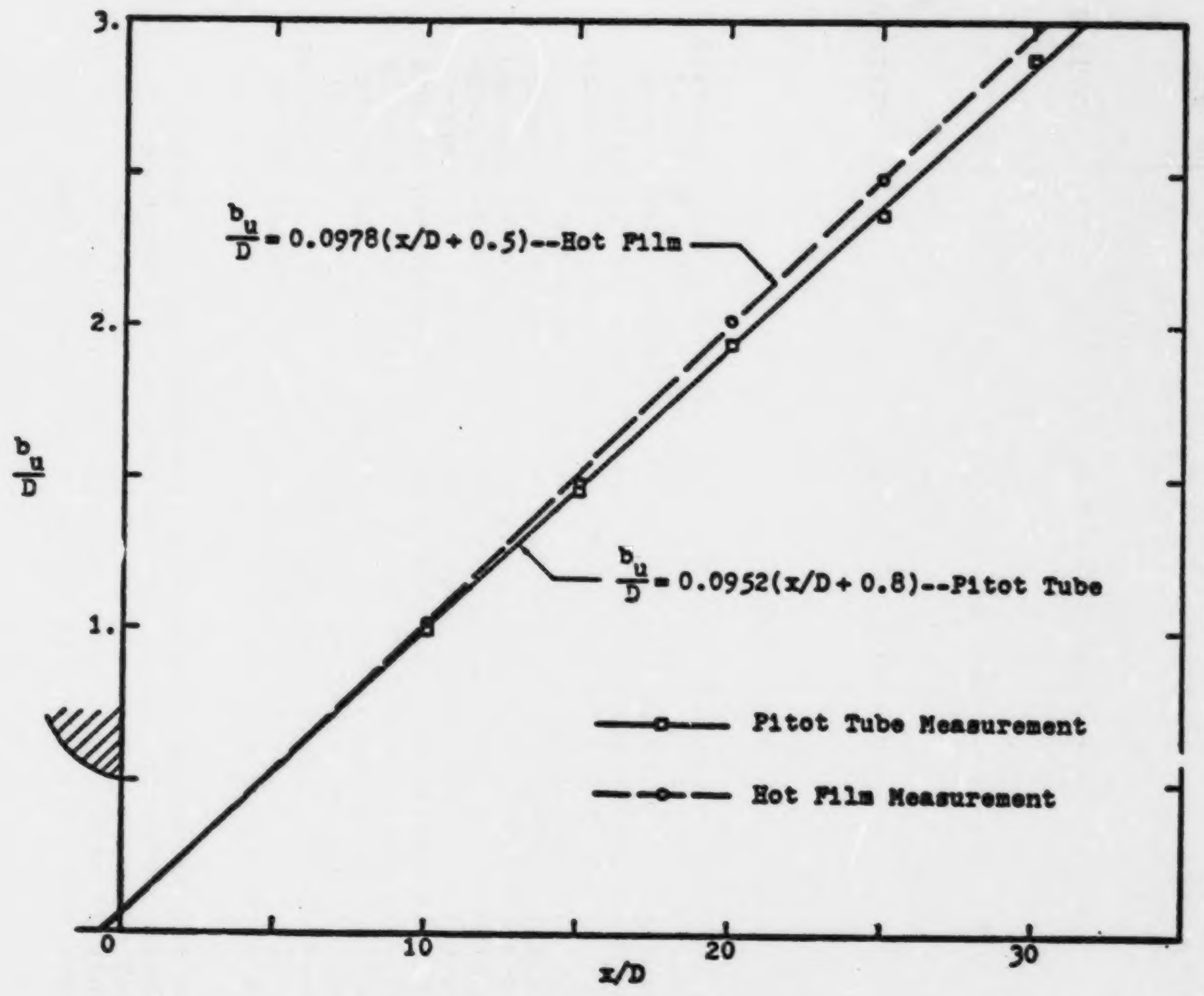

FIG. 10 VELOCITY HALF WIDTH (WITH SYRINGE TUBE)

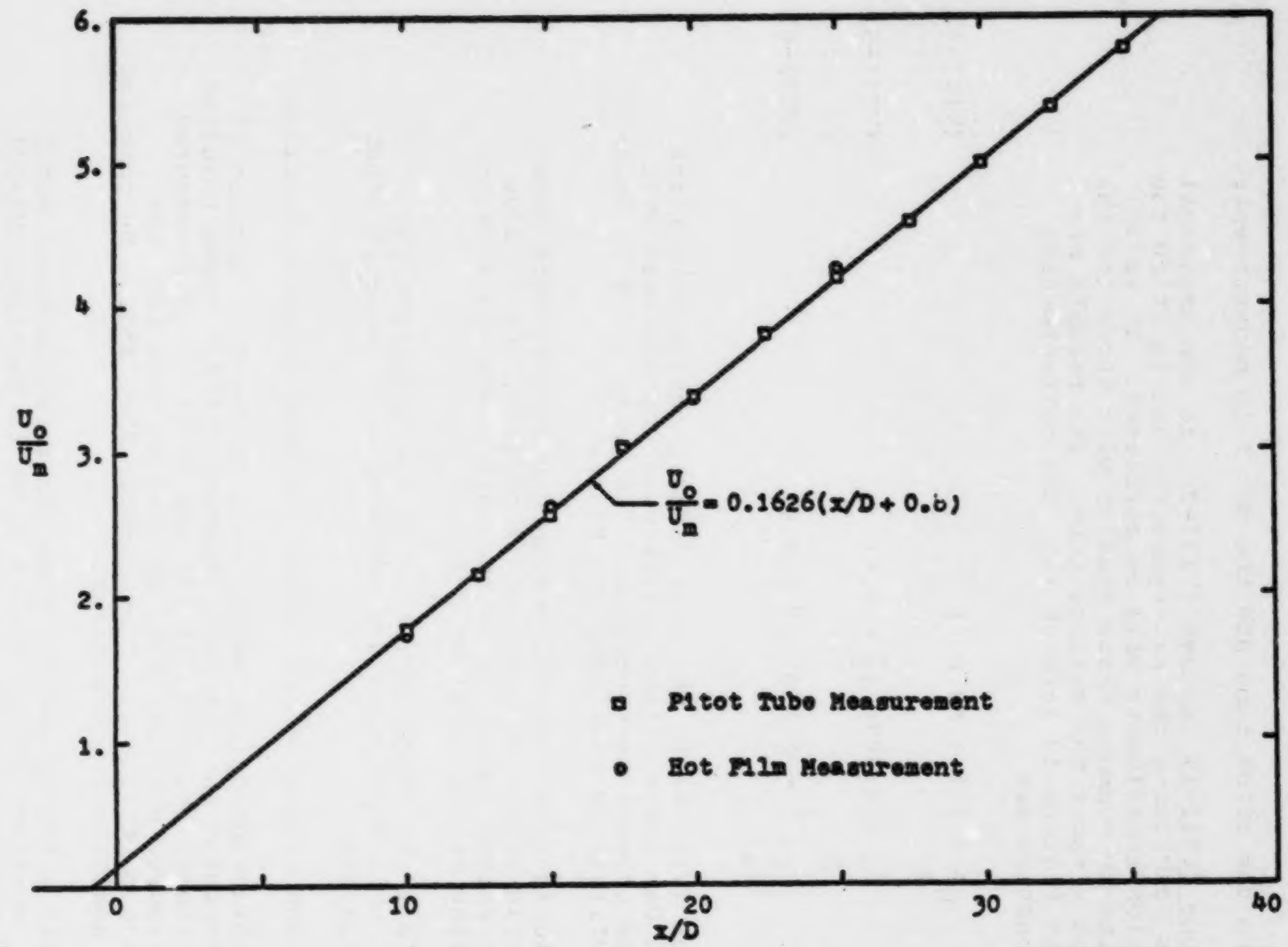

FIG. 11 VELOCITY DISTRIBUTION ALONG JET AXIS (WITH SYRINGE TUBE)

$$\left(\frac{U_m}{U_o}\right)^{-1} = 0.1626\ (\frac{x}{D} + 0.8) \qquad \text{(VIII-3)}$$

for both the pitot tube and the hot film measurements.

Equations (VIII-1) through (VIII-3) are the empirical results describing the axi-symmetric jet in which the dispersion experiments will be performed. It is interesting to compare these results with those for the jet flow without the syringe tube. The results are shown in Figures 12 through 14. The corresponding relationships are

$$\frac{U}{U_m} = [\ 1 + 63.8\eta^2]^{-2} \qquad \text{(VIII-4)}$$

$$\frac{b_u}{D} = 0.0806\ (\frac{x}{D} + 0.6) \qquad \text{(VIII-5)}$$

$$\left(\frac{U_m}{U_o}\right)^{-1} = 0.1562\ (\frac{x}{D} + 0.6) \qquad \text{(VIII-6)}$$

Equation (VIII-4) is the relationship obtained by Hinze and Van Der Hegge Zijnen (1949) which agrees very well with the present measurements. The curve given by Equation (VIII-4) is also shown in Figure 12.

The results show that the presence of the syringe tube has little effect on the virtual origins, but it does cause a faster spreading of the half width and a faster decreasing of the axial velocity in the jet.

In table 1 the characteristics of the submerged jet used in this experiment are compared with those of other investigators.

Comparison with proposed Models for Mean Velocity Profiles:

Three phenomenological models were proposed in Section VI for describing the jet mean velocity field. These resulted in Equations, (VI-11), (VI-14) and (VI-17). The measured mean velocity profiles will be used to calculate the diffusion coefficient. Consequently they should be compared to the analytical predictions.

The axial velocity profile from the first proposed model with ε_m constant everywhere is given in Equation (VI-11). The constant coefficient $U_m\ (x+a)/8\varepsilon_m$, obtained by minimizing the mean square error of the measured data fitted to this model is found to be 46.02. The corresponding

Table 1 Comparison of Various Axi-symmetric Turbulent Jet Measurements

Author		Half Width Spreading Coefficient k_b (see Eq.III-4)	Virtual Origin Based on the Half Width Spreading	Center Line Vel. Decaying Rate k_u (See Eq. III-5)	Virtual Origin Based on the Center Line Vel. Decaying	Potential Core Length	Reynolds Number	Remark
Keuthe (1935)		0.068	4.4D	-	-	-	-	Air Jet
Squire & Trouncer (1944)		0.0906	3.6	0.1506	3.4	6.19D	-	Air Jet
Hinze & Van Der Hegge Zijnen (1948)		0.0826	0.6D	0.1563	0.6D	-	$6.7(10^4)$	Air Jet
Albertson et al (1948)		0.0956	-	0.1612	-	6.2D	$2\text{-}10(10^4)$	Air Jet
Keagy & Weller (1949)		0.0888	0	0.1722	0	-	-	Air Jet
Corrsin & Uberoi (1950)		0.085	0	0.148	0	6.0D	$5.5(10^4)$	Air Jet
Forstall & Gaylord (1955)		0.0920	0	0.161	0	-	$4(10^4)$	Water Jet
Trentacoste & Sforza (1966)		0.093	-1.2D	0.143	-1.2D	7.0D	-	Air Jet
Present Study	With Syringe Tube	0.0952	0.8D	0.1626	0.8D	-	$4.5(10^4)$	Water Jet (Pitot Tube)
		0.0978	0.5D	0.1626	0.8D	-	$4.5(10^4)$	(Hot Film)
	Without Syringe Tube	0.0806	0.6D	0.1562	0.6D	-	$4.5(10^4)$	(Pitot Tube)

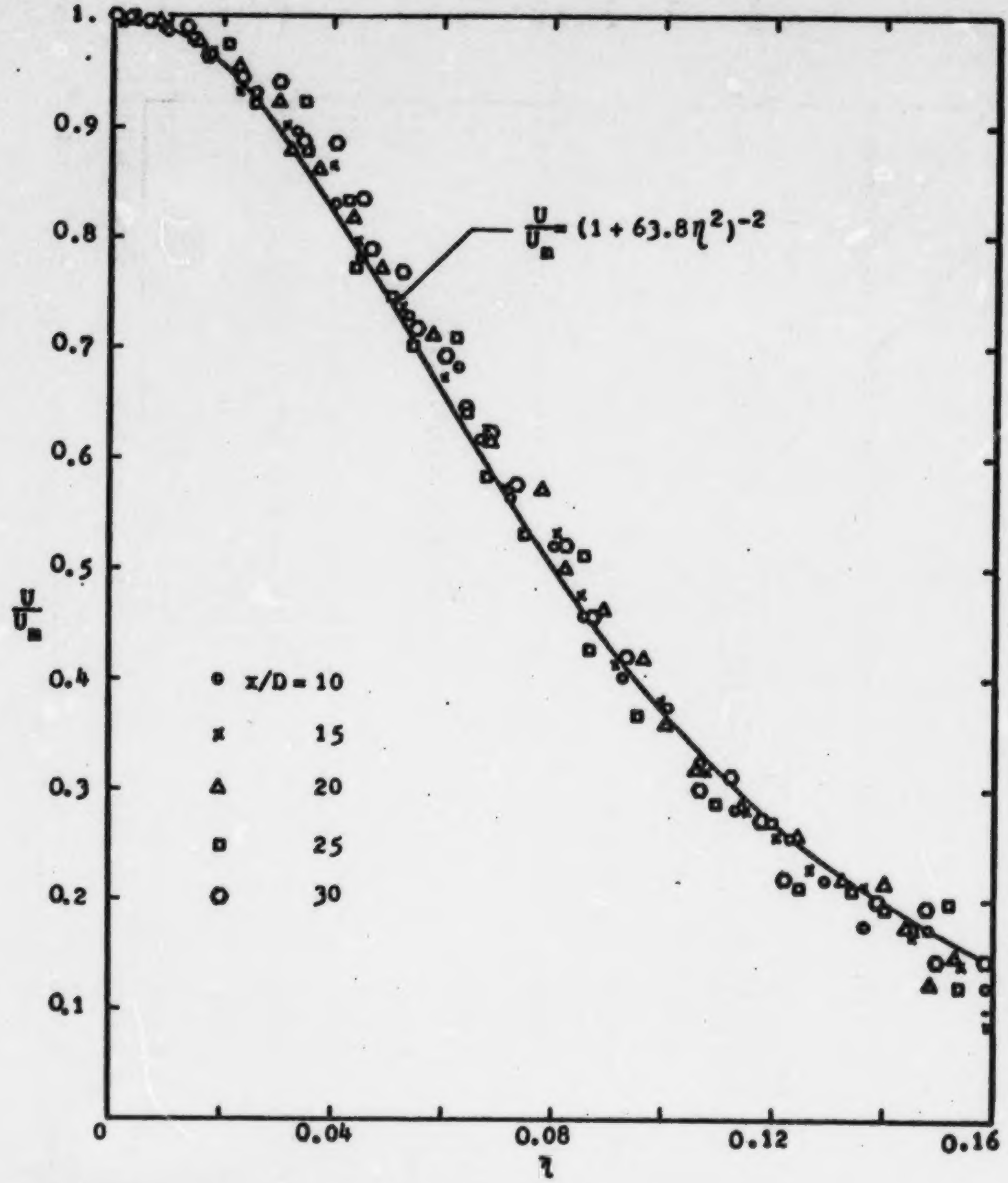

FIG. 12 NORMALIZED VELOCITY PROFILE (WITHOUT SYRINGE TUBE)

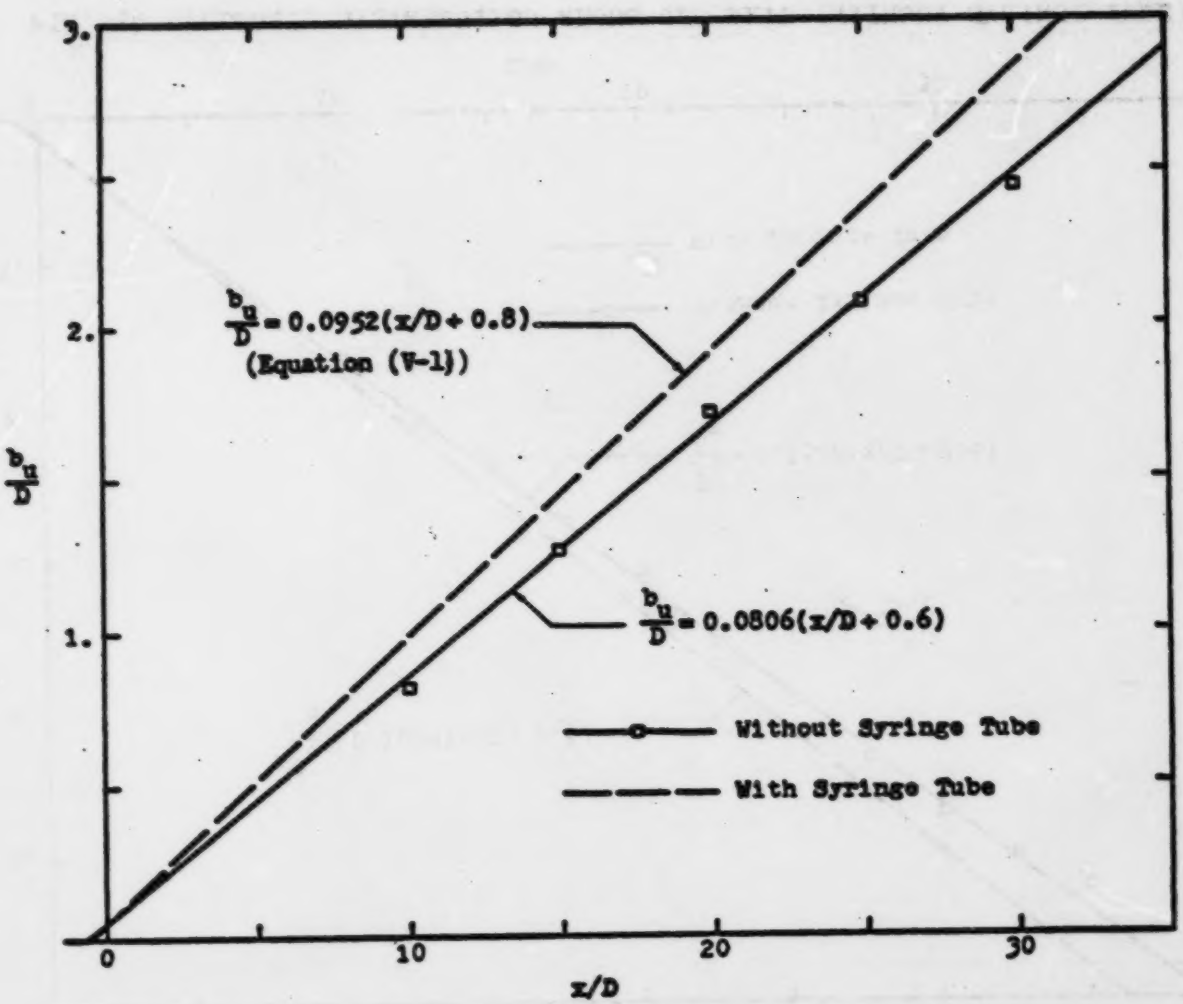

FIG. 13 VELOCITY HALF WIDTH (WITHOUT SYRINGE TUBE)

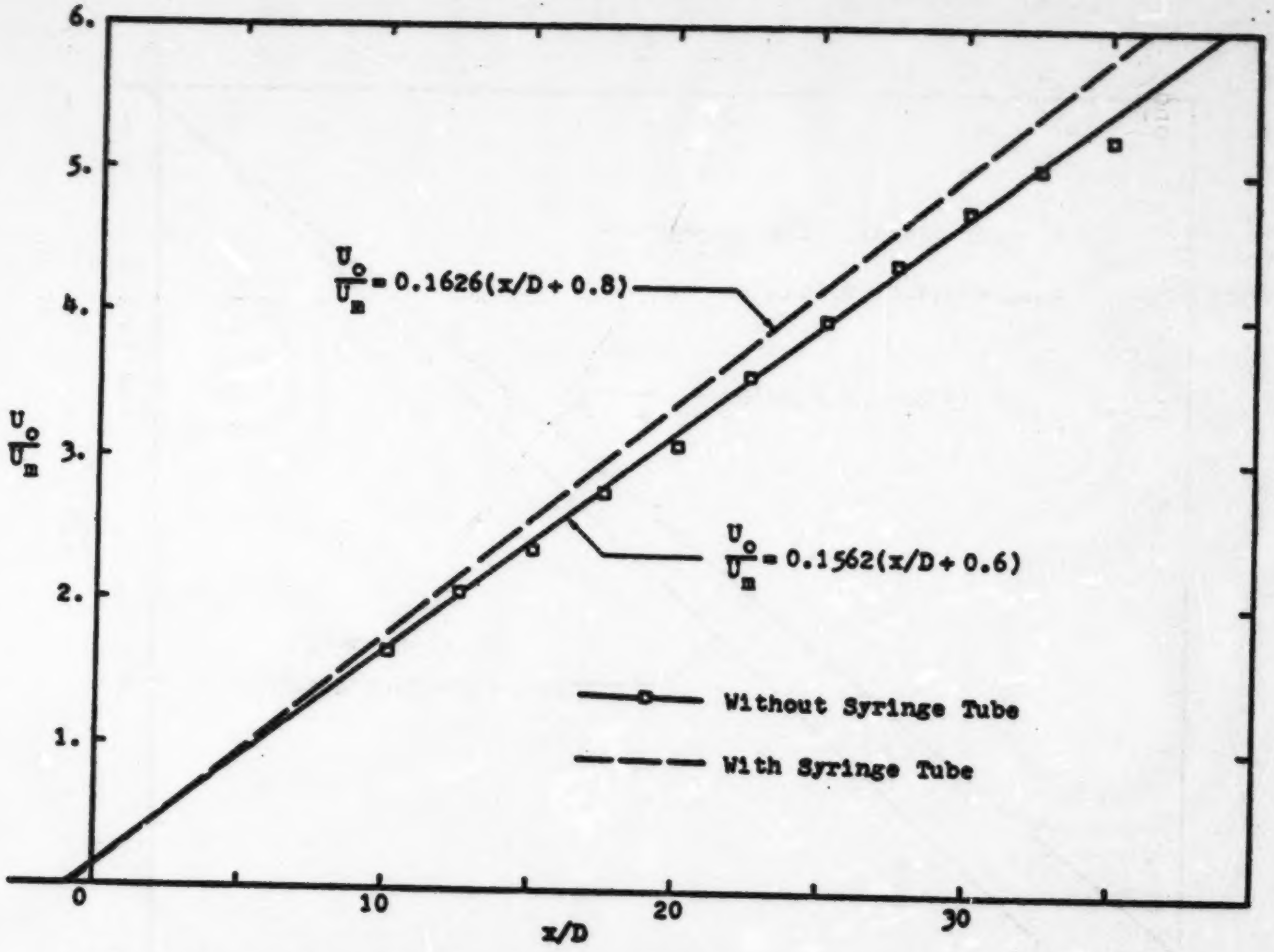

FIG. 14 VELOCITY DISTRIBUTION ALONG JET AXIS (WITHOUT SYRINGE TUBE)

constant eddy viscosity, ε_m, is then equal to $0.0027U_m (x+a)$ and the resulting velocity profile reads:

$$\frac{U}{U_m} = (1 + 46.02\eta^2)^{-2} \qquad \text{(VIII-7)}$$

The similar regression procedure applied to the second proposed model yields a numerical coefficient $(C_\omega^2/2)^{-1/3}$ equal to 11.8 and a velocity profile given by

$$\frac{U}{U_m} = \frac{1-2\sqrt{2}}{3\sqrt{3}} (11.8\eta)^{3/2} + \frac{11}{81} (11.8\eta)^3 - \frac{1363\sqrt{2}}{61236\sqrt{3}} (11.8\eta)^{9/2} \qquad \text{(VIII-8)}$$

Similarily, the third proposed model gives:

$$\frac{U}{U_m} = e^{-73.04\eta^2} \qquad \text{(VIII-9)}$$

The analytical curves given in Equations (VIII-7) through (VIII-9) are plotted together with the measured data in Figure 9. It is seen that the velocity profile given by Equation (VIII-7) fits the experiment data best of all.

As discussed in Chapter VI, the corresponding eddy viscosities ε_m for the second and third models are not constant in the flow field. They depend on η as described in Equation (VI-16) and (VI-18), respectively. Figure 15 depicts the dependence of ε_m on η in this particular jet flow measurement as inferred for the three different models.

FLUCTUATION VELOCITY MEASUREMENT

Since the velocity components in a turbulent jet flow field are random functions of space and time, it would be necessary to measure moments and cross moments of all orders to understand the whole statistics of the flow field. In this study only the rms value of the axial fluctuation component was measured.

The sensor was calibrated in the potential core of the water jet. The calibration curve is shown in Figure 16. From Figure 16 the corresponding sensitivity S_u, the slope of the calibration curve which is directly measured from the calibration curve, can be obtained. It is shown in Figure 17.

The fluctuation level is then defined as $\sqrt{\overline{e^2}}/S_u$ where $\sqrt{\overline{e^2}}$ is the rms value of the fluctuation voltage output. The axial turbulent levels were measured at x/D = 10, 15, 20, and 25. The data are shown in Figure 18. It is seen that the turbulent levels at each section are approximately similar

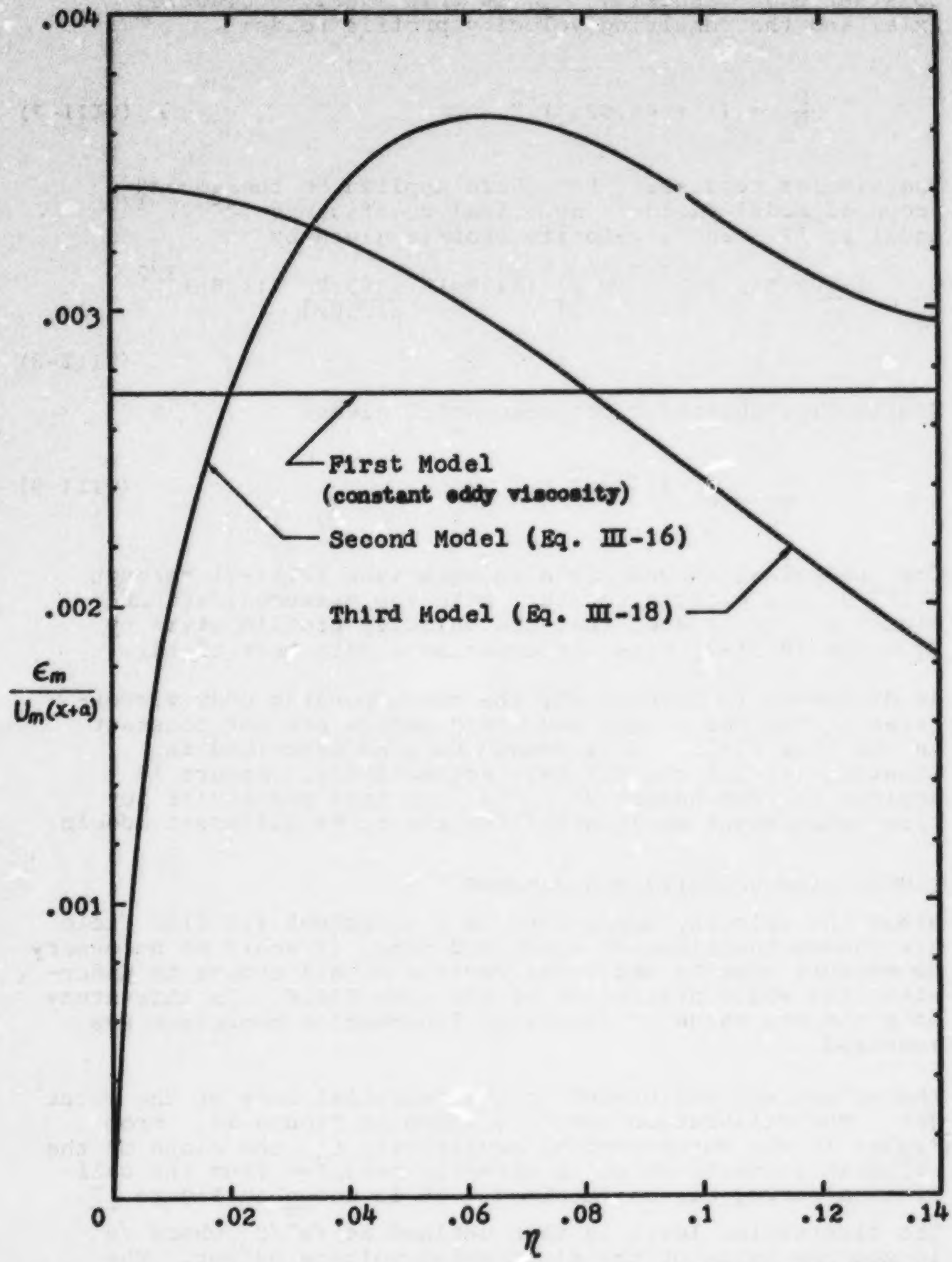

FIG. 15 DISTRIBUTION OF EDDY VISCOSITY BASED ON DIFFERENT MODELS

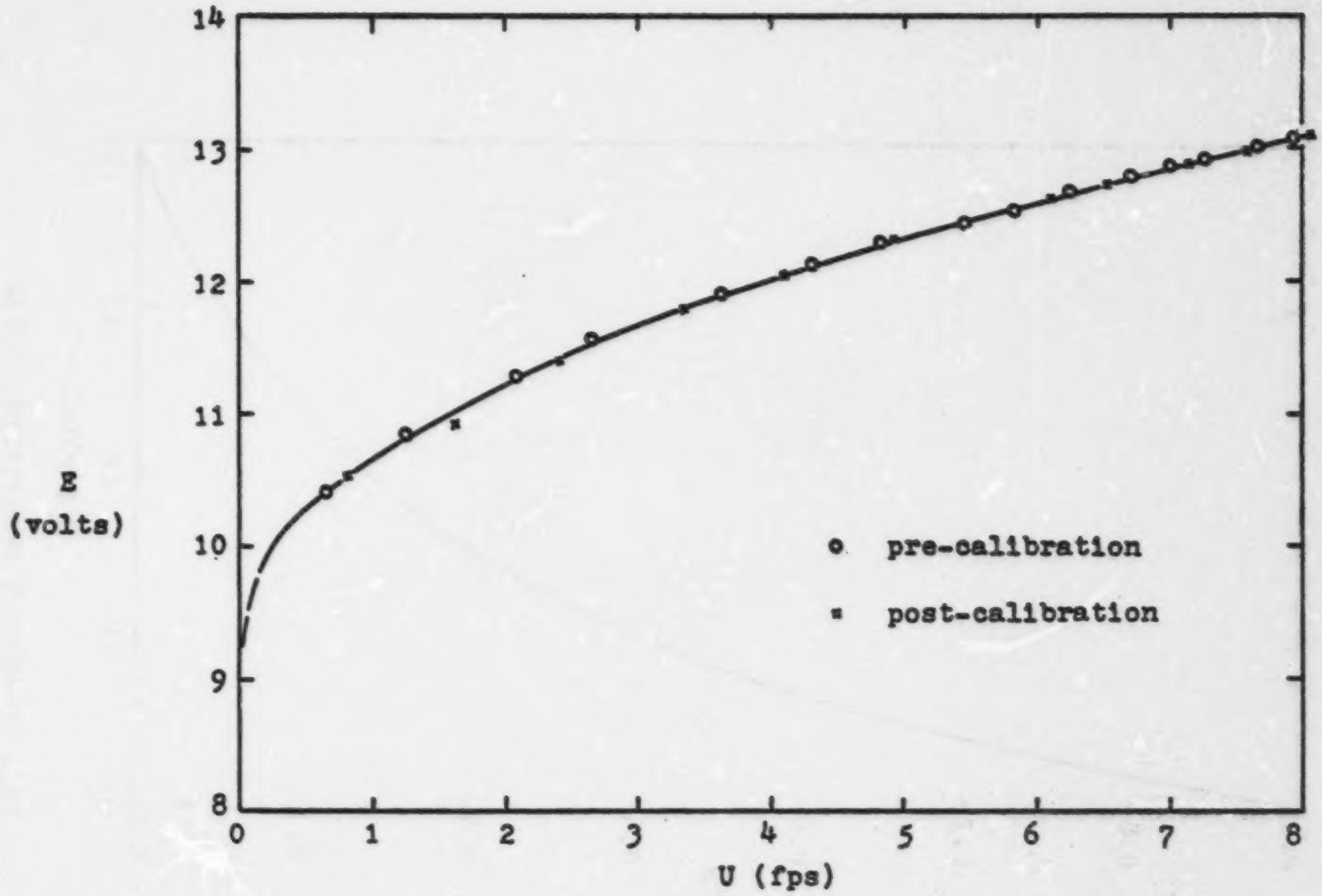

FIG. 16 SENSOR CALIBRATION CURVE

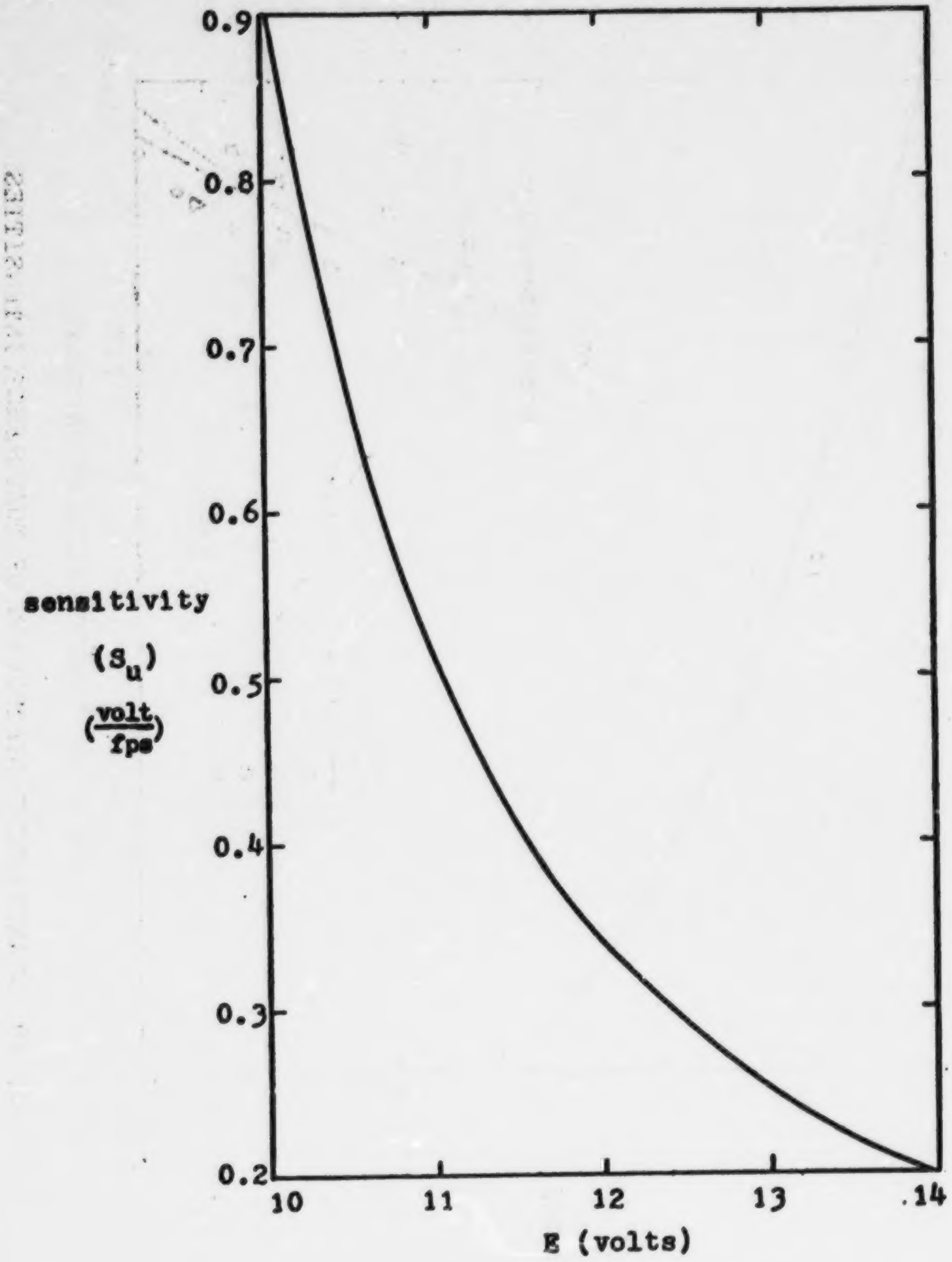

FIG. 17 SENSOR SENSITIVITY CURVE

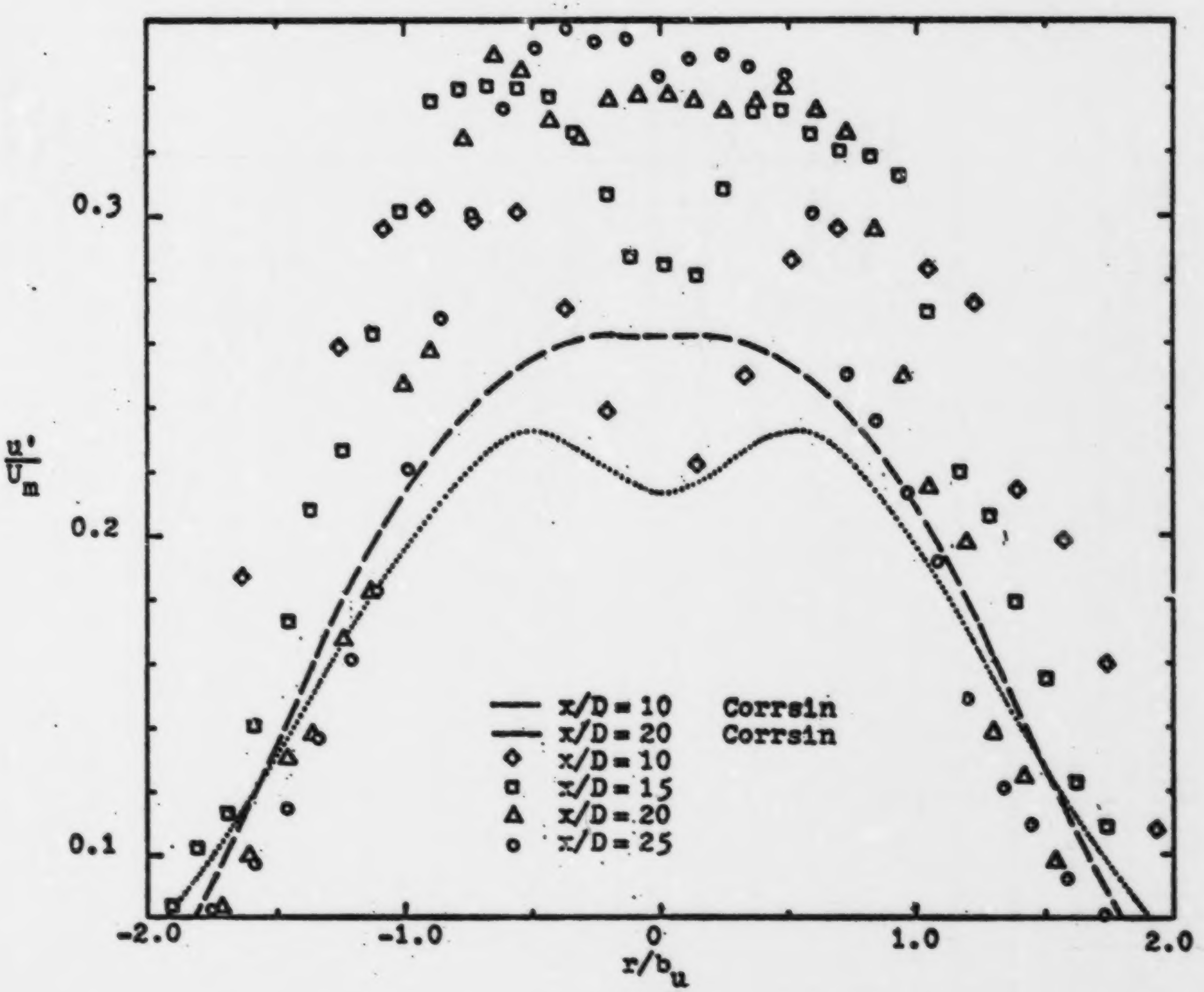

FIG. 18 TRANSVERSE DISTRIBUTION OF TURBULENCE INTENSITIES

in shape and have the maxima at r/b_u about equal to ± 0.5 to ± 0.8. The measured turbulent levels reveal that there is a trend of increasing turbulence level along the axial direction.

The results of air jet turbulence level distribution measured by Corrsin (1943) for x/D = 10 and 20 are also shown in Figure 18. It is seen that the turbulence level obtained from the present measurement is higher than Corrsin's results.

ENERGY SPECTRUM AND TURBULENT SCALES

Experimentally the energy spectrum is obtained by taking the ratio of the mean square voltage response $\overline{e_f^2}$ at a particular frequency band centered at a frequency f to the total mean square fluctuation voltage $\overline{e^2}$ of the sensor output divided by the effective band width of the filter (Curtis (1960)). Energy spectra were obtained from measurements performed at stations with x/D=10, 20, and 30 along the jet axis. The resulting curves are plotted in a normalized form as F(K) versus K such that $\int_0^\infty F(K)dK = 1$ where K is the wave number and is defined as $K = 2\pi f/U$, where f is the frequency and U is the mean velocity at the measurement location. Figure 19 shows such plots. The procedure for making energy spectrum measurements was the following:

a. Determined the characteristics of the wave analyzer used (General Radio Type 1900-A Wave Analyzer) by feeding in a known frequency sine wave signal and measuring the output of the wave analyzer at various center frequencies, $\sqrt{\overline{e_f^2}}$. The attenuation factor, which is defined as $\int_0^\infty \overline{e_f^2}df/\overline{e^2}$, was then calculated and found to be equal to 5.17.

b. The turbulent signal was then fed into the wave analyzer and the output at various center frequencies $\overline{e_f^2}$ was measured. With it $\overline{e_f^2}$ was calculated. The normalized energy spectrum F (f) is then defined as $\overline{e_f^2}/(5.17\overline{e^2}$ where $\overline{e^2}$ is the total fluctuation energy and was simultaneously measured through a Brüel and Kjaer Wave Analyzer.

c. The measured data were then plotted as F(f) versus f. The total area under the F(f) curve should be equal to unity. If not, another correction factor is obtained and the values of F(f) corrected through this factor.

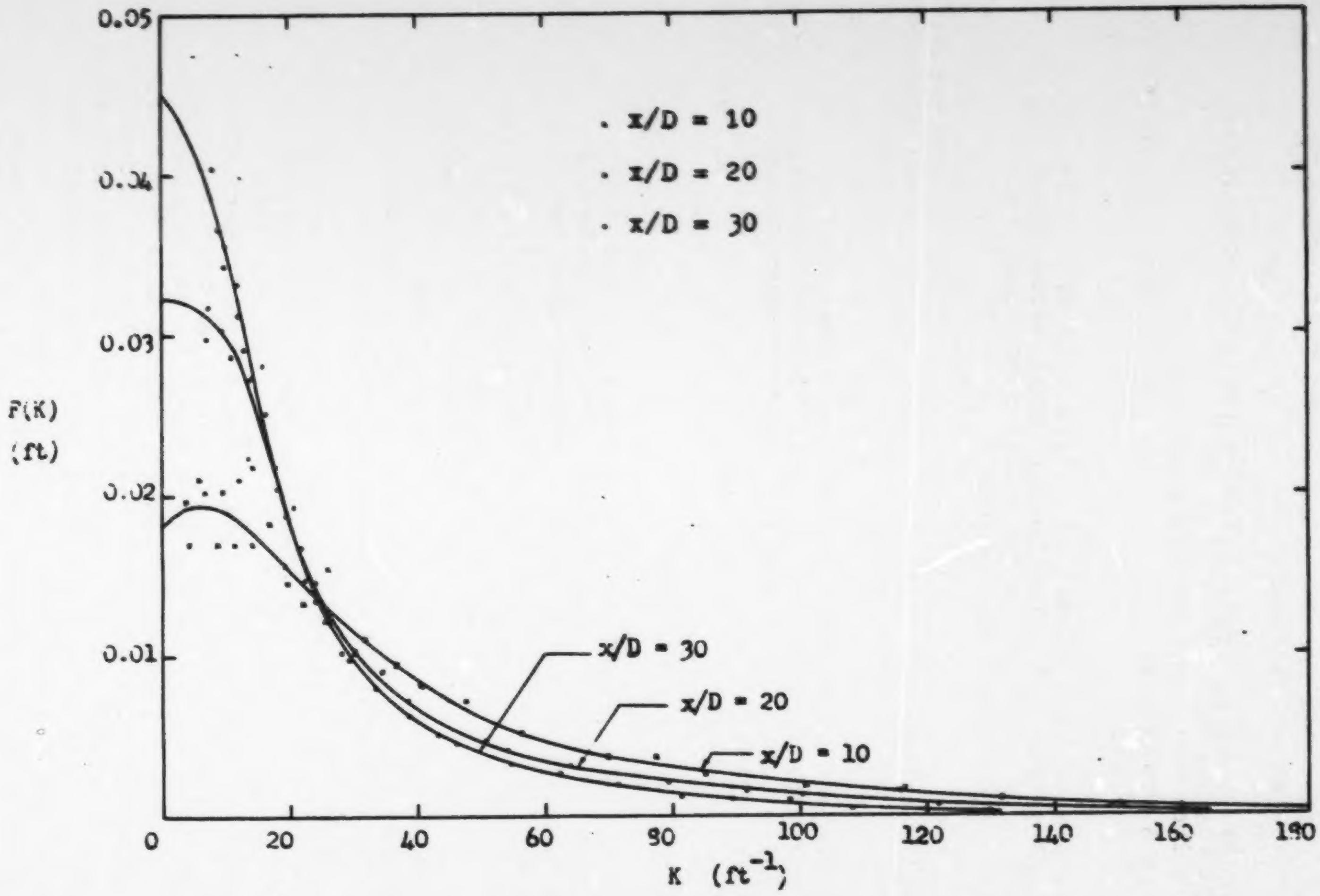

FIG. 19 ENERGY SPECTRUM ALONG CENTER LINE OF THE JET

d. The curves were then changed to F(K) versus K, where K is as previously defined and $F(K) = \frac{U}{2\pi} F(f)$. The resulting curves of F(K) versus K are shown in Figure 19.

The longitudinal macro scale of the turbulence, defined as

$$\Lambda_x = \frac{\pi}{2} \lim_{K \to 0} F(K) \tag{VIII-10}$$

can be calculated from Figure 19. Figure 20 shows the plot of Λ_x/D versus x/D. The longitudinal macro scale increases linearly along the jet axial direction, following the approximate relationship

$$\frac{\Lambda_x}{D} = 0.0492 \left(\frac{x}{D} + 2.5\right) \tag{VIII-11}$$

Comparing Fig. 20 with Fig. 13 shows that the longitudinal macro scale along the jet axis is approximately half the value of the half width b_u, and follows the expected linear growth.

CONCENTRATION FLUX MEASUREMENT

In this experiment the efflux velocity of the turbulent water jet was 10.83 feet per second. The generated bubbles were measured directly through a microscope for four different sets of runs. When the stroboscopic illumination frequency is synchronized with the bubble generation frequency, the generated series of bubbles will appear stationary. Their size can then be measured by a microscope placed outside the jet tank. The corresponding average bubble sizes were 343, 527, 780 and 970 microns with a standard deviation of less than 15 percent.

As described in Section VII the mean concentration flux is obtained by counting the number of bubble impactions on a cylindrical hot film sensor. If A_s is the upstream cross sectional area containing bubbles ultimately touching the cylindrical hot film, Γ the actual number of bubbles per unit volume of the flow field at the measuring location, and V_b the mean bubble velocity at this location, the concentration flux measured will be $N=\Gamma V_b A_s$. Theoretically A_s is related to the impaction coefficient (defined as the ratio of the area containing particles touching the collector to the frontal area of the collector) and is not a constant value with velocity. Householder (1968) made an extensive study of the impaction coefficient by assuming that the particle trajectory in the vicinity of a cylindrical collector is governed by the particle inertial and

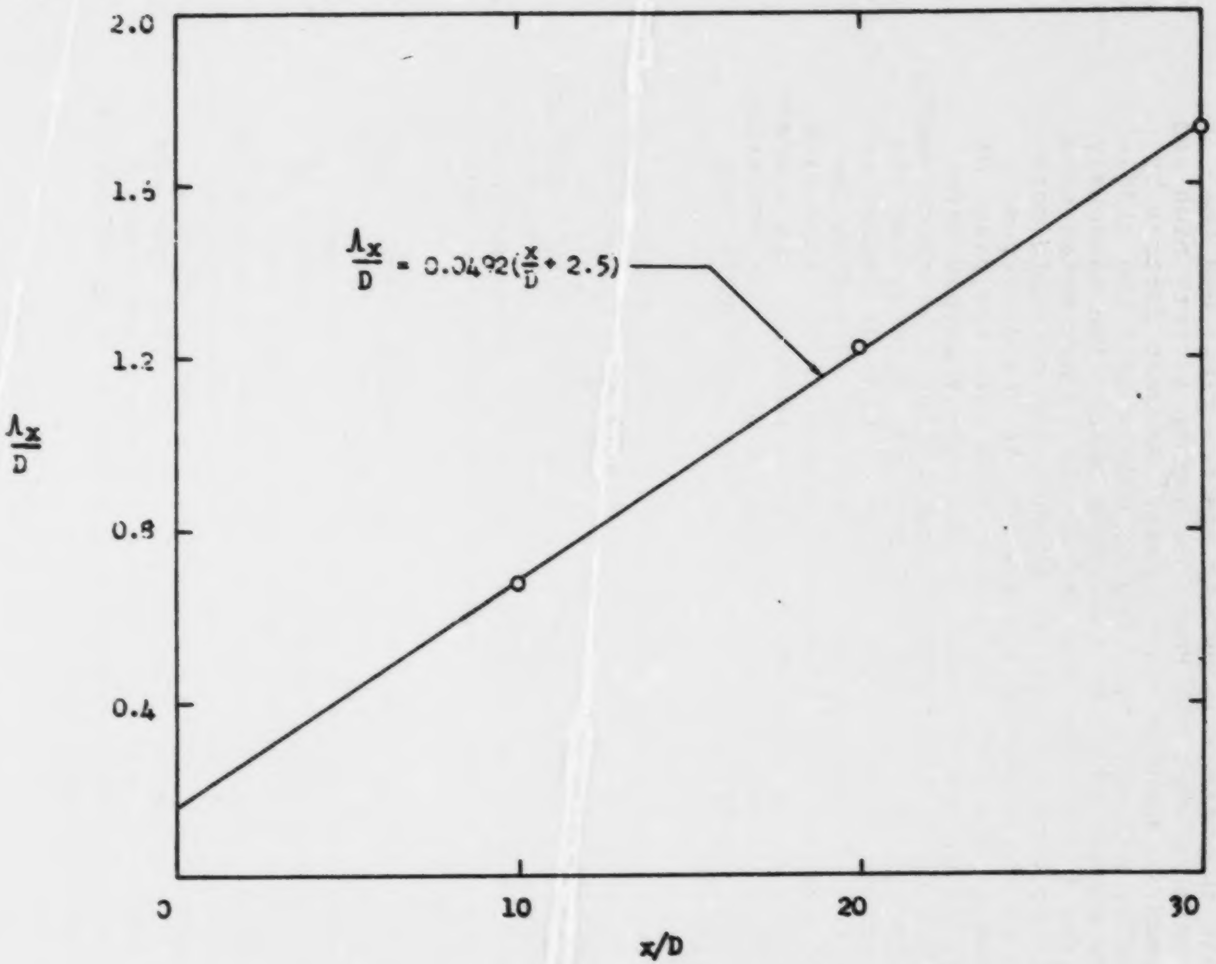

FIG. 20 LONGITUDINAL MACRO SCALE ALONG THE TURBULENT JET AXIS

viscous forces only. He further assumed that the stream flow field is not affected by the presence of the particles. He obtained a solution for two extreme cases. The first case is when the Reynolds number is extremely low such that the stream is solely viscous flow; and the second case is when the Reynolds number is very high and the stream is assumed non-viscous. He went further by empirically extrapolating two solutions into the middle Reynolds number range by fitting a model simultaneously satisfying the two extreme cases. It is attempted here, by applying such results, to predict the possible correction on the intercepting area A_s at the different locations of the flow field. In this work the range of the carrier stream velocity in the axi-symmetric water jet within which the bubble concentration flux measurements are performed is from 1.4 to 7 feet per second, and the corresponding range of the collector Reynolds number is from 24 to 120 based on sensor diameter. Based on the reported results the maximum difference in the impaction coefficient would then be less than 2 percent. This error is within the accuracy of the concentration flux measuring system and any correction in the impaction coefficient was neglected.

If the impaction coefficient is then assumed constant in the whole flow field and if furthermore the partial hit effect is similar throughout, then for e/e_p fixed the intercepting area, A_s, within which every bubble hitting the sensor will give a signal perceptible by the measuring system will be constant. e and e_p are as defined in the Appendix; for all sets of measurements e/e_p was fixed to be 0.15.

The absolute concentration flux was measured by two different means. First the flux over a whole cross section was measured at the jet nozzle by counting the number of bubbles generated per unit time. This was achieved by snychronizing the bubble generation frequency with a stroboscope. Second the actual concentration flux measurements were integrated over a whole cross sectional area assuming an impaction coefficient and neglecting partial hit effects. The actual wire sampling area was $6.5\text{x}10^{-4}\text{cm}^2$. A count of 200/min. on the counter would then correspond to a concentration flux of $4.8\text{x}10^5$ counts per ft^2 per second.

TABLE 2

Total Bubble Concentration of the Experiments

Diffusion Experiments	N_o (Efflux bubble rate, 1/sec.)		Efflux Volume Concentration (percent)
	by Stroboscope Measurement	by Hot Film Measurement	
343μ case	9.64×10^3	11.13×10^3	0.048
527μ case	6.26×10^3	5.93×10^3	0.116
780μ case	4.24×10^3	4.02×10^3	0.252
970μ case	3.41×10^3	2.97×10^3	0.390

The concentration flux was measured at $x/D=10$, 15, 20 and 25. All the data were obtained in a form of N versus r. The data so obtained were normalized in terms of N_m.

Check for Bubble Coalescence and/or Breakage

If there is neither bubble breakage nor bubble coalescence, the conservation of mass requires that at each successive section the following relation must be satisfied:

$$\int_0^\infty N\, r\, dr = \dot{M} \qquad \text{(VIII-12)}$$

Equation (VIII-12) was calculated by graphical integration for four sets of measurements. Figure 21 is the plot of $\dot{M}$ normalized by the mean of the four section measurements. It shows that $\dot{M}$ at four different sections deviated by less than 6 percent from the mean. As a 6 percent deviation is probably due to the inaccuracy of the measurements, $\dot{M}$ can be considered to be essentially constant. This suggests the absence of coalescence and/or breakage of the bubbles.

Transverse Profiles of the Concentration Flux

In order to check the similarity of the concentration flux profiles, the measured data were normalized and plotted as $N/N_m (r/b_n)$, where N_m is the maximum value of the concentration flux profile and b_n is the half width of the concentration flux profile defined as the radial distance from the center line to the point where the concentration flux is one-half the maximum value. The resulting plots for four bubble sizes are shown in Figures 22 through 25. All of these figures indicate that the similarity characteristics of the concentration flux are preserved.

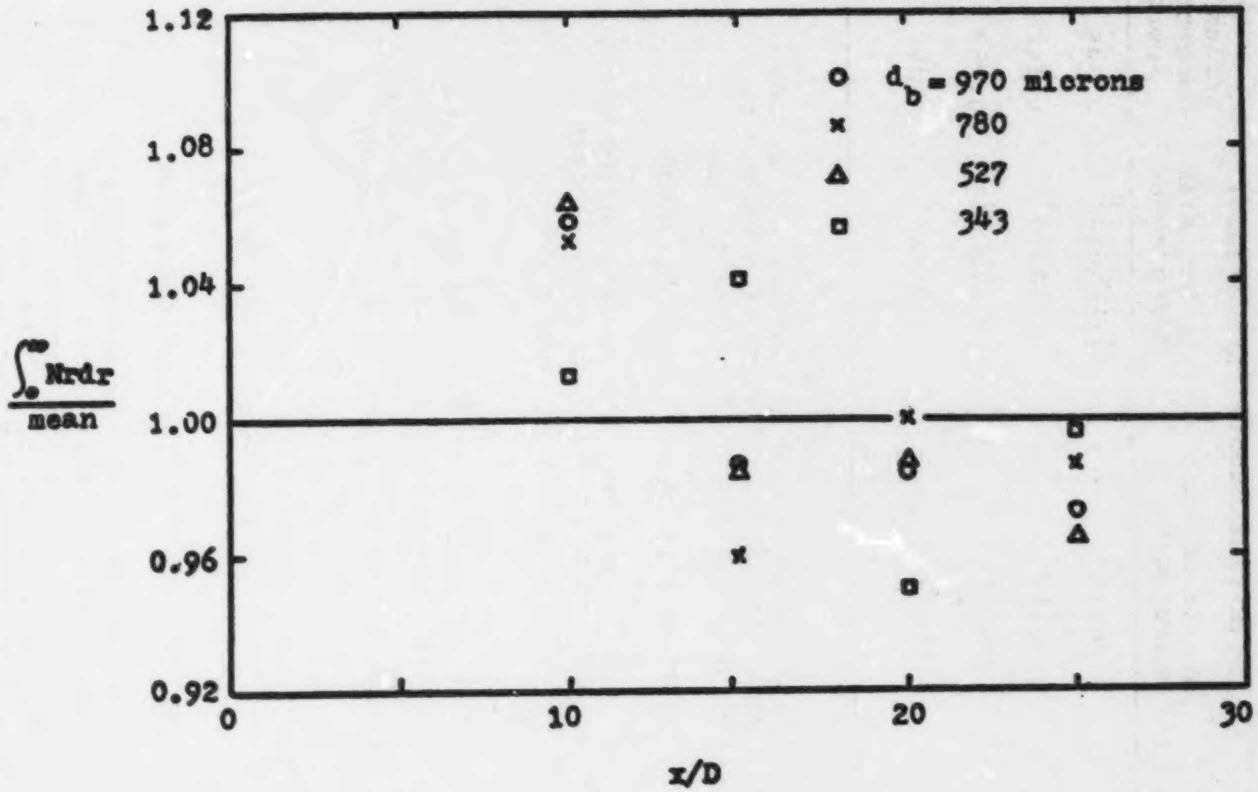

FIG. 21 VARIATION OF THE INTEGRATED CONCENTRATION FLUX ALONG THE AXIAL DIRECTION

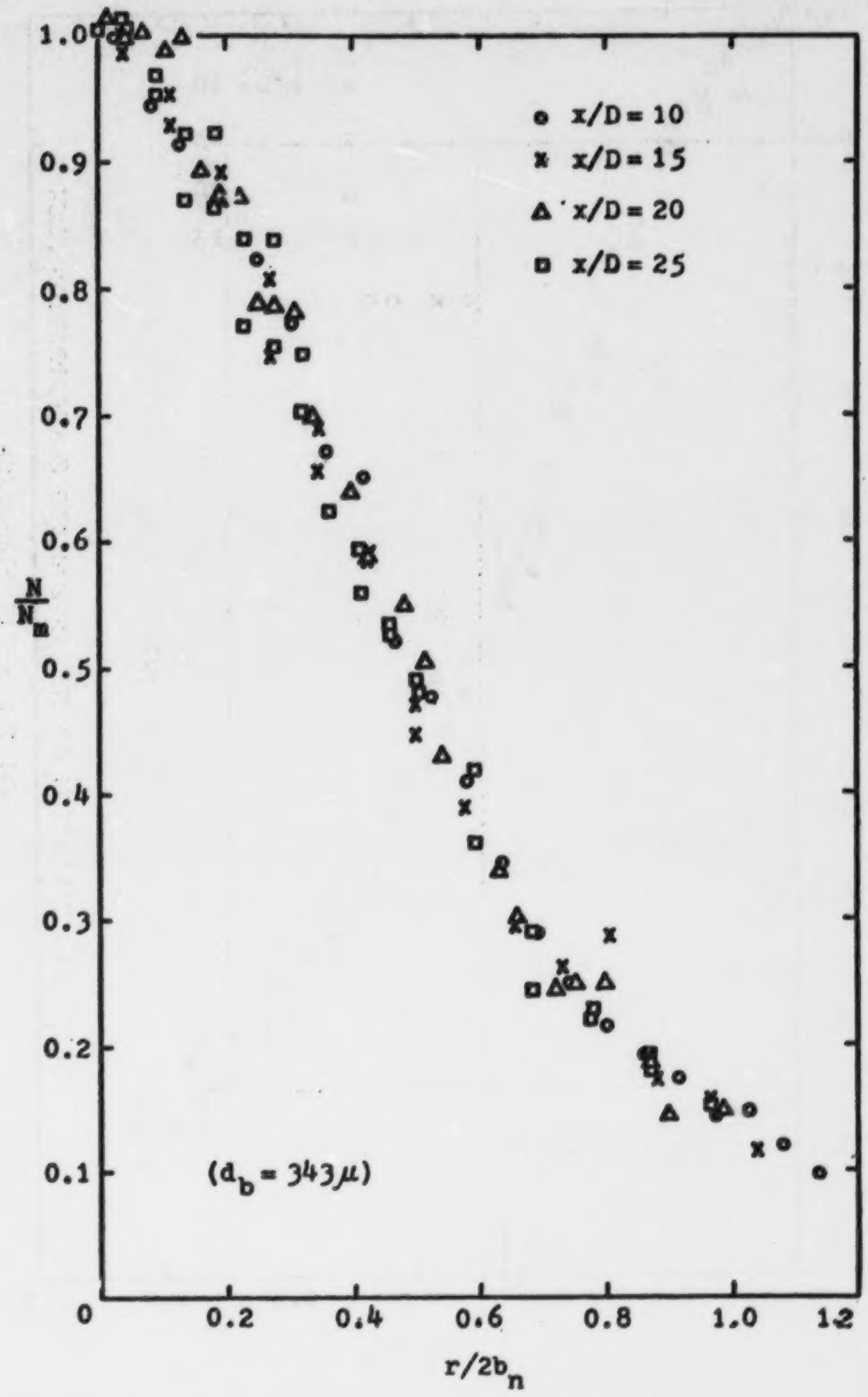

FIG. 22 CONCENTRATION FLUX PROFILE

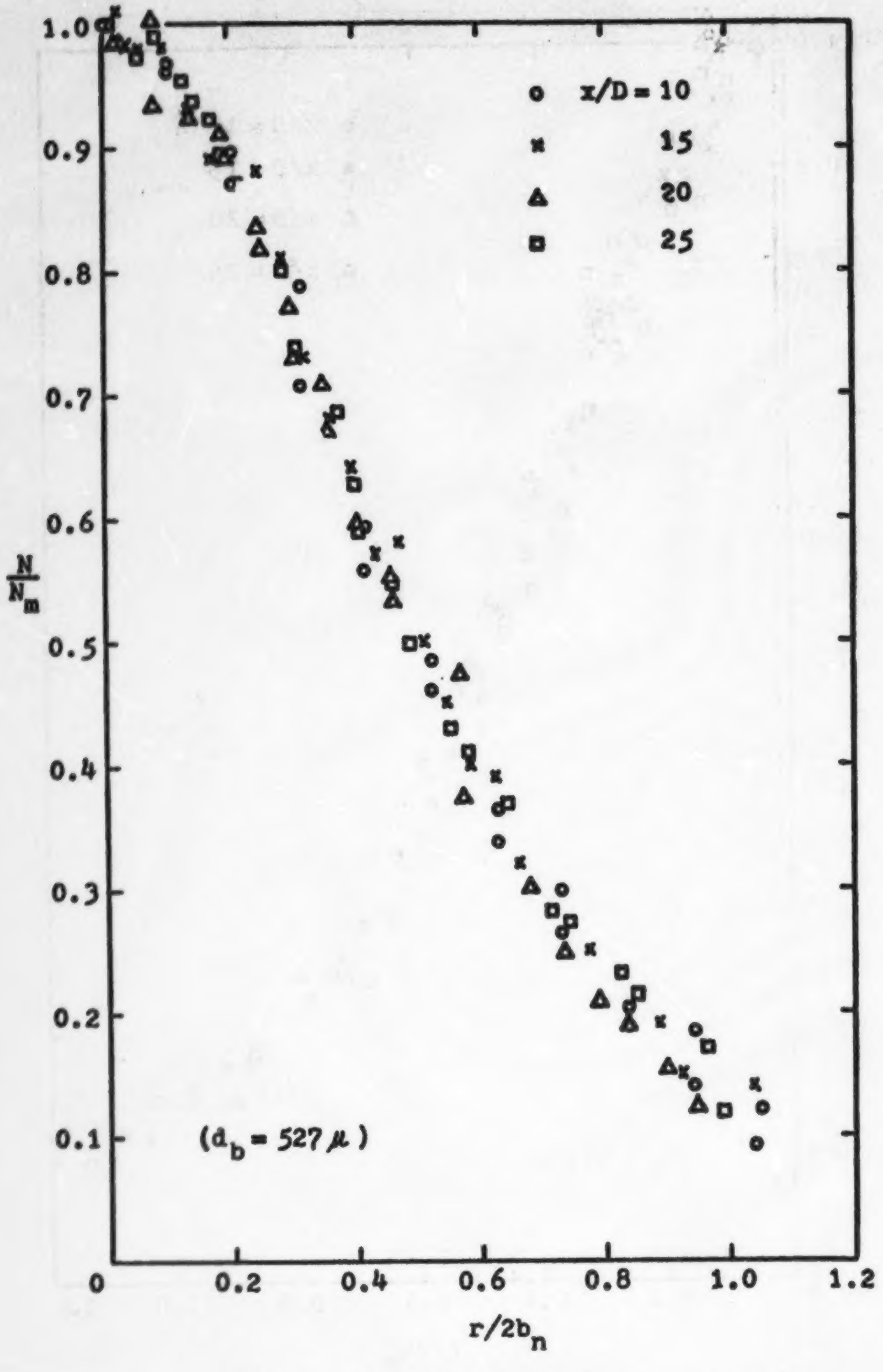

FIG. 23 CONCENTRATION FLUX PROFILE

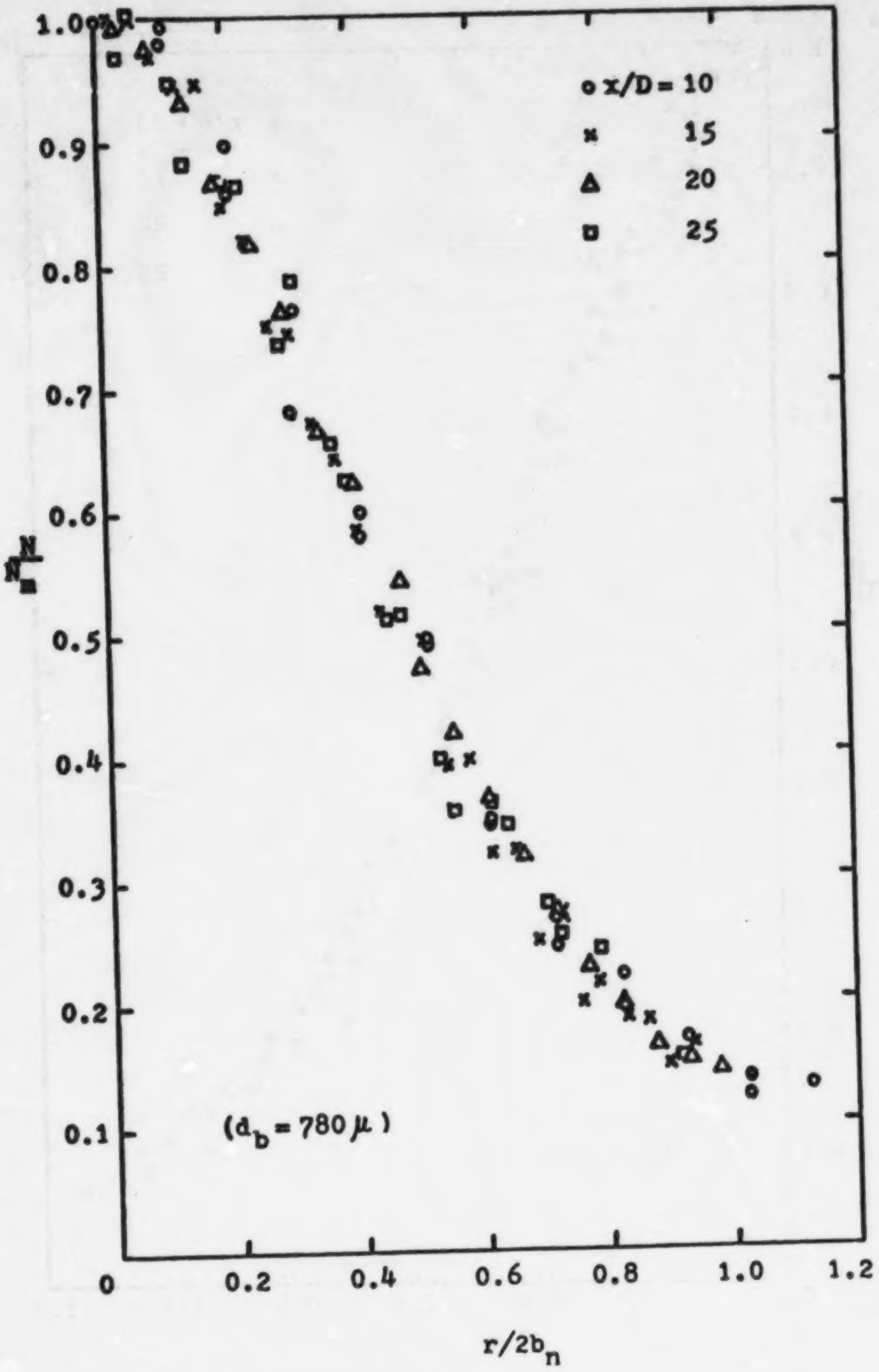

FIG. 24 CONCENTRATION FLUX PROFILE

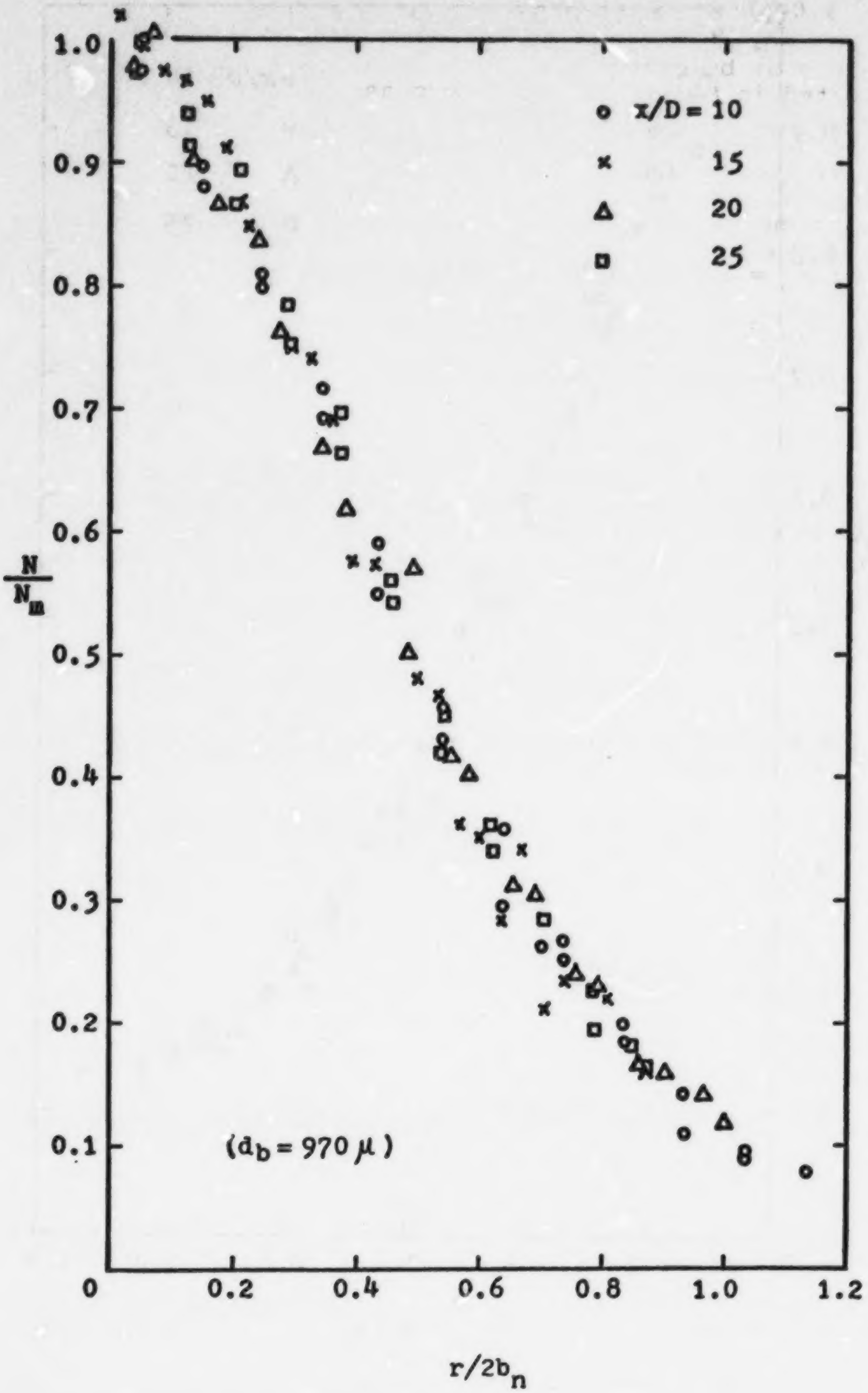

FIG. 25 CONCENTRATION FLUX PROFILE

Half Width Dependence

The values of b_n versus x/D for four different bubble sizes are plotted in a dimensionless form as b_n/D versus x/D in Figure 26. Figure 26 indicates that the concentration flux half width spreads linearly along the axial direction from a virtual origin at 0.8D from the jet nozzle plane. Coincidentally, this coincides with the virtual origin of the momentum flux. The plots of Figure 26 give:

$$\text{for } d_b = 343\mu \quad b_n/D = 0.0650(x/D + 0.8) \tag{VIII-13}$$

$$d_b = 527\mu \quad b_n/D = 0.0683(x/D + 0.8) \tag{VIII-14}$$

$$d_b = 780\mu \quad b_n/D = 0.0708(x/D + 0.8) \tag{VIII-15}$$

$$d_b = 970\mu \quad b_n/D = 0.0735(x/D + 0.8) \tag{VIII-16}$$

From the above four expressions it is seen that the rate of spread of the concentration flux half width consistently increases when the bubble size increases. Qualitatively this implies that larger size bubbles diffuse faster. To evaluate the diffusion coefficients a careful quantitative analysis accounting for all the measured data will be done in the next Section.

Center Line Concentration Flux Decay

From the similarity requirement and the principle of mass conservation, the following relations must be true

$$N_m b_n^2 \sim \int_o^\infty Nrdr = \text{Constant} \tag{VIII-17}$$

Furthermore, from the form of equations (VIII-13) to (VIII-16)

$$N_m\ b_n^2 \sim N_m\ x^2 = \text{Constant} \tag{VIII-18}$$

and hence

$$N_m{}^{-1/2} \sim x \tag{VIII-19}$$

The center line decay of the concentration flux is thus plotted as $(N_o/N_m)^{1/2}$ versus x/D in Figure 27, where N_o is defined as

$$N_o = \frac{2\pi \int_o^\infty \Gamma Urdr}{\frac{\pi D^2}{4}} \qquad A_s = \frac{8}{D^2} \int_o^\infty Nrdr \tag{VIII-20}$$

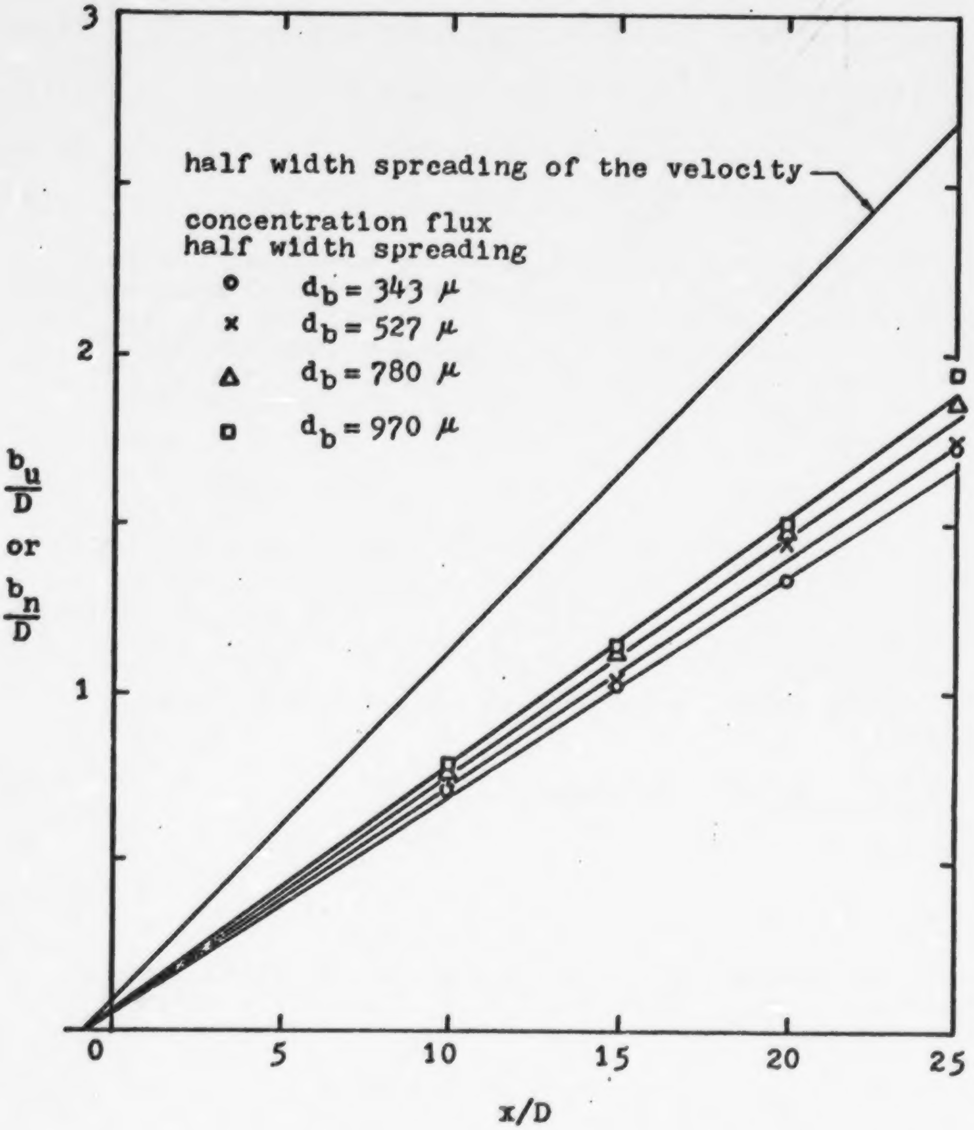

FIG. 26 HALF WIDTH SPREADING OF THE CONCENTRATION FLUX

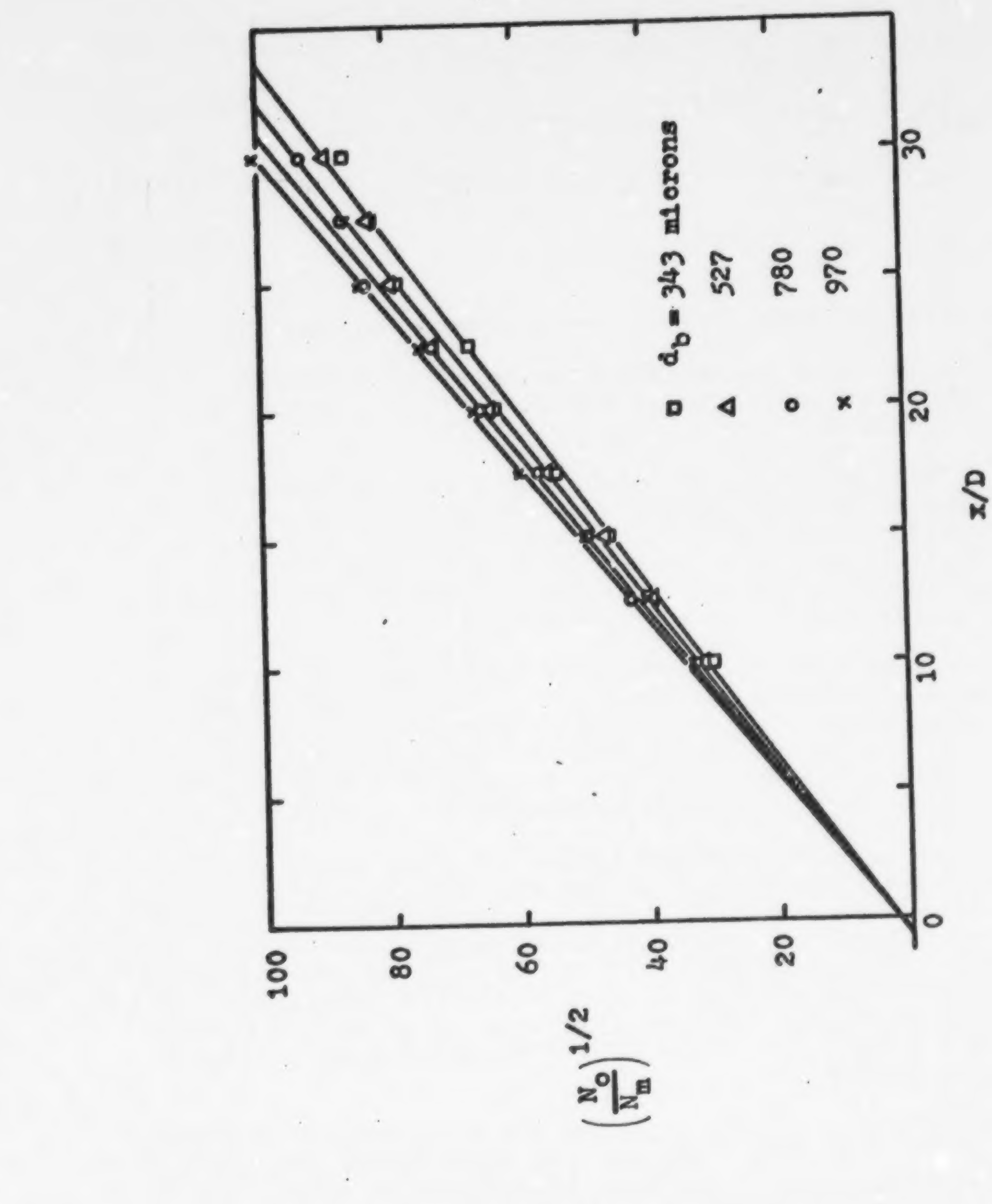

FIG. 27 CENTERLINE CONCENTRATION FLUX DECAY

The slopes of the corresponding plots in Figure 27 depend upon the size of the bubbles. The following results are noted

for $d_b = 343\mu$ $\quad (N_o/N_m)^{1/2} = 29.2(\frac{x}{D} + 0.8)$ (VIII-21)

$d_b = 527\mu$ $\quad (N_o/N_m)^{1/2} = 30.5(\frac{x}{D} + 0.8)$ (VIII-22)

$d_b = 780\mu$ $\quad (N_o/N_m)^{1/2} = 31.5(\frac{x}{D} + 0.8)$ (VIII-23)

$d_b = 970\mu$ $\quad (N_o/N_m)^{1/2} = 32.5(\frac{x}{D} + 0.8)$ (VIII-24)

EFFECT OF BUBBLE CONTAMINATION ON THE CARRIER STREAM

When a turbulent flow field is contaminated with foreign particles the characteristic of the flow field itself will probably be changed.

Soo et al (1960) carried out measurements on the diffusion of helium gas in air and in suspensions which contained 0.0005 to 0.003 volume fraction of glass beads of diameter less than 0.01 inches in a horizontal pipe. They found that the presence of the solid particles did not affect the diffusion in the fluid phase.

Kada and Hanratty (1960) investigated the effect of particles on the diffusion characteristics of turbulence. They concluded that foreign particles with volume concentration less than 2.5 percent do not appear to have a large effect on the diffusion rate unless there is an appreciable average slip velocity between the solid particles and the fluid.

Brandon (1968) investigated the effect of glass beads on the longitudinal turbulent intensity and the friction coefficient of a pipe flow. He concluded that (1) there is no detectable effect of the solids on the longitudinal turbulent intensity for particle sizes ranging from 20 to 60 microns and solid sphere volume fraction of about 0.003, (2) the friction factor increases with particles size from 20 up to 170 microns and remains constant for sizes up to 560 microns for volume fraction less than 0.01.

Hetsroni and Sokolov (1969) measured the longitudinal turbulent intensity in an aerosol contaminated two dimensional jet with aerosol consisting of oil droplets 13 microns in size. They reported that the intensity of turbulence is lowered by the particles and that the suppression of turbulence is proportional to the concentration of the droplets.

In this section the effect of the bubbles on the characteristics of the flow field is considered both in the mean flow property, fluctuation components, momentum flux deviation and the energy spectrum. For the case treated the bubble concentration is about 0.4 percent volume at the nozzle efflux of the jet. It compares to the highest concentration used in the diffusion measurements (see Table 2). The bubble size used in this experiment is about 950 microns which is comparable to the largest bubble size (970 microns) used for the diffusion measurements.

Effect on the Mean Flow Properties

The mean velocity profiles in the now bubble contaminated flow field were re-measured with the hot film anemometer. The bubble when impacting on the sensor will change the cooling of the sensor and hence introduce errors both in the DC and RMS voltages. For the bubble concentrations treated they may be neglected.

The measured velocity profiles are shown in Figure 28. They are noted to preserve the similarity characteristics and to practically coincide with the bubble-free profiles. The half width spreading coefficient k_b in this measurement is of 0.0961. This value is comparable to the k_b of 0.0978 obtained for the single phase jet. The distance from the virtual origin obtained by the intersection of the half width spreading line and the jet axis to the jet nozzle plane, a, is now 0.9D and this value is comparable to the value of 0.5D obtained for the single phase jet (Figure 29). The center line velocity decaying rate, k_u, in this measurement is 0.162 which agrees well with the single phase jet measurement. However, the distance from the virtual origin to the jet nozzle plane obtained by the decay of the center line velocity is now 2.3D. This is bigger than the single phase result of 0.8D (Figure 30). This is probably due to the fact that the presence of the bubbles in the potential core disturbs and shortens the length of the potential core thus shifting the virtual origin toward the upstream end.

Effect on the Turbulence Intensities

When a turbulent flow field is contaminated with foreign particles distinguishable in their size and density from the carrier stream, the relative motion of the particles with respect to the fluid (slip velocity) may cause extra dissipation of the turbulent kinetic energy of the turbulent fluid and hence a decrease in the turbulent intensity (Hetsroni and Sokolov (1969)). Plots of the measured turbulence levels at x/D=10, 15, 20 and 25 for the bubble contaminated flow field are shown in Figure 31. For comparison, the fluctuation levels for the single phase jet measurement (as per Figure 18) are re-plotted in Figure 31. The following intensities are noted at the axis of the jet.

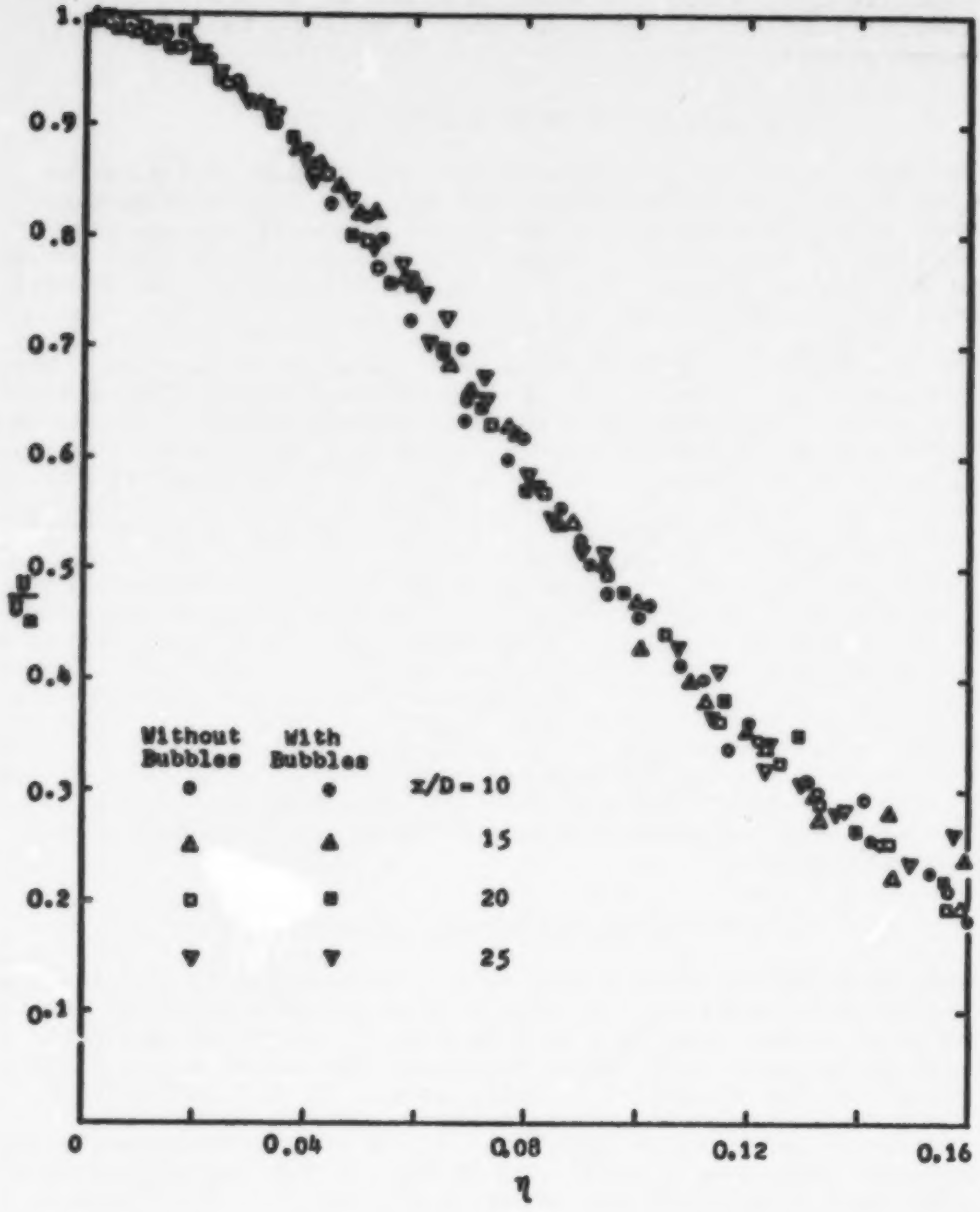

FIG. 28 NORMALIZED VELOCITY PROGILE (WITH & WITHOUT CONTAMINATION)

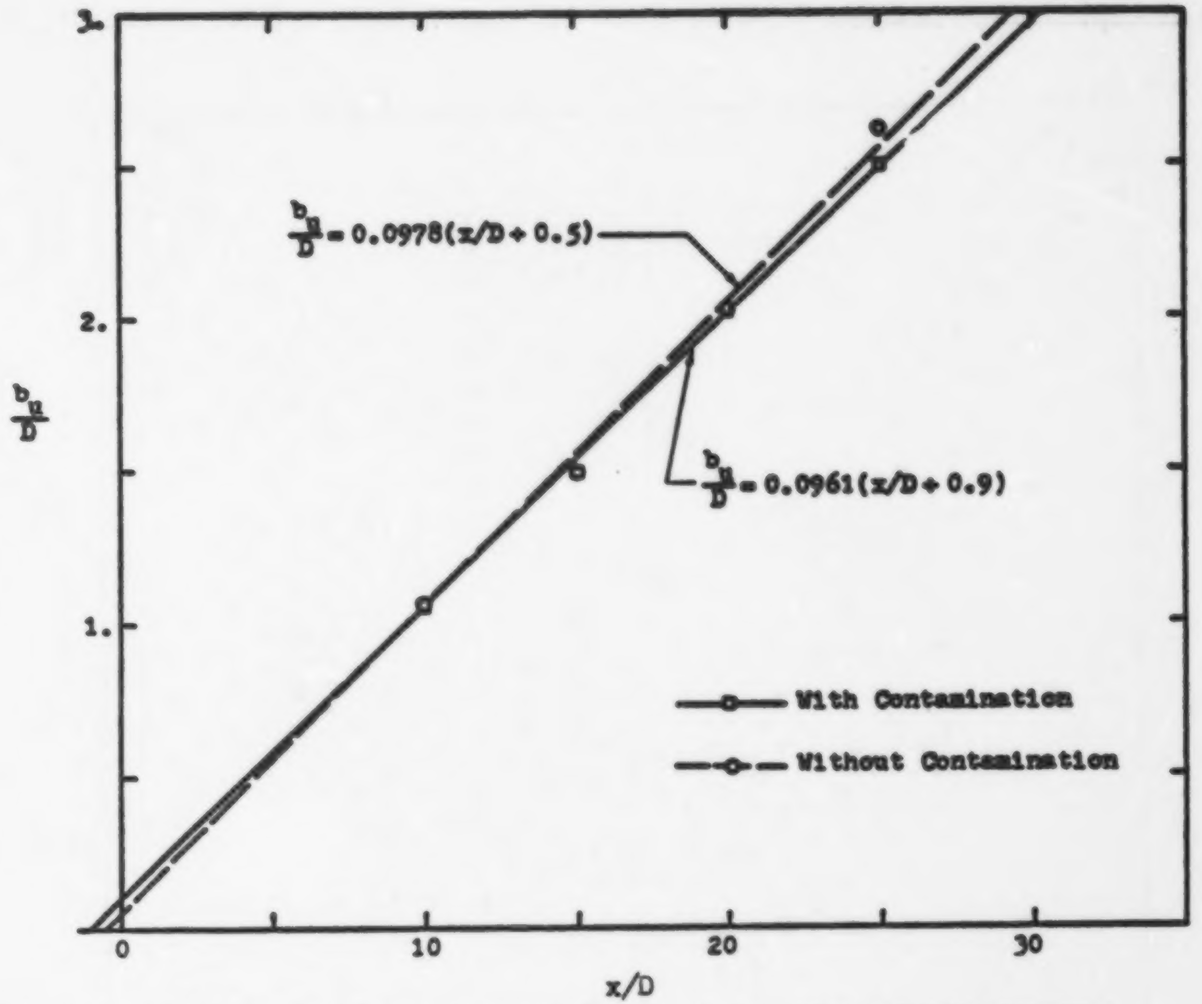

FIG. 29 VELOCITY HALF WIDTH (WITH & WITHOUT BUBBLE CONTAMINATION)

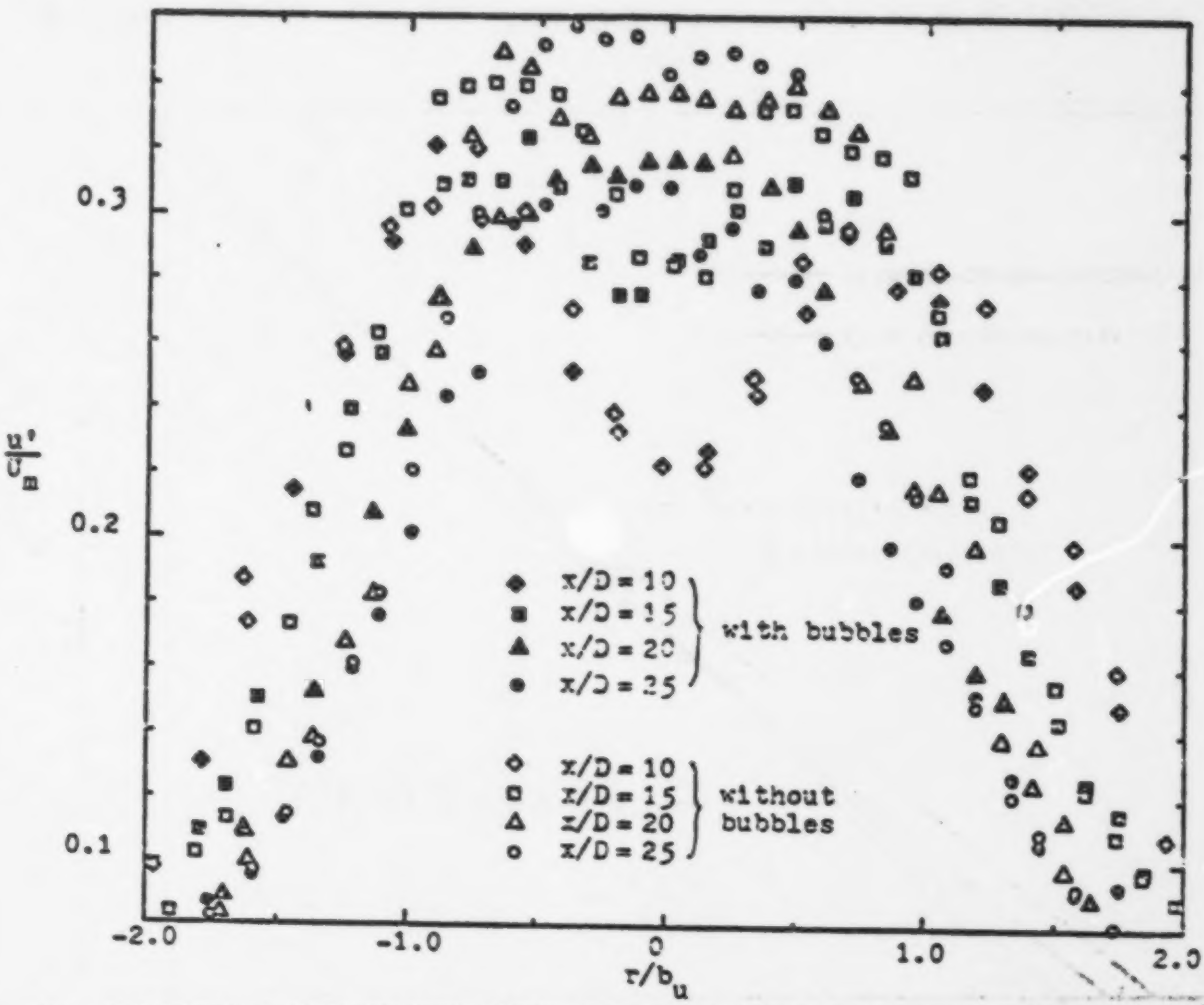

FIG. 30 VELOCITY DISTRIBUTION ALONG JET AXIS (WITH & WITHOUT BUBBLE CONTAMINATION)

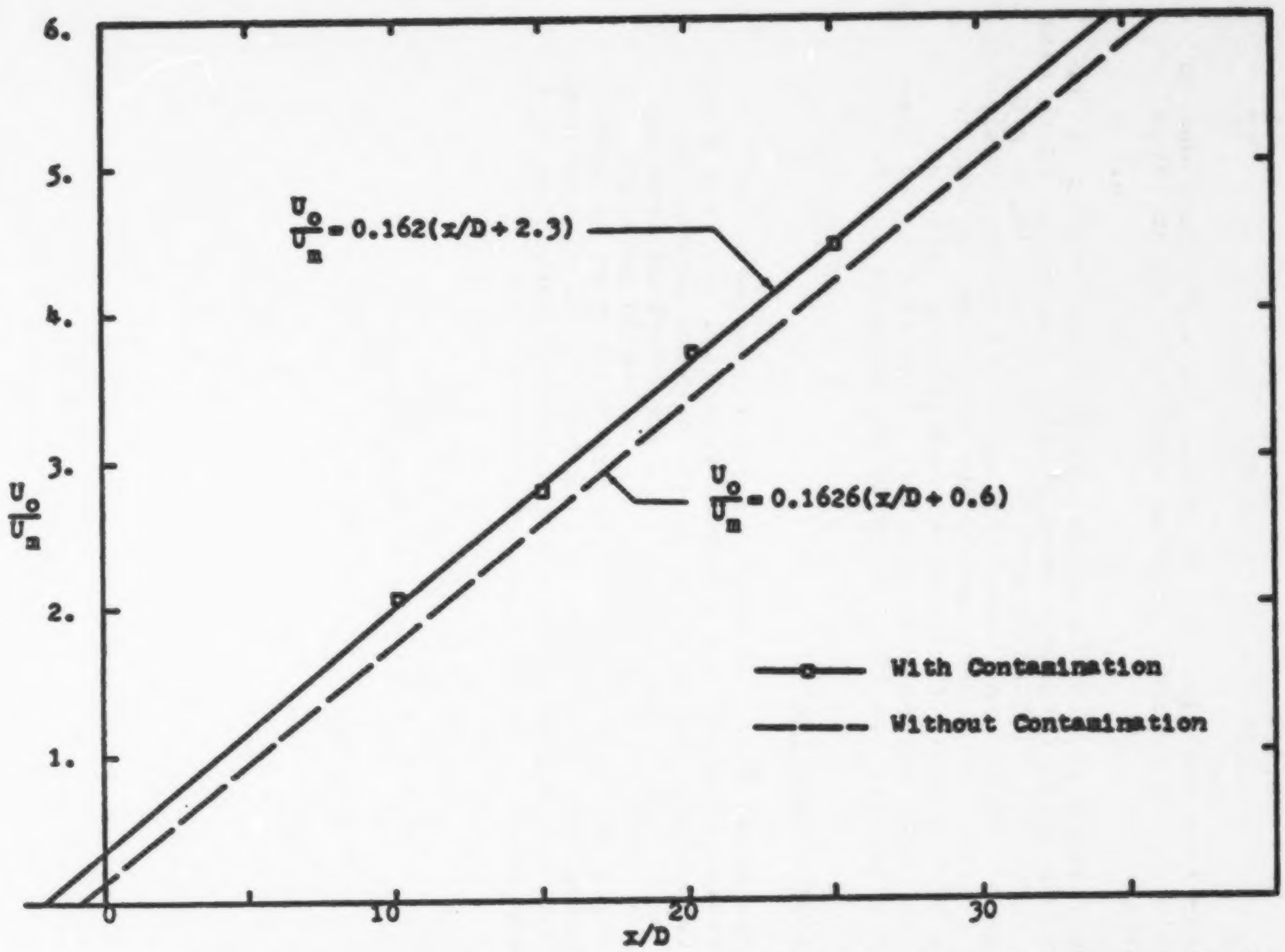

FIG. 31 TRANSVERSE FLUCTUATION LEVEL (WITH AND WITHOUT BUBBLES CONTAMINATION)

x/D	With Bubbles	Without Bubbles	Percent Decrease
10	0.220	0.225	2
15	0.275	0.285	3
20	0.318	0.336	5
25	0.305	0.35	12

It is seen that the fluctuation levels are attenuated due to the bubble contamination. This is especially so at large axial distances.

The result seems reasonable since the relative motion of the contaminants would dissipate more kinetic energy and hence damp out the turbulent fluctuations. At a relatively large x/D the range of mixing, and hence the amount of energy dissipated, will be greater, and consequently the deviation between the two sets of turbulent fluctuation measurements (with and without the bubbles) becomes greater. This result, as discussed previously, has been observed by Hetsroni and Sokolov (1969).

CONCENTRATION PROFILES

It must be noted that the measured quantities were the concentration flux, N, and the mean velocity, U. From these the corresponding half widths, b_u and b_n were determined. The actual concentration profiles, Γ, are obtained from the measured N and U as discussed in the following section. When looking at figures such as Figure 26 it must be noted that although the concentration flux half width always grows slower than the velocity half width, the concentration half width need not.

SECTION IX

TURBULENT DIFFUSIVITIES

The bubble concentration, Γ, can be obtained from the measured concentration flux, N, as

$$\Gamma = \frac{N}{V_b\ A_s} \tag{IX-1}$$

In the above A_s is the effective area sampled by the sensor, as defined in Chapter VIII, and V_b is the velocity of the bubbles.

The bubble velocity is given as $V_b=U+v_b$, where U is the mean velocity of the carrier stream and v_b is the mean relative velocity between the bubble and the carrier stream. Baker and Chao (1965) suggest that the mean relative velocity between the bubble and the mean flow of the turbulent carrier stream can be taken as the rise velocity of the bubble in a quiescent liquid. Based on this assumption, v_b is then a function only of bubble size. Haberman and Morton (1953) measured rising bubble velocities leading to the following:

Table 3 Rising Bubble Velocity

d_b (Microns)	v_b (fps)
343	0.105
527	0.186
780	0.301
970	0.397

The normalized concentration is then calculated by

$$\frac{\Gamma}{\Gamma_m} = \frac{N}{N_m}\ \frac{U_m + v_b}{U + v_b} \tag{IX-2}$$

where N/N_m is obtained from Section VIII, U and U_m are described by one of the three different models as given in Section VIII and v_b is obtained from Haberman and Morton's measurement. The normalized concentration profile can thus be calculated based on Equation (IX-2) and the corresponding diffusivities computed with Equations (VI-25), (VI-27), or (VI-28).

First Model: (Constant Eddy Viscosity and Constant Eddy Diffusivity)

Assuming the velocity profile to be given by Equation (VIII-6) the normalized concentration profiles can then be calculated from Equation (IX-2). The profiles for 343, 527, 780 and 970 micron

Table 4 Turbulent Schmidt Number

Bubble Size (Microns)	First Model (Constant ε_m and ε_γ Model)		(Tomotika's Solution)	(Gaussian Solution)
	$\frac{\varepsilon_\gamma}{U_m(x+a)}$	S_t	S_t	S_t
343	0.0025	1.06	1.19	1.17
527	0.0029	0.92	1.00	1.07
780	0.0030	0.90	0.98	1.00
970	0.0031	0.88	0.94	0.93

Note: In the second and third models, ε_γ and ε_m are dependent on η as shown in Figure VII-17 bubbles are respectively shown in Figures 32 to 35. It is seen that the normalized concentration data preserve the similarity characteristics. (This point will be further discussed in the next section).

Combining Equations (VIII-6) and Equation (VI-25), one obtains

$$\frac{\Gamma}{\Gamma_m} = (1 + 46.02\eta^2)^{-2\,\varepsilon_m/\varepsilon_\gamma} \tag{IX-3}$$

The computed concentration profiles are given in terms of η. The corresponding turbulent Schmidt number for the bubble diffusion, ($S_t=\varepsilon_m/\varepsilon_\gamma$), can be obtained by comparing Equation (IX-3) with the data of Figures 32 to 35. The resulting coefficients of the eddy particle diffusivities and the corresponding turbulent Schmidt numbers for the four bubble sizes tested are tabulated in Table 4. These were obtained by minimizing the mean square difference between the data and Equation (IX-3) with different exponents. The theoretical curves given by Equation (IX-3) with the regressed coefficients are also plotted in Figures 32 to 35. It is seen that the general shape of the curves agrees very well with the values computed based on the actual measurements.

Second Model: (Taylor's Vorticity Transport Theory)

Assuming that the velocity profile of the flow field is given by Equation (VIII-8), the normalized concentration profiles calculated with Equation (IX-2) for the 343, 527, 780 and 970 micron bubbles will differ from those of figures 32 to 35. The corresponding values are shown in Figures 36 to 39.

Combining Equations (VIII-8) and Equation (VI-27) the assumed concentration profile takes the form

$$\frac{\Gamma}{\Gamma_m} = \left\{ \mathrm{Exp}\left[\int_0^{11.8\eta} 11.8\,d\eta \frac{\frac{1}{2}(11.8\eta)^{\frac{1}{2}} - \frac{2}{7}a_1(11.8\eta)^2 + \frac{a_2}{5}(11.8\eta)^{\frac{7}{2}} - \frac{2a_3}{13}(11.8\eta)^5}{-\frac{3}{2}a_1 + 3a_2(11.8\eta)^{3/2} - \frac{9a_3}{2}(11.8\eta)^3} \right] \right\}^{\frac{\varepsilon_m}{\varepsilon_\gamma}} \tag{IX-4}$$

Equation (IX-4) can be numerically integrated for various values of η provided the exponent $\varepsilon_m/\varepsilon_\gamma$ is assumed to be known. In this manner, repeating the calculation of the concentration profile by considering different values for $\varepsilon_m/\varepsilon_\gamma$, the value for which the calculated concentration profile appears to best fit the measured data can be found. This is then taken to be the representative turbulent Schmidt number.

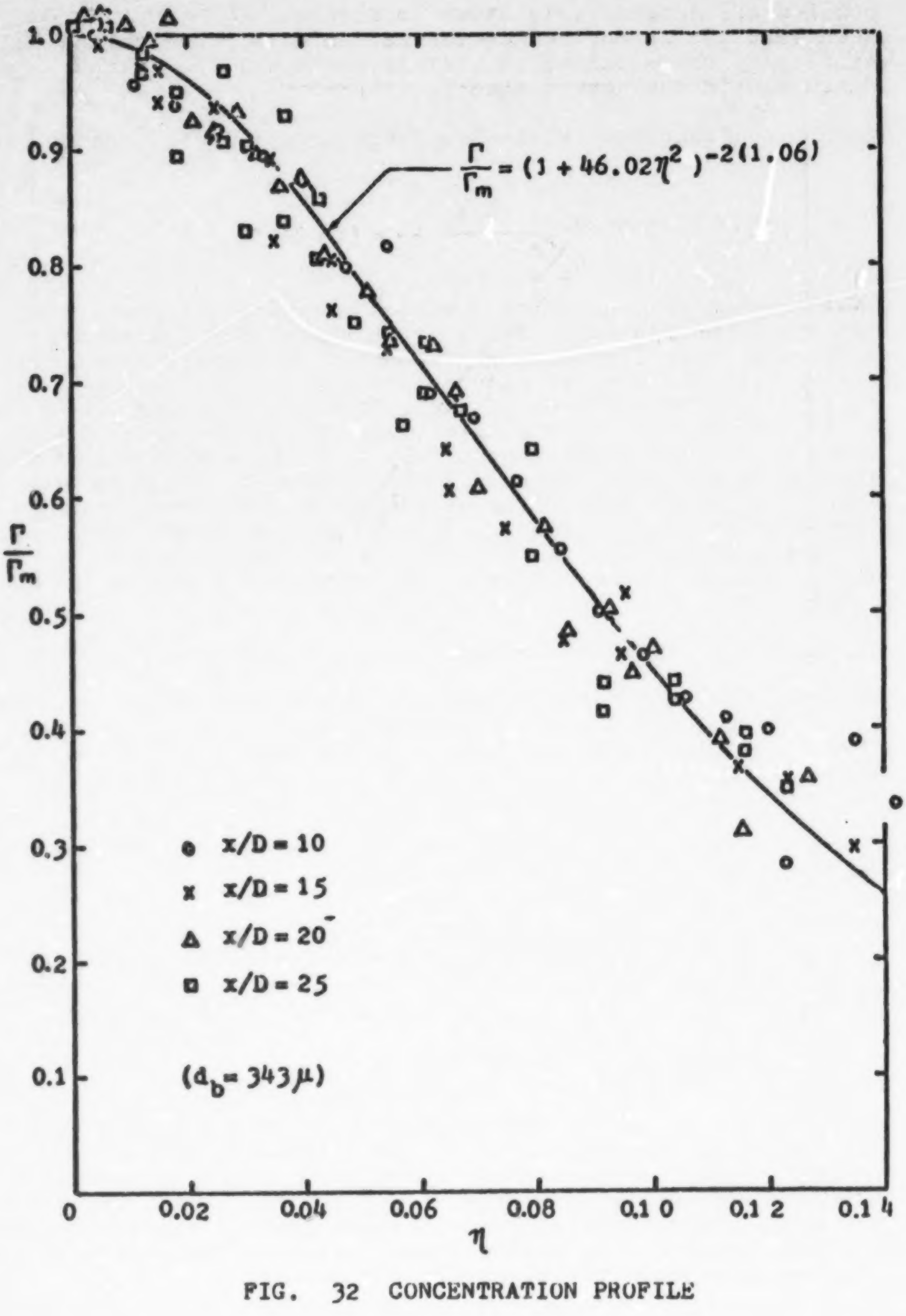

FIG. 32 CONCENTRATION PROFILE

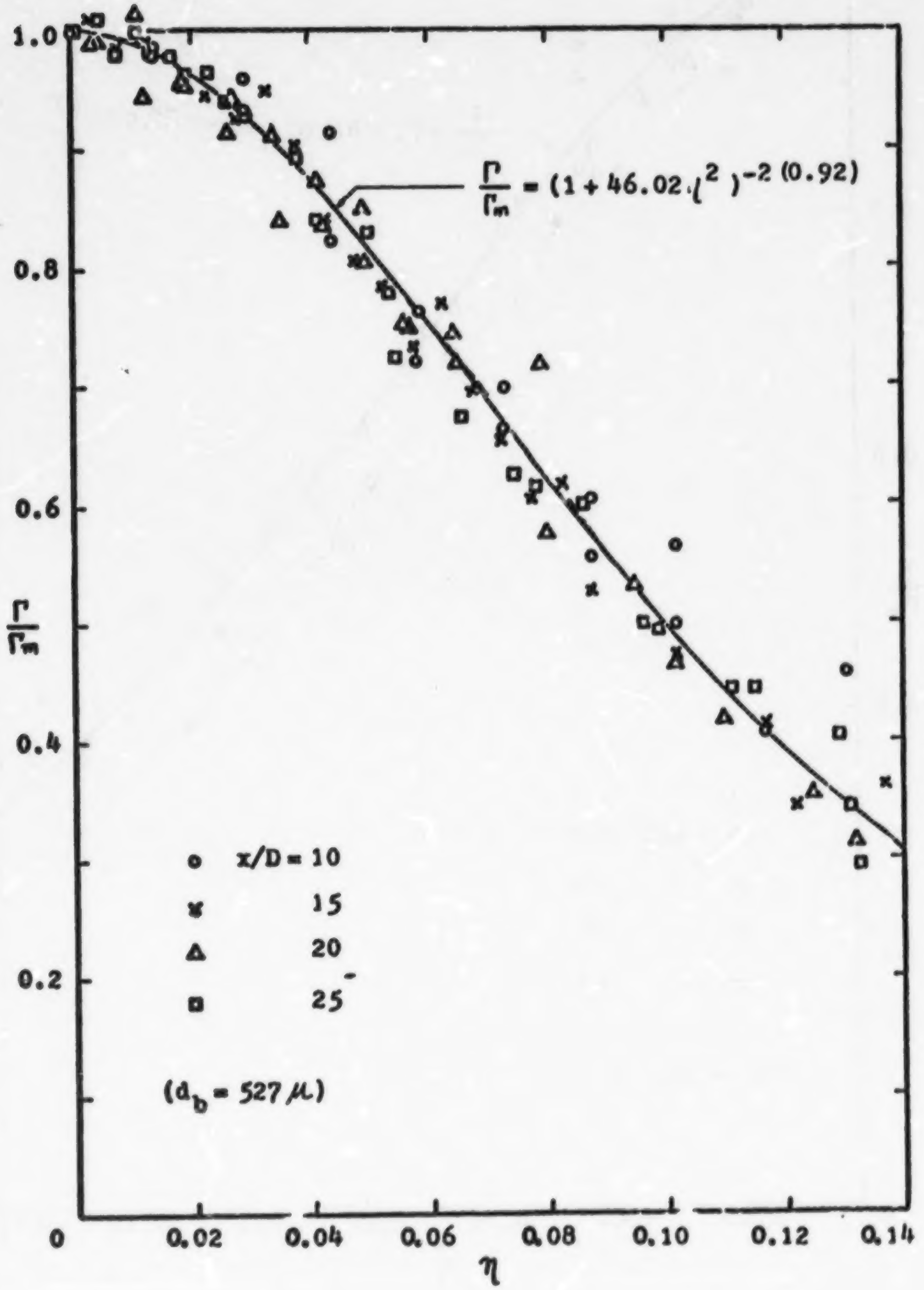

FIG. 33 CONCENTRATION PROFILE

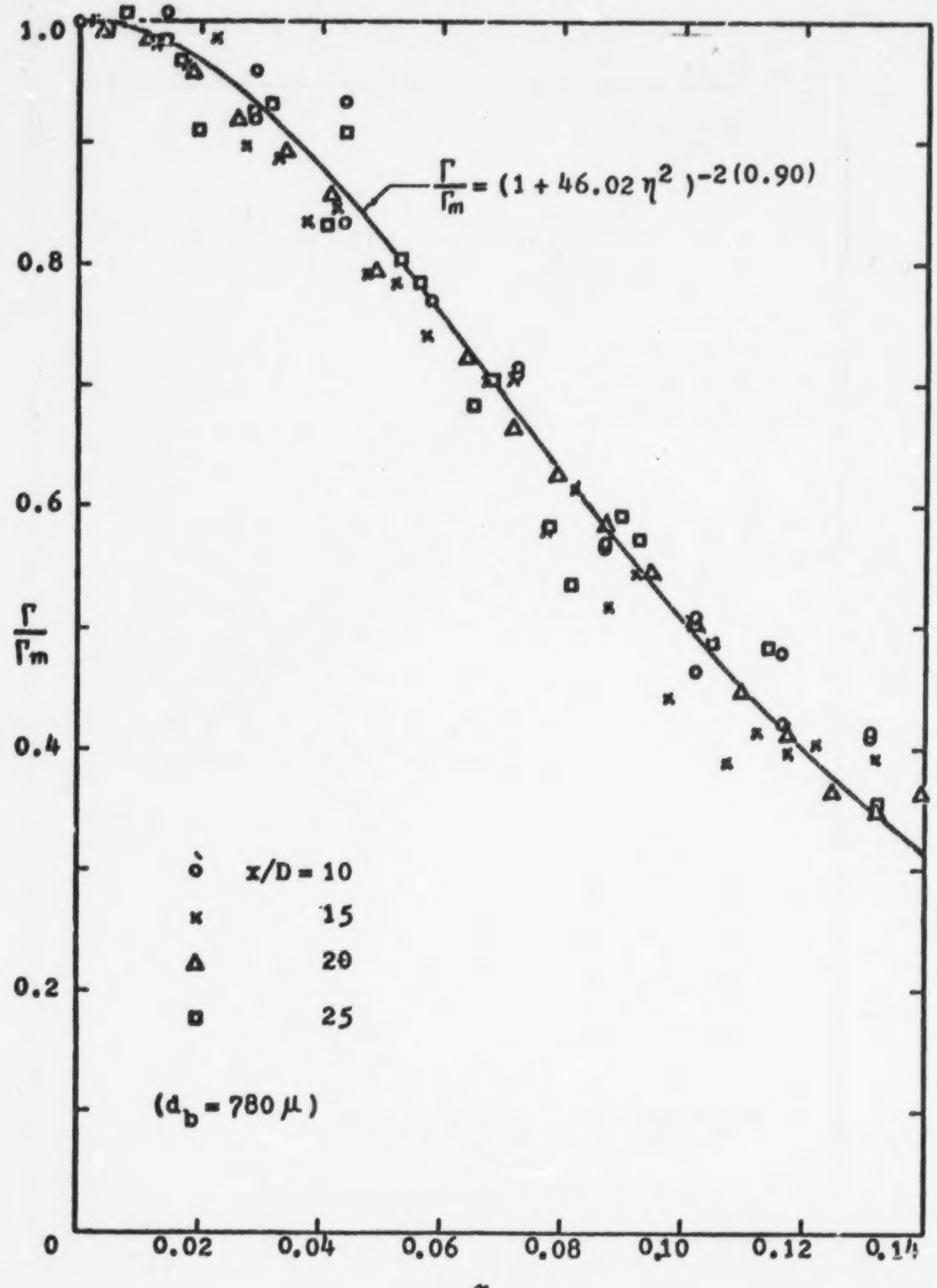

FIG. 34 CONCENTRATION PROFILE

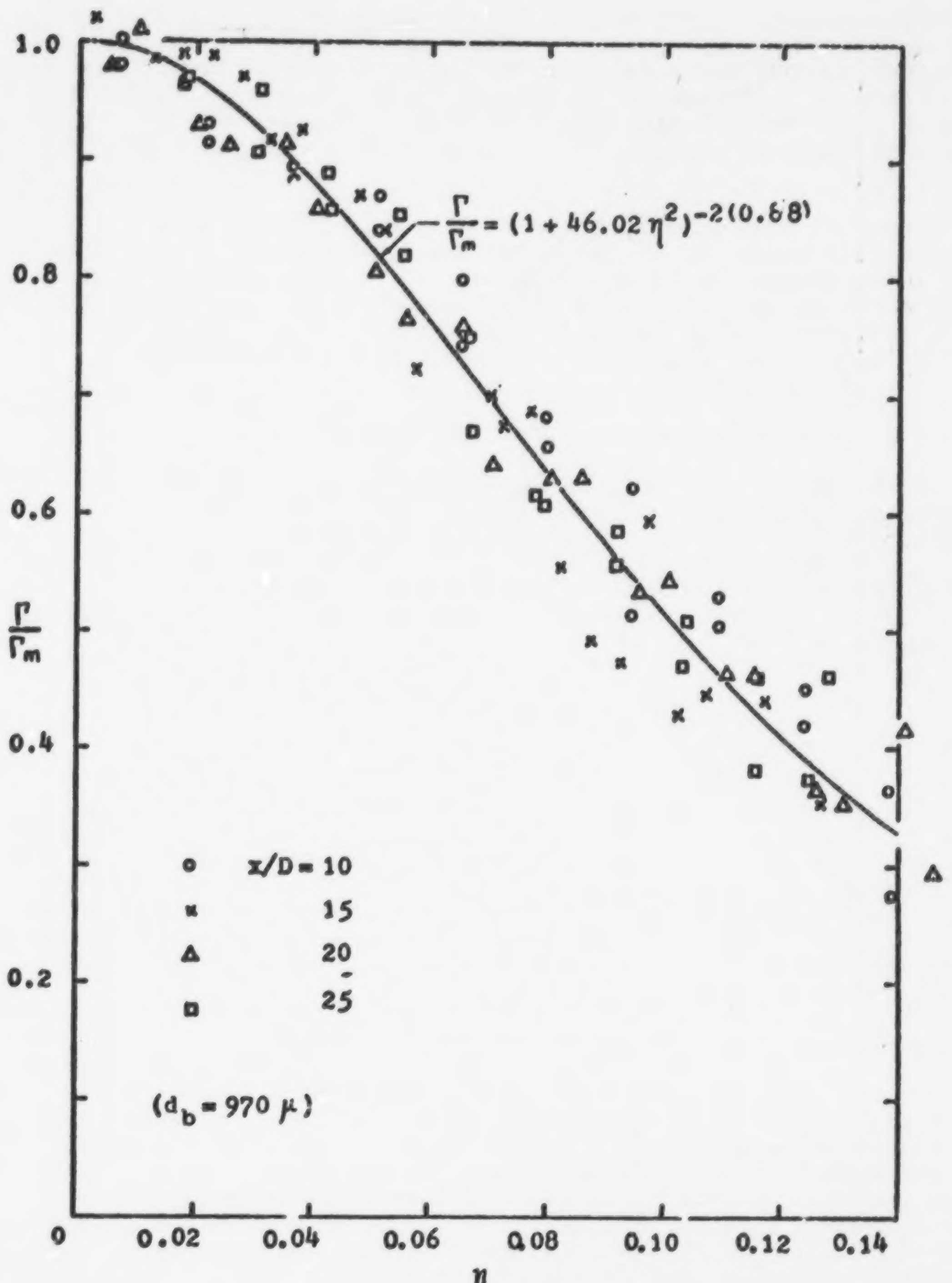

FIG. 35 CONCENTRATION PROFILE

The corresponding theoretical curves calculated with the best fit coefficients of $\varepsilon_m/\varepsilon_\gamma$ are shown in Figures 36 to 39. In order to see how sensitive the plots given in Figures 36 to 39 are to a change in S_t the curves of Equation (IX-4)with S_t=0.8, 1.0 and 1.4 are also included in Figure 36. The numerical values of $\varepsilon_m/\varepsilon_\gamma$ leading to a best fit are shown in Table 4.

In comparing the general shape of the theoretical curves with the measurements, it is seen that the theoretical curves show a greater curvature at small values of η. The general shape of the curves does not agree with the measured concentration profiles very well. The same deviation (between measured values and model) was observed in the velocity profiles as shown in Figure 9.

Third Model: (Reichardt's Inductive Theory)

The data can also be analyzed considering the third model proposed. Assuming that the velocity profile is given by Equation (VIII-9), the corresponding concentration profiles calculated from Equation (IX-2) for the 343, 527, 780 and 970 micron bubbles are shown in Figures 40 to 43. From Equations (VIII-9) and VI-28) the assumed concentration profile takes the form

$$\frac{\Gamma}{\Gamma_m} = \mathrm{Exp}\left\{- 73.04 \frac{\varepsilon_m}{\varepsilon_\gamma} \eta^2\right\} \qquad \text{(IX-5)}$$

The corresponding turbulent Schmidt number $\varepsilon_m/\varepsilon_\gamma$ leading to a best fit, as shown by the plots of Figures 40 to 43 are tabulated in Table 4. The calculated curves show a smaller curvature near the center line region and under predict near the edge of the jet. The general shape of the analytical curve does not agree very well with the measured data. The same deviation has been observed in the velocity profile when calculated using this model as shown in Figure 9.

The comparison of the analytical and semi-empirical curves given by the above models indicates that the first model seems to fit the measured concentration profile best. Hence it is concluded that the particle diffusivity and the corresponding turbulent Schmidt number obtained from the first model should be the most reliable of the three. No thorough statistical measures were sought to compare the predictions made by the three models. An attempt at using a simple regression analysis did not lead to a better interpretation of the results. This was primarily due to the spread of the data.

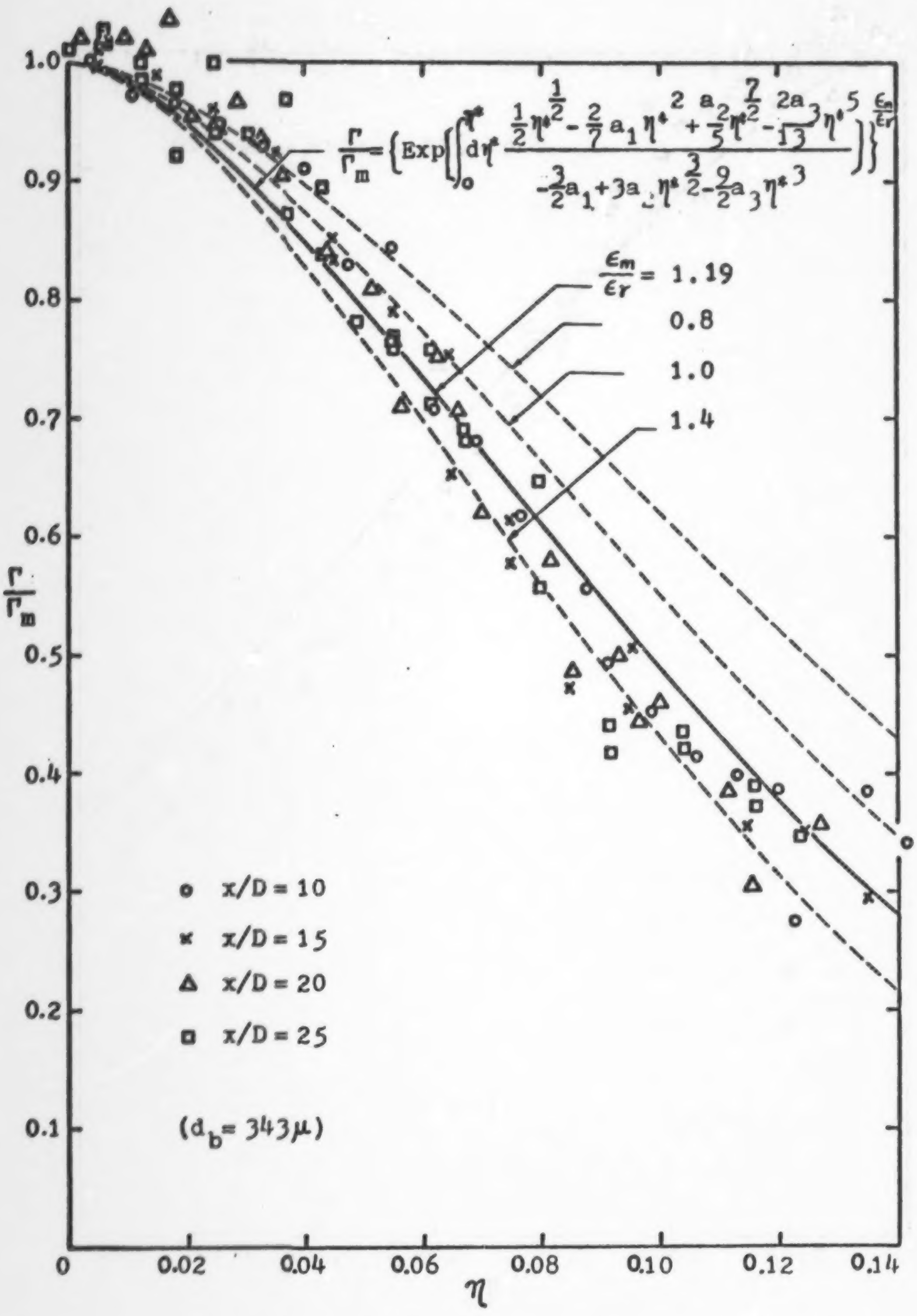

FIG. 36 CONCENTRATION PROFILE

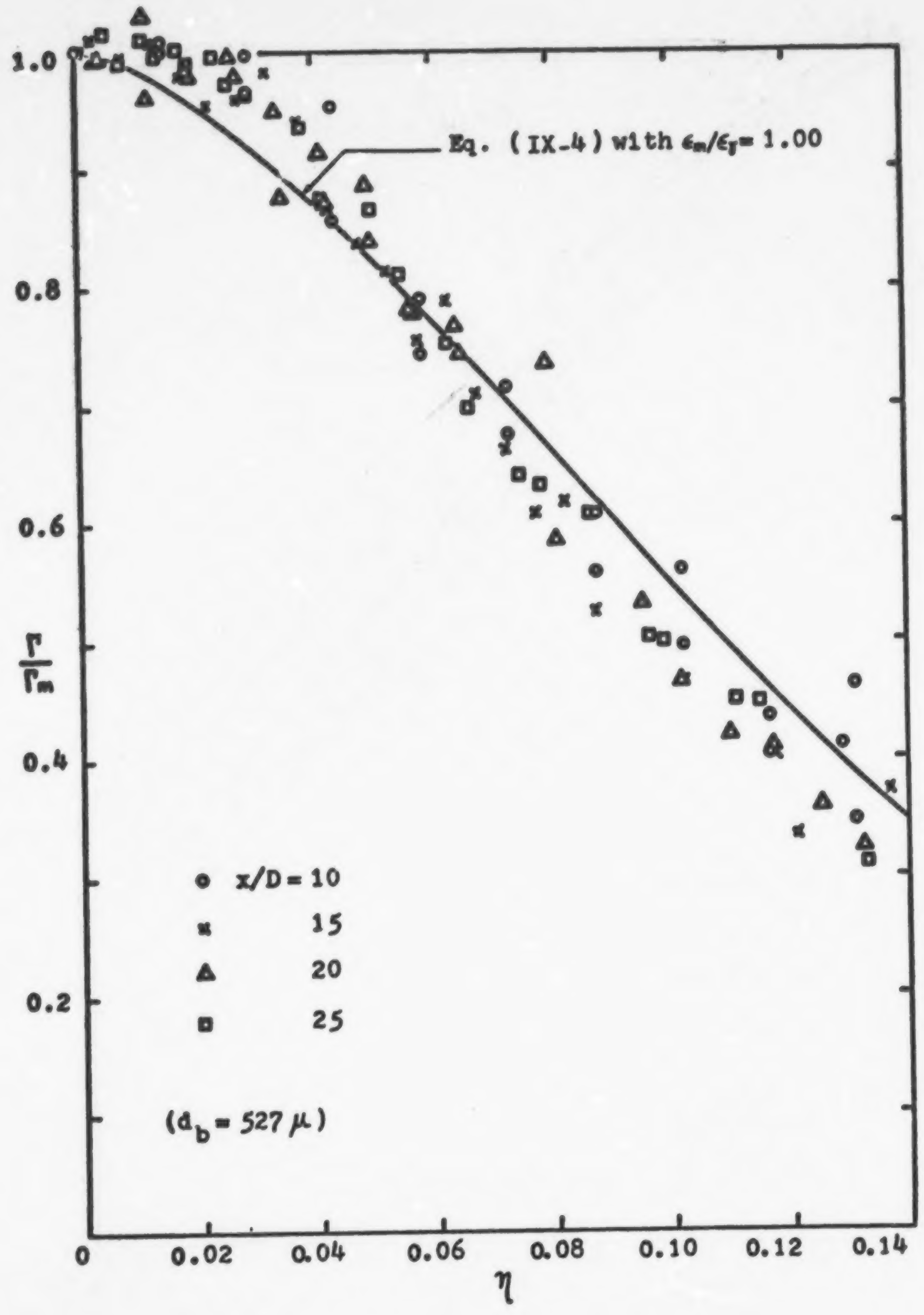

FIG. 37 CONCENTRATION PROFILE

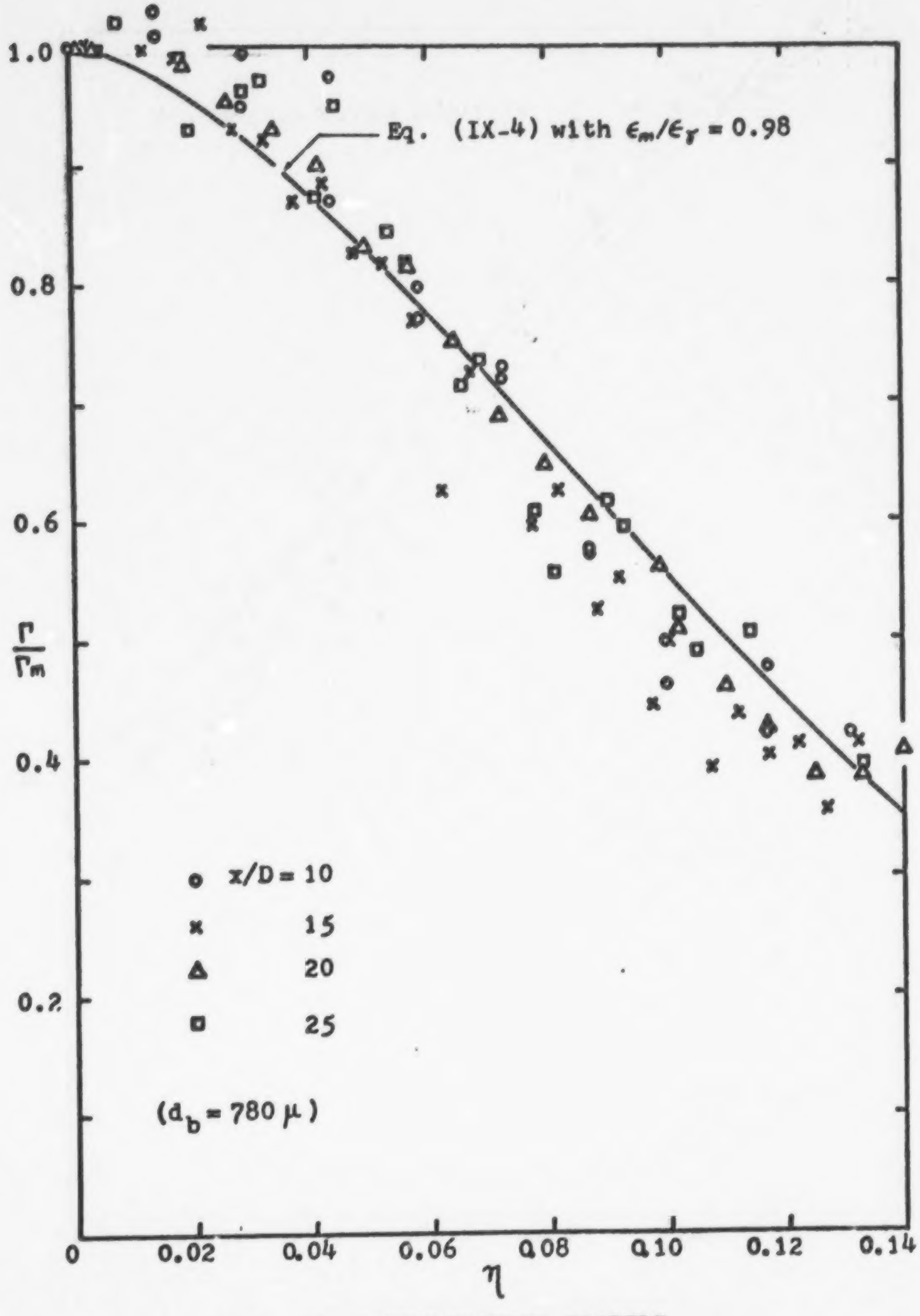

FIG. 38 CONCENTRATION PROFILE
(With Bubble Rising Vel. Corr.)

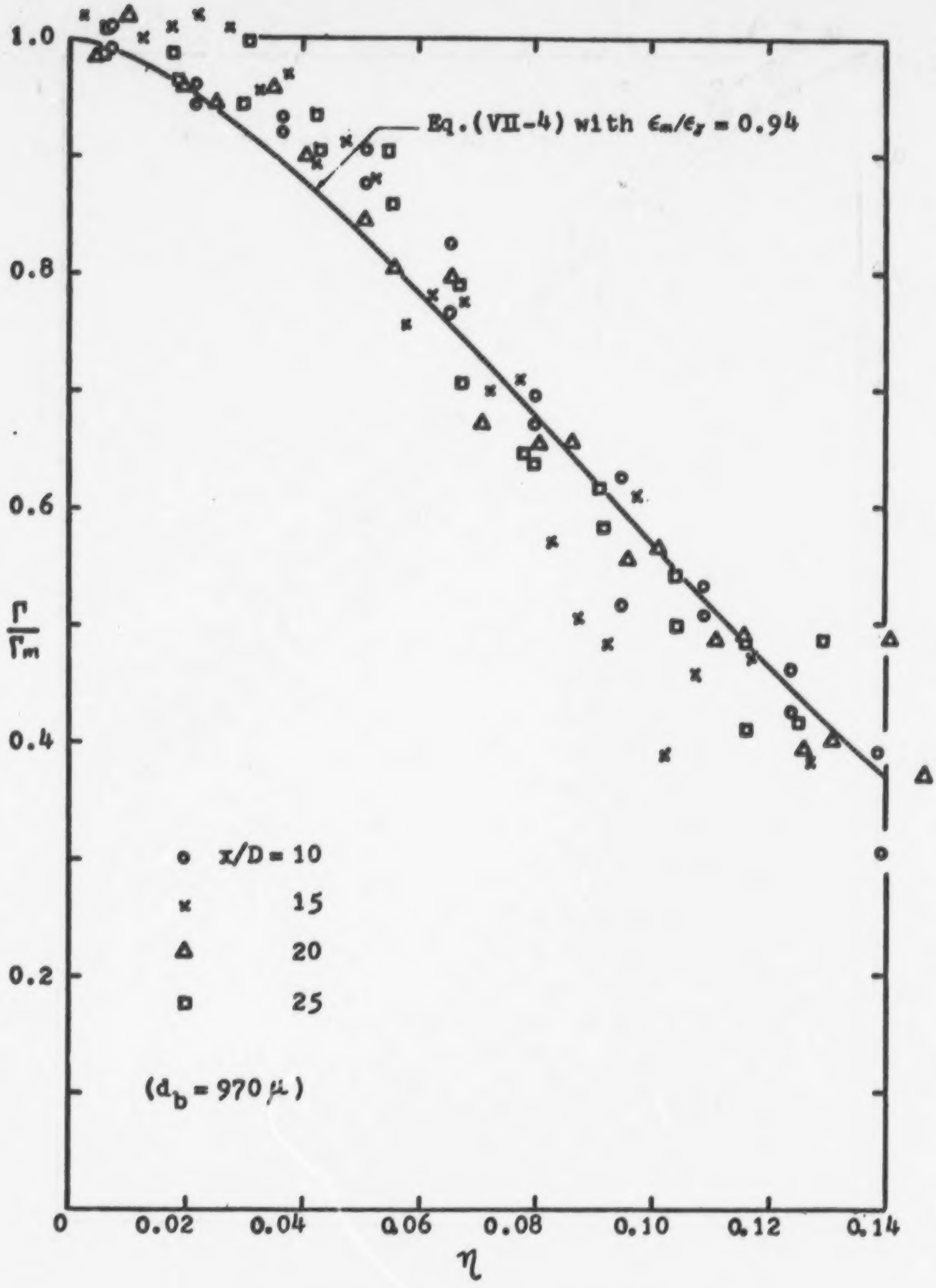

FIG. 39 CONCENTRATION PROFILE
(With Bubble Rising Vel. Corr.)

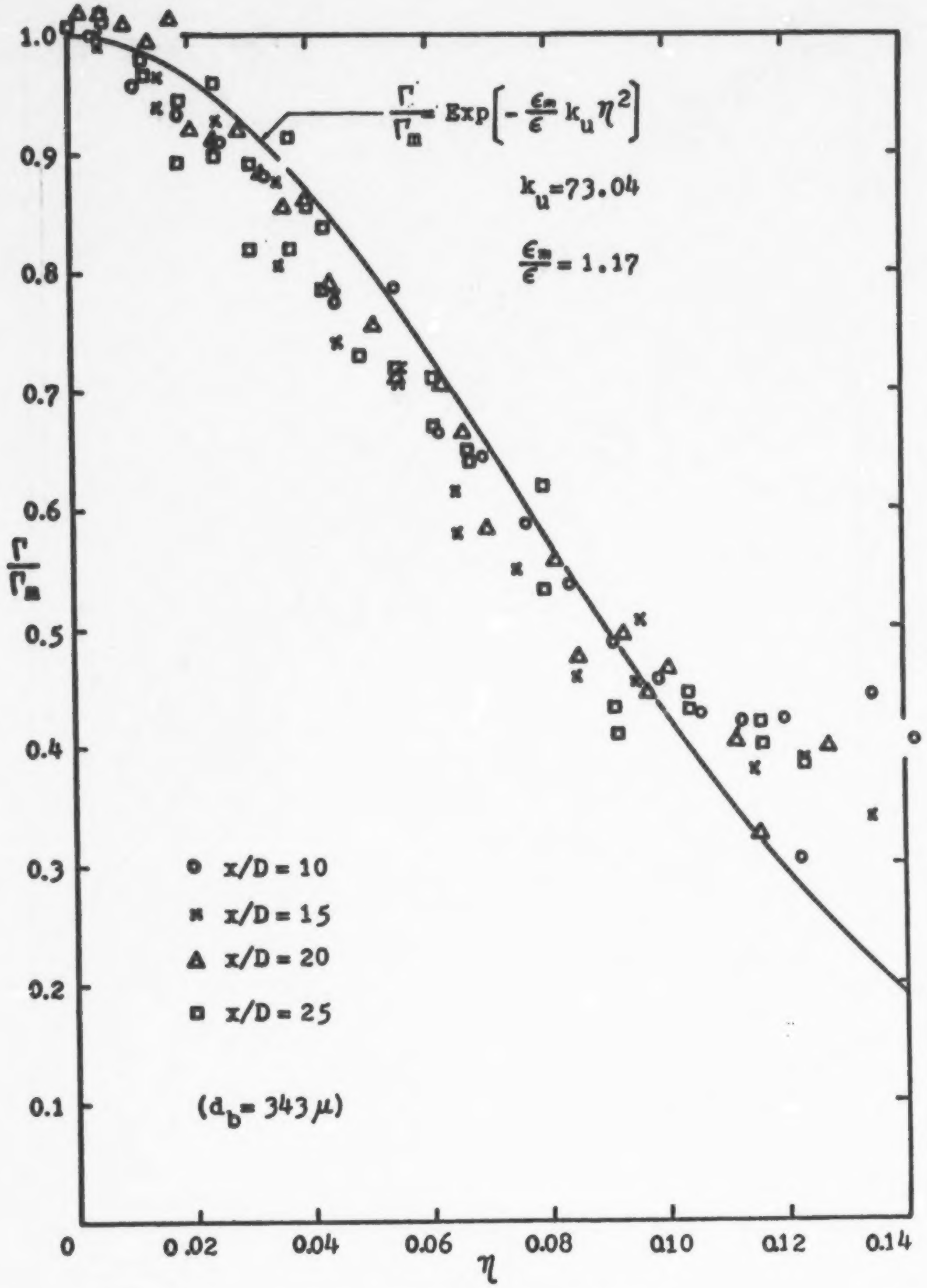

FIG. 40 CONCENTRATION PROFILE
(With Bubble Rising Vel. Corr.)

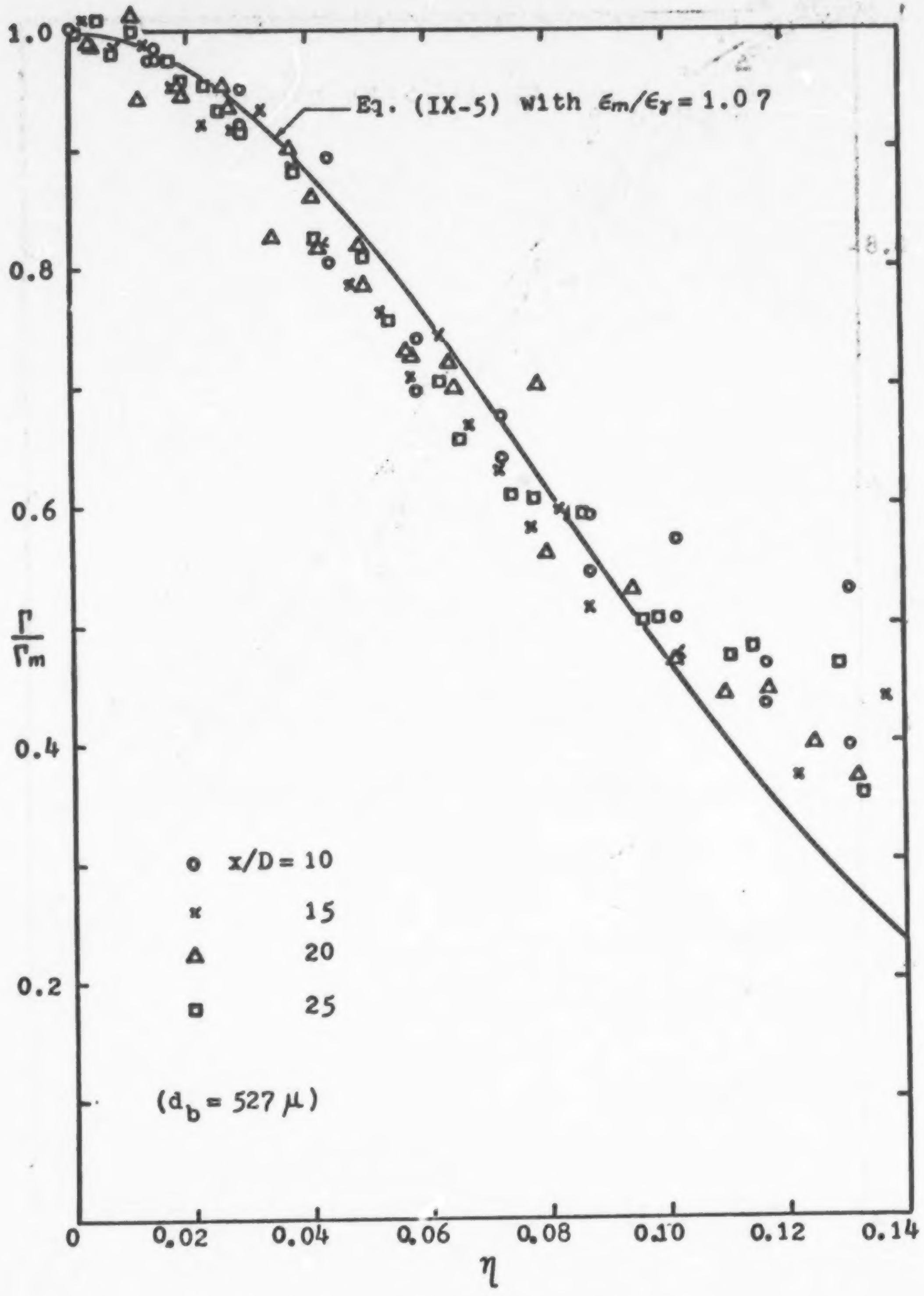

FIG. 41 CONCENTRATION PROFILE
(With Bubble Rising Vel. Corr.)

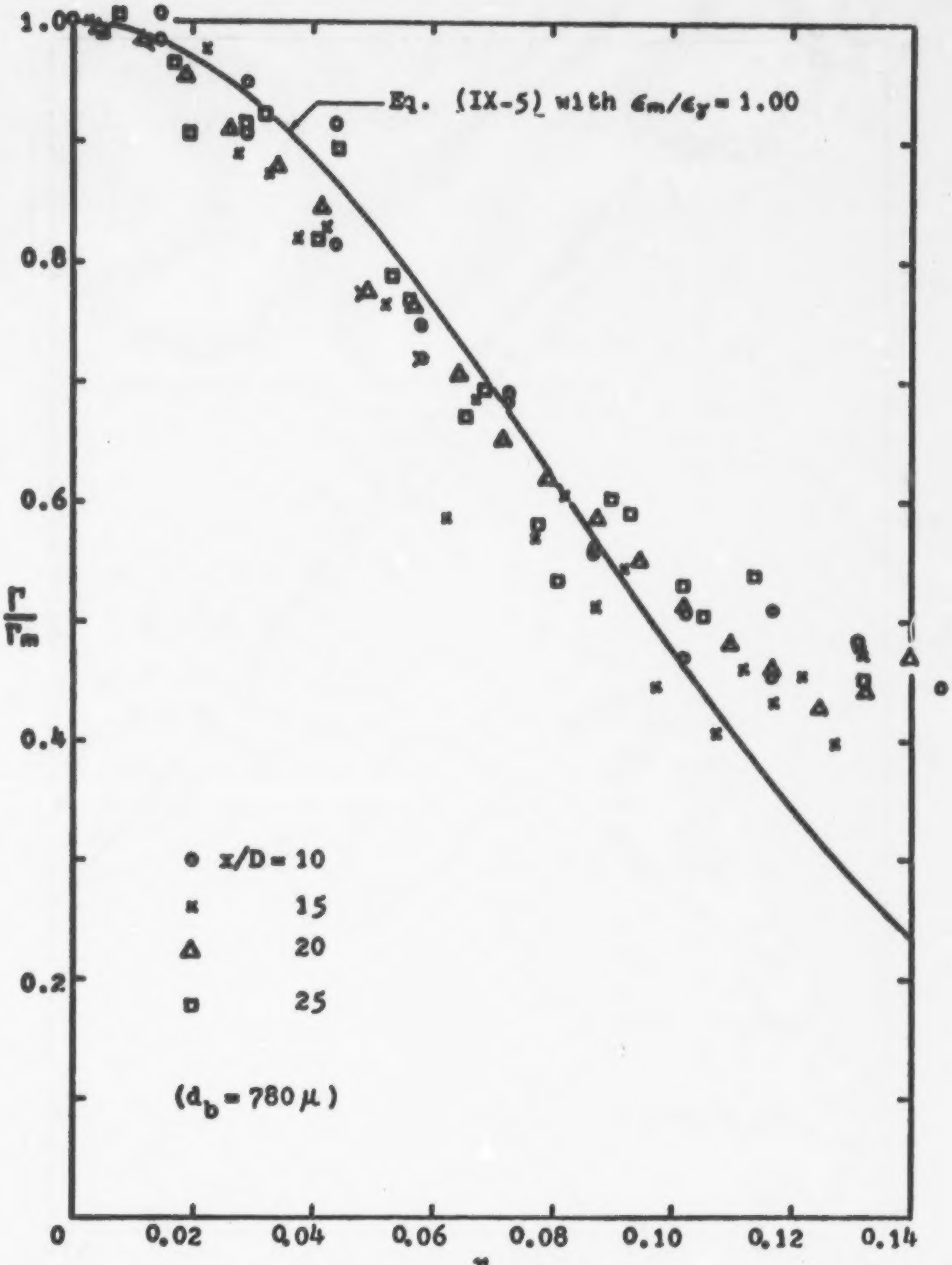

FIG. 42 CONCENTRATION PROFILE
(With Bubble Rising Vel. Corr.)

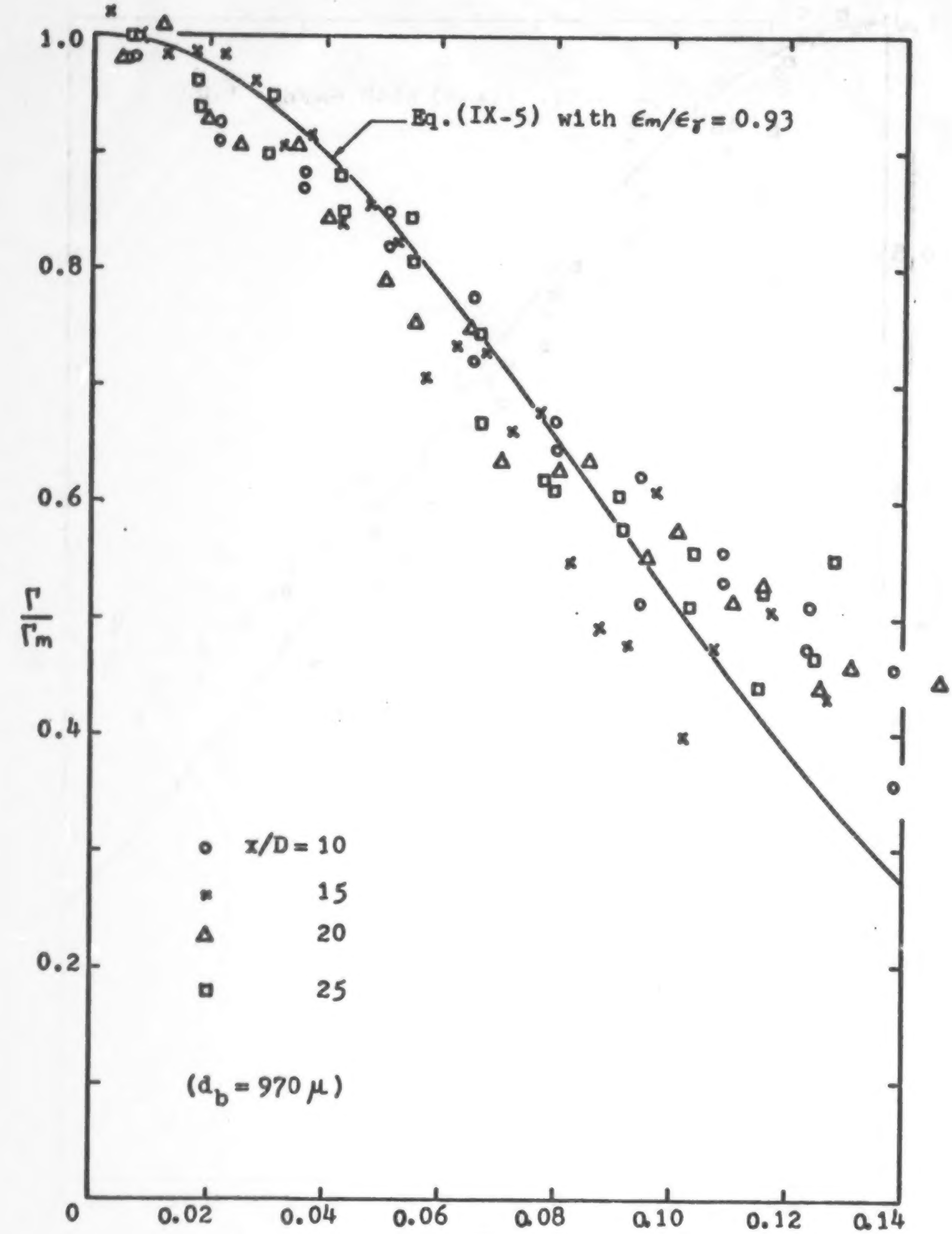

FIG. 43 CONCENTRATION PROFILE
(With Bubble Rising Vel. Corr.)

SECTION X

TURBULENT DIFFUSION CHARACTERISTICS

Dependence of Turbulent Schmidt Number on the Particle Parameter ψ_T

The results reported in the previous sections dealt with the dispersion of bubbles in a liquid jet. As noted by Householder and Goldschmidt (1969) it is possible to compare the diffusion of particles in entirely different flow fields by using a correlation based on ψ_T.

This is because the turbulent transport is related primarily to the immediate structure of the turbulent flow and the particle size, shape and density. In selecting a parameter to make this comparison they selected the ratio of the Stokesian response time of the particle in a carrier stream to a characteristic time scale of the flow. Ahmadi (1970) extended this idea using the turbulent time macroscale as the specific characteristic time. He defined the corresponding particle parameter as

$$\psi_T = \frac{\sqrt{\overline{u^2}}\,\Lambda_x}{\nu}\left(\frac{d_b}{\Lambda_x}\right)^2\left(\frac{2\rho_p}{\rho_f}+1\right) \qquad \text{(X-1)}$$

where Λ_x is the longitudinal turbulent macroscale of the flow field. What is to be investigated is whether or not S_t is a function of ψ_T. Knowledge of such a function would permit comparison of experimental results of the previous section to those of other investigators and an extension to other flow fields as well.

When the particle in concern is a bubble of gas in water the particle parameter given in Equation (X-1) simplifies to

$$\psi_T = \frac{\sqrt{\overline{u^2}}}{\nu}\,\frac{d_b^2}{\Lambda_x} \qquad \text{(X-2)}$$

which can then be re-written as

$$\psi_T = \frac{\sqrt{\overline{u^2}}}{U_m}\,\frac{U_m D}{U_o \Lambda_x}\,\frac{U_o D}{\nu}\left(\frac{d_b}{D}\right)^2 = \frac{\sqrt{\overline{u^2}}}{U_m}\,\frac{U_m D}{U_o \Lambda_x}\,R_e\left(\frac{d_b}{D}\right)^2 \qquad \text{(X-3)}$$

$\sqrt{\overline{u^2}}/U_m$, U_o/U_m and Λ_x/D are given in Figures 31, 11 and 20, respectively. An average value of ψ_T can be computed for each bubble size throughout the region in which measurements were taken. The relationship used is $\psi_T = 7.25\text{x}10^3 \left(\frac{d_b}{D}\right)^2$, an average for 10<x/D<25, computed along the axis. The resulting relationship between the inverse of the turbulent Schmidt number and the particle parameter ψ_T for the four bubble sizes is shown in Figure 44. The dynamic numerical prediction of Ahmadi (1970) and the data for the pipe and open channel experiments collected by Householder and Goldshmidt (1969) are also included. In addition, results of two other jet diffusion experiments by Singamsetti (1966) and Brush (1962), one plane jet diffusion experiment by Householder (1968) and one "isotropic" turbulent diffusion experiment by Kennedy (1965) are included in Figure 44. The results of Householder include one questionable data point currently under a separate study.

From Figure 44, it is seen that the data obtained from the circular jet measurements (i.e. Singamsetti, Brush and present study) seem to fall below the other measurements and Ahmadi's prediction.

Such deviation suggests that the relationship between S_t and ψ_T may have different trends, one for the reported pipe, channel and plane jet measurements (which follow the theoretical curve predicted by Ahmadi) and another for the circular jet measurements.

The difference between these may be either due to an essential difference in their geometries or to some inherent difference in the specific experiments reported. The predictions of Ahmadi, as well as the selection of ψ_T assumed that the particle Reynolds number (which according to Ahmadi is defined as $R_{e_p} = 2\sqrt{\overline{u^2}}\, d_b/\nu$) is in the order of one or smaller. This condition was satisfied for Householder's experiment and most of the data gathered by him. Unfortunately it was not for the current measurements nor for the other reported for circular jets (all of which has values of R_{e_p} in the order of 10^2-10^3).

It is desirable to attempt to find another particle parameter. Hopefully a university relationship could be found between S_t and this new particle parameter

Dependence of Turbulent Schmidt Number on the Particle Parameter ψ'_T

Recalling the definition of ψ_T, one can decompose it as

$$\psi_T = \frac{36\,\overline{u^2}}{\Lambda_x}\,\frac{d_b^2}{36\nu}\left(\frac{2\rho_p}{\rho_f} + 1\right) = \frac{36\,\overline{u^2}}{\Lambda_x}\,\tau_s \qquad \text{(X-4)}$$

Where τ_s is the Stokesian response time of the particle. It is quite obvious then that the particle parameter ψ_T is meaningful in describing the particle diffusion only for the cases where the particle Reynolds number lies within the

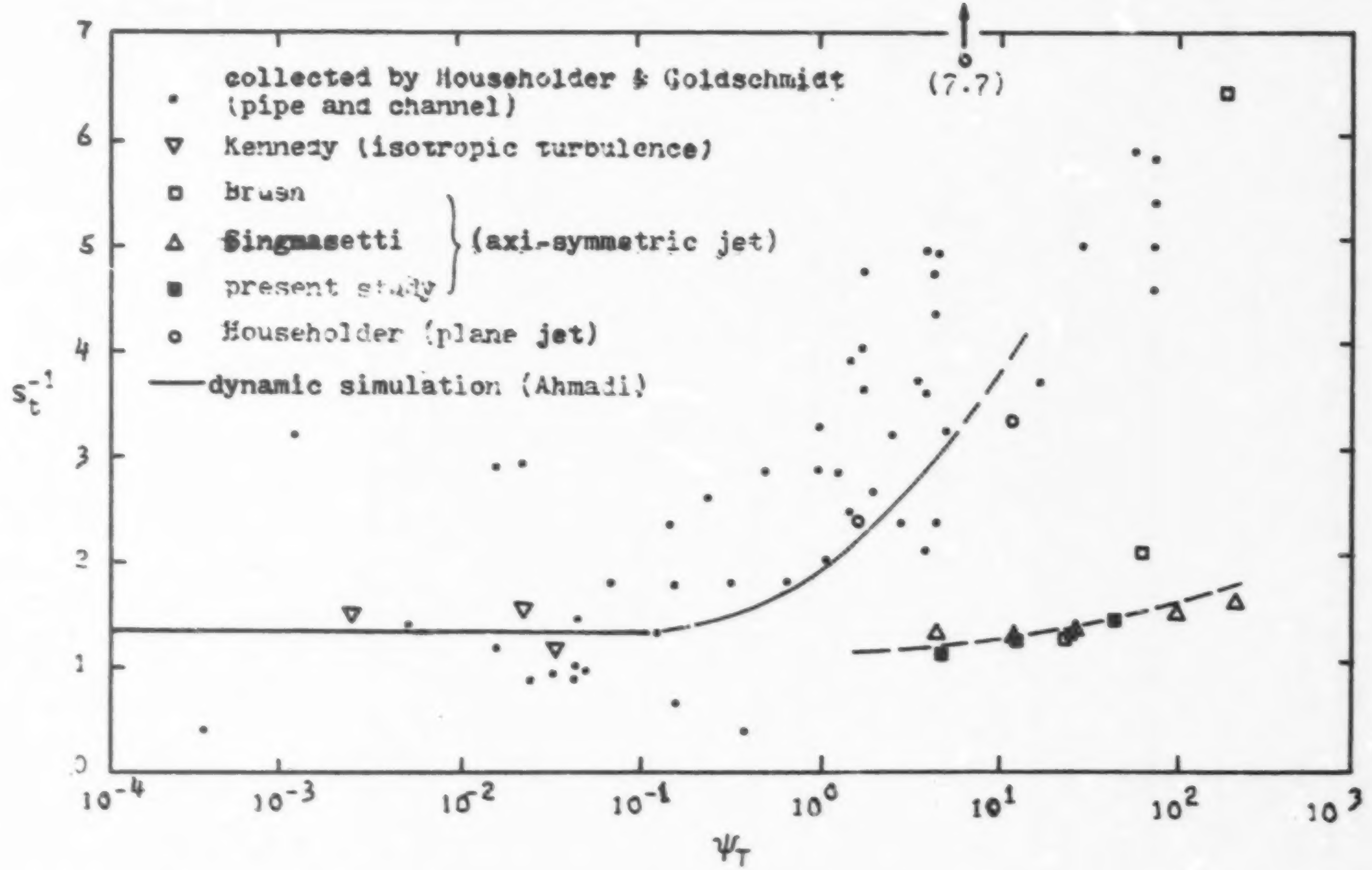

FIG. 44 DEPENDENCE OF S_t^{-1} ON PARTICLE PARAMETER ψ_T

Stokes range. For the present and the other two circular jet measurements where the particle Reynolds numbers are in the order of 10^2 to 10^3 another particle parameter has to be defined. Let this be

$$\psi_T' = \frac{36\sqrt{\overline{u^2}}}{\Lambda_x}\tau \tag{X-5}$$

where τ is the actual particle response time. An expression is then sought for τ.

Neglecting the potential force, nonlinear effect and Basset term, the B.B.O. Equation takes the form

$$\frac{\pi}{6} d_b^3\rho_p \frac{d}{dt}(v_p) = C_D \frac{\pi d^2_b}{4}\frac{\rho_f}{2} \mid v_p - v_f \mid^2 + \frac{1}{2}\frac{\pi}{6} d^3_b \rho_f \frac{d}{dt}|v_p - v_f| \tag{X-6}$$

where v_p and v_f are respectively the particle and fluid velocities. Assuming one dimensional steady flow such that $\frac{dv_f}{dt} = 0$, Equation (X-6) simplifies to

$$\frac{d}{dt}|v_p - v_f| + \frac{3C_D}{2d_b\left(\frac{2\rho_p}{\rho_f} + 1\right)}|v_p - v_f|^2 = 0 \tag{X-7}$$

Note that in Stokesian motion $C_D = 24/Re_p = 24\,\nu/|v_p - v_f|d_b$. The expression for the Stokesian response time, τ_s, as defined in Equation (X-4) follows from Equation (X-7).

Consider first the case where the particle Reynolds number is in between 2 and 500. In this Reynolds number range, Bird, Stewart and Lightfoot (1960) suggested that

$$C_D = \frac{18.5}{R_{e_p}^{3/5}} = \frac{18.5}{\left\{\frac{|v_p - v_f|d_b}{\nu}\right\}^{3/5}} \tag{X-8}$$

Equation (X-7) then simplifies to

$$\frac{d}{dt}|v_p - v_f| + \frac{111\,\nu^{3/5}}{4d_b^{8/5}\left(2\frac{\rho_p}{\rho_f} + 1\right)}|v_p - v_f|^{7/5} = 0 \tag{X-9}$$

Assuming that the initial condition is $|v_p - v_f|_{t=0} = 2\sqrt{\overline{u^2}}$, Equation (X-9) can be integrated to yield

$$|v_p - v_f| = \left\{ \frac{11.1\ \nu^{3/5}}{d_b^{8/5}(2\ \frac{\rho_p}{\rho_f} + 1)}\ t + (2\sqrt{\overline{u^2}})^{-2/5} \right\}^{-5/2} \qquad \text{(X-10)}$$

Defining particle response time   as the value of t where $|v_p - v_f|/2\sqrt{\overline{u^2}}$ equals to $e^{-1} = 0.368$ the expression for becomes

$$\tau = 0.0335 \times \frac{d_b^{1.6}\ (2\ \frac{\rho_p}{\rho_f} + 1)}{(\ \overline{u^2}\ 0.4\,\nu^{0.6}}\ \text{for } 2 < R_{e_p} < 500 \qquad \text{(X-11)}$$

or

$$\frac{\tau}{\tau_s} = \frac{1.21\ \nu^{0.4}}{(\sqrt{\overline{u^2}})^{0.4} d_b^{\ 0.4}} = \frac{\psi_T'}{\psi_T} = \frac{1.59}{R_{e_p}^{\ 0.4}} \qquad \text{(X-12)}$$

Consider next the case where the particle Reynolds number is between 500 and 10^5. In this range $C_D=0.44$ Equation (X-7) then becomes

$$\frac{d}{dt}\,|v_p - v_f| + \frac{0.66}{d_b\ (2\frac{\rho_p}{\rho_f} + 1)}\,|v_p - v_f|^2 = 0 \qquad \text{(X-13)}$$

With the same initial condition as in Equation (X-8), Equation (X-13) can be integrated to yield

$$|v_p - v_f| = \left\{ \frac{0.66}{d_b\ (2\frac{\rho_p}{\rho_f} + 1)}\ t - \frac{1}{2\sqrt{\overline{u^2}}} \right\}^{-1} \qquad \text{(X-14)}$$

The expression for τ then becomes

$$\tau = \frac{1.16 d_b (2\frac{\rho_p}{\rho_f} + 1)}{\sqrt{\overline{u^2}}}\ \text{for } 500 < R_{e_p} < 10^5 \qquad \text{(X-15)}$$

or $$\frac{\tau}{\tau_s} = \frac{41.8\nu}{\sqrt{\overline{u^2}}\,d_b} = \frac{\psi_T'}{\psi_T} = \frac{83.6}{R_{e_p}} \qquad \text{(X-16)}$$

With τ defined, the values of ψ_T' in Equation (X-5) can be calculated for various measurements. These are shown in Table 5.

Figure 45 shows the relationship now between S_t^{-1} and ψ_T'. Better agreement is now noted. However the deviation between the circular jet measurements and the two dimensional flow field measurements (together with the theoretical two-dimensional prediction) is still noted.

In comparing the results of the present bubble diffusion measurements with the other diffusion measurements in circular jets with solid particles as contaminants (i.e. sediment in Singamsetti's and glass beads in Brush's), it is seen that the agreement is very good except for a point in Brush's data. This interesting result could be explained in the following conjecture. For a relatively small bubble moving in a turbulent liquid stream the bubble shape will remain approximately spherical due to the surface tension effect. If this is the case, the bubble can be considered as a rigid particle. The density effect of the particle has been accounted for by the particle parameter ψ_T'. Consequently the measured results unified through ψ_T' give a comparable S_t^{-1} - ψ_T' relationship as shown in Figure 45. Such results lead to the conclusion that with ψ_T' so defined the dependence of S_t^{-1} on the particle parameter ψ_T' is universal for measurements in similar flow fields regardless on whether the particle is heavier or lighter than the carrier stream. In other words the relationship between S_t^{-1} and ψ_T' is the same for similar flow fields for bubbles in water, solid particles in water or even aerosols in air streams.

One point yet unclarified, as noted previously, is that a two-dimensional and a three-dimensional flow field, appear to give different trends of S_t^{-1} - ψ_T'. This dilemma could be clarified by extending the experimental study to larger ψ_T' domain, such as measuring the diffusion of larger aerosols in both circular and plane air jets to see whether there exists a large deviation in between these two.

The relationship for S_t^{-1} versus ψ_T' as just described is originated form a rather intuitive background. The theoretical basis for the universality of such relationship is rather weak, and although confirmed by experiments, it deserves further study.

TABLE 5 Calculation of S_t^{-1} versus ψ'_T

Authors	$d_b(\mu)$	Particle Reynolds Number, R_{ep} $2\sqrt{\overline{u^2}}\,d_b/\nu$,	τ_s (10^{-3}sec.)	ψ_T	τ/τ_s		ψ'_T		S_t^{-1}
Present	343	338	3.52	5.28	0.154	(0.203)	0.81	(1.07)	0.94
Work	527	519	8.32	12.46	0.161	(0.172)	2.00	(2.14)	1.09
	780	768	18.07	27.30	0.109	(0.147)	2.97	(4.01)	1.11
	970	954	28.10	42.30	0.088	(0.134)	3.70	(5.67)	1.14
Singamsetti	68	136	3.43	4.68	0.223	(0.293)	1.04	(1.37)	1.23
	115	227	9.54	13.38	0.182	(0.238)	2.43	(3.18)	1.20
	230	454	38.20	53.40	0.138	(0.180)	7.37	(9.61)	1.24
	320	631	73.70	101.50	0.132	(0.158)	13.40	(16.00)	1.37
	460	907	152.20	213.00	0.092	(0.138)	19.60	(29.40)	1.44
Brush	190	374	17.55	23.50	0.148	(0.195)	3.48	(4.58)	1.00
	320	631	49.90	67.00	0.132	(0.158	8.85	(10.60)	2.00
	550	1084	147.80	196.00	0.080	(0.160)	15.60	(31.30)	6.70

Reproduced from best available copy.

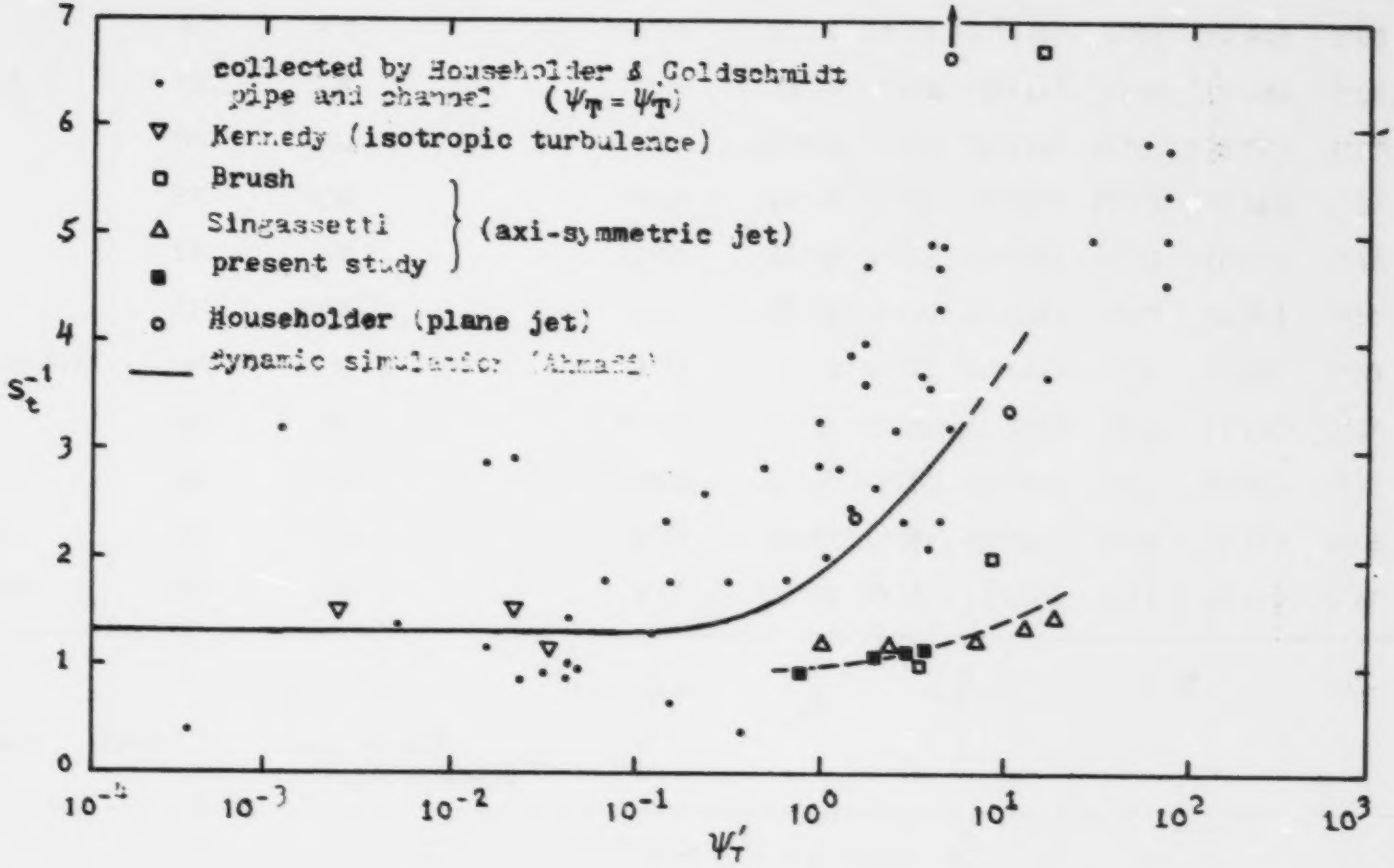

FIG. 45 DEPENDENCE OF S_t^{-1} ON PARTICLE PARAMETER ψ_T'

SECTION XI

SIGNIFICANCE OF RESULTS

The experiments convincingly show that the turbulent transport coefficient of suspended particles is not necessarily equal to that of momentum. As a matter of fact an increasing eddy diffusivity coefficient with particle size is noted. This is observed for small particles in the Stokes regime, smaller than the turbulent macroscale of the carrier stream.

The results of Figure 44 exhibit then when a particle can be considered to have a turbulent transport same as that for the momentum of the carrier stream. As an example, a grain of sand, 50 microns in diameter, when suspended in water flowing from a plane 2 inch nozzle at about 5 ft./sec. would have a ψ_T parameter of about 0.05. For such a case the transport coefficients (of the sand and carrier stream momentum) would be equivalent. However, if the channel width were to be in the order of 1/16 of an inch (then $\psi_T \approx 1.5$ and) the transport coefficient of the sand would now be in the order of three times more than that of the momentum of the fluid! Estimates of the corresponding dispersion of the effluent sand should then correctly account for this somewhat startling result.

SECTION XII

ACKNOWLEDGEMENTS

The reported work was the result of the Ph.D. research of Dr. Strong C. Chuang. Professor Victor W. Goldschmidt acted as supervisor of his work.

The support of the project by the Water Quality Office Environmental Protection Agency, and the help provided by Mr. George Ditsworth, Project Representative is acknowledged.

The assistance of the staff of the School of Mechanical Engineering and its Ray W. Herrick Laboratories during the final stages of the work reported is also gratefully acknowledged.

Preceding page blank

SECTION XIII

REFERENCES

Ahmadi, G. "Analytical Prediction of Turbulent Dispersion of Finite Size Particles," Ph.D Thesis, Purdue University, Lafayette, Indiana 1970.

Albertson, M. L., Dai, Y. B., Jensen, R. A., and Rouse, H. "Diffusion of Submerged Jets," American Society of Civil Engineers, Vol. 74, Dec., 1948, pp. 1571-1596.

Baker, James L. L. and Chao, Bei T. "An Experimental Investigation of Air Bubble Motion in a Turbulent Water Stream," American Institute of Chemical Engineers Journal, Vol. II, No. 2, March, 1965, pp. 268-273.

Batchelor, G. K. "Diffusion in a Field of Homogeneous Turbulence, I. Eulerian Analysis," Australian Journal of Scientific Research, Series A, Vol. 2, No. 4, 1949, pp. 437-450.

Batchelor, G. K. "Diffusion in a Field of Homogeneous Turbulence, II. The Relative Motion of Particles," Proc. Cambridge Phi. Soc., Vol. 48, 1952, pp. 345-362.

Batchelor, G. K. and Townsend, A. A. "Turbulent Diffusion," Surveys in Mechanics, Cambridge University Press, 1956, pp. 352-399.

Benzing, R. J. and Myer, J. E. "Low Frequency Bubble Formation at Horizontal Circular Orifices," Ind. & Eng. Chem. 47, 1955, pp. 2087-2090.

Binnie, A. M. "The Turbulent Spreading of the Water Jet," Engineering, Vol. 153, 1942, pp. 503.

Bird, Byron R., Stewart, Warren E., and Lightfoot, Edwin N. Transport Phenomena, John Wiley & Sons, Inc., New York, 1960, pp. 192-194.

Boussinesq, J. "Theory de L'Ecoulement Tourbillant," Mem. Pres. Par. Div. Sav. XXIII, Paris, 1877.

Brandon, C. A. "An Investigation of the Interaction of Solid Particles with Fluids in Turbulent Pipe Flow," Oak Ridge National Lab., Oak Ridge, Tenn., ORNL TM-2124, September, 1968.

Brooks, N. H. Discussion of "Acceleration Motion of a Spherical Particle" by M. R. Carstens Transactions, A. G. U., Vol. 34, 1953, pp. 947-950.

Brush, L. M. Jr. "Exploratory Study of Sediment Diffusion," J. of Geophysical Research, Vol. 67, No. 4, 1962, pp. 1427-1433.

Preceding page blank

Brush, L. M., Ho, H. W., and Singamsetti, S. R. "A Study of Sediment in Suspension," Publication No. 59 of the I. A. S. H. Commission of Land Erosion, 1965, pp. 293-310.

Calderbank, P. H. "The Inter-dispersion of Immiscible Fluid Phases," Brit. Chem. Engr., Vol. 1, 1956, pp. 206-209 and 267-274.

Carstens, M. R. "Accelerated Motion of a Spherical Particle" Trans., Ame. Geophysical Union, Vol. 33, No. 5, 1952, pp. 713-721.

Cermak, J. E. "Lagrangian Similarity Hypothesis Applied to Turbulent Shear Flow", J. of Fluid Mech., Vol. 15, 1963, pp. 49-64.

Chuang, S. C. and Goldschmidt, V. W. "The Response of a Hot Wire Anemometer to a Bubble of Air in Water", Symposium on Turbulence Measurement in Liquids, 9, 1969, Univ. of Mo., Rolla, Mo.

Chuang, S. C. and Goldschmidt, V. W. "Bubble Formation Due to a Submerged Capillary Tube in Quiescent and Co-flowing Streams", ASME Nucleonics Symposium, May, 1970. (ASME, Paper No. 70-FE-21)

Collis, D. C. and Williams, N. J. "Two-dimensional Convection from Heated Wires at Low Reynolds Number," J. of Fluid Mech., Vol. 6, 1959, pp. 357-384.

Corrsin, S. "Investigation of Flow in an Axially Symmetric Heated Jet of Air," NACA W-94 ACR No. 3123, 1943.

Corrsin, S. and Uberoi, M. S. "Further Experiments on the Flow and Heat Transfer in a Heated Turbulent Air Jet," NACA Tech. Note No. 1865, 1949.

Corrsin, S. and Lumley, J. "On the Equation of Motion for a Particle in Turbulent Flow," Appl. Sci. Research, Vol. 6A 1956, pp. 114.

Corrsin, S. "Theory of Turbulent Dispersion", Proc. for Turb. Diff., Marseille, France, 1962, pp. 27-52.

Curtis, A. J. "Shock and Vibration Handbook", Edited by Harris and Crede, McGraw-Hill, 1960, Ch. 22.

Datta, R. L., Mapier, D. H. and Newitt, D. M. "The Properties and Behavior of Gas Bubbles formed at a Circular Orifice," Trans. Inst. Chem. Engr., Vol. 28, 1950, pp. 14-26.

Davidson, L. "A Study of the Formation of Gas Bubbles from Horizontal Circular Submerged Orifices," Ph.D. Thesis, Columbia U., 1951.

Davidson, L. and Schuler, B. O. G. "Rapid Formation of Gas Bubbles in a Viscous Liquid," Trans. Inst. Chem. Engr. Vol. 38, 1960, pp. 144-154.

Delhaye, J. W. "Hot-film Anemometry in Two Phase Flow," Two Phase Flow Instrumentation, Presented at 11th Nat'l American Society of Mechanical Engineering, American Institute of Chemical Engr. Heat Transfer Conf. 8 1969, Minneapolis, Minn. pp. 58-69.

Eckert, E. R. G. and Drake, R. M. Jr. Heat and Mass Transfer, McGraw Hill, Inc., N. Y., 1959.

Eversole, W. G.; Wagner, G. H. and Stackhouse, E., "Rapid Formation of Gas Bubbles in Liquids," Ind. Engr. Chem., Vol. 33, 1941, pp. 1459-1462.

Flora, J. J. J. and Goldschmidt, V. W. "Virtual Origin of a Free Plane Turbulent Jet" AIAA Journal Vol. 7, No. 12, 12, 1969, pp. 2344-2346.

Folsom, R. G. "Review of the Pitot Tube", Trans. ASME, Oct., 1956, pp. 1450.

Forstall, W. and Gaylord, E. W. "Momentum and Mass Transfer in a Submerged Water Jet," J. of Applied Mech., ASME Trans., Vol. 22, No. 2, 1955.

Frenkiel, F. N. "Turbulent Diffusion of Mean Concentration Distribution in a Flow Field of Homogeneous Turbulence," Advance in Applied Mech., Academic Press, Inc., 1953, pp. 61-107.

Frielander, S. K. "Behavior of Suspended Particles in a Turbulent Fluid" AIChE J. Vol. 3, No. 3, 9, 1957, pp. 381-385.

Goldschmidt, V. W. "Measurement of Aerosol Concentrations with a Hot Wire Anemometer," J. of Colloid Science, Vol. 20, No. 6, 1965, pp. 617-634.

Goldschmidt, V. W. and Eskinazi, S., "Two-Phase Turbulent Flow in a Plane Jet," Journal of Applied Mechanics, Vol. 33, Series E, No. 4, Dec., 1966, pp. 735-747.

Goldschmidt, V. W. and Householder, M. K. "Measurement of Aerosols by Hot Wire Anemometry," AFOSR Final Report, AFOSR No. 68-1492, July 1968, pp. 134-152.

Goldschmidt, V. W. and Householder, M. K., "The Hot Wire Anemometer as an Aerosol Droplet Size Sampler," Atmospheric Environment, Vol. 3, Nov., 1969, pp. 643-652.

Haberman, W. L. and Morton, R. K. "An Experimental Study of Bubbles Moving in Liquids," ASCE Trans. Paper No. 2799, 1953, pp. 227-252.

Heskestad, G. "Hot Wire Measurements in a Plane Turbulent Jet," J. of Applied Mech. Dec., 1965, pp. 721-739.

Hetsroni, G. and Sokolov, M. "Distribution of Mass, Velocity and Intensity of Turbulence in a Two Phase Turbulent Jet," Dept. of Nuclear Sci. and Mech. Engr., Technion, Israel Institute of Technology, Haifa, Israel, 1969.

Hinze, J. O. Turbulence McGraw Hill Co., Inc. 1959.

Hinze, J. O. and Van Der Hegge Zijnen B. G. "Transfer of Heat and Matter in the Turbulent Mixing Zone of an Axially Symmetrical Jet," Applied Sci. Research A. Mech. Heat, Vol. 1, 1949, pp. 435.

Ho, H. W. "Fall Velocity of a Sphere in a Field of Oscillating Fluid." Ph.D Thesis, Univ. of Iowa, Iowa City, Iowa, 1964.

Householder, M. K. "Turbulent Diffusion of Small Particles in a Two-dimensional Free Jet," Ph.D Thesis, School of Civil Engr., Purdue Univ., W. Lafayette, Ind., 1968.

Householder, M. K. and Goldschmidt, V. W. "Turbulent Diffusion and Turbulent Schmidt Number of Small Particles-Part I," Journal of the Engineering Mechanics Division, EM6, December 1969, pp. 1345-1367.

Hsu, Y. Y., Simon, F. F. and Graham, R. W. "Application of Hot-wire Anemometer for Two Phase Flow Measurements Such as Void Fraction and Slip Velocity," ASME Winter Meeting, Philadelphia, Pa., Nov., 1963.

Ismail, H. M. "Turbulent Transfer Mechanism and Suspended Sediment in Closed Channels," Trans. ASCEE Vol. 117, 1952, pp. 409-446.

Jones, B. G., Chao, B. T. and Shirazi, M. A. "An Experimental Study of the Motion of Small Particles in a Turbulent Fluid Using Digital Techniques for Statistical Data Processing," Nuclear Engr. Dept., Univ. of Ill., Urbana, Ill., 1966.

Kada, H. and Hanratty, T. J. "Effects of Solids on Turbulence in a Fluid," AIChE J. Vol. 6, No. 4, 12, 1960, pp. 624-630.

Kalinske, A. A. and Pien, C. L. "Eddy Diffusion," Ind. Engr. Chem., Vol. 36, 1944, pp. 220.

Kampe de Feriet, J., Proc. 5th Intern. Congr., Appl. Mech., Cambridge, Mass., 1938, pp. 352.

Keagy, W. R. and Weller A. E., Proc., Heat Transfer and Fluid Mechanics Inst., Berkeley, Calif., 1949, pp.89.

Kennedy, D. A. "Some Measurements of the Dispersion of Spheres in a Turbulent Flow," Ph.D. Thesis, Dept. of Mechanics, The John Hopkins Univ., Baltimore, Maryland, 1965.

Kraichnan, R. H. "Dispersion of Particle Pair in Homogeneous Turbulence" The Physics of Fluids, Vol. 9, No. 10, 1966, pp. 1937-1943.

Kuethe, A. M. "Investigations of the Turbulent Mixing Regions Formed by Jets," J. Appl. Mech., Vol. 2, No. 3, 1935, pp. A-87-95.

Kumar, A. "Bubble Formation in Fluids of Low Viscosity Under Constant Flow Conditions," Chem. Tech., Vol. 19, 1967, pp. 78-82.

Laursen, E. M. "The Total Sediment Load of Stream," Proc., ASCE, Feb., 1958, pp. 1-36.

Leibson, I., Holcomb, E.G., Cacoso, A.G. and Jacmic, J.J. "Rate of Flow and Mechanics of Bubble Formation From Single Submerged Orifices," AICHE J., Vol. 2, 1956, pp. 296-306.

Levich, V.G. and Kuchanov, S.I. "Motion of Particles Suspended in Turbulent Flow," Soviet Physics Doklady, Vol. 12, No. 6, 12, 1967, pp. 546-548.

Lin, C.C. "On a Theory of Dispersion by Continuous Movement-I," Proc. Nat. Academy of Sci., Vol. 46, 1960a, pp. 566-570.

Lin, C.C. "On a Theory of Dispersion by Continuous Movement-II," Stationary Anisotropic Process," Proc., Nat. Academy of Sci., Vol. 46, 1960b, pp. 1147-1150.

Liu, C.L. "Characteristics of Hot Wire and Hot Film Sensors for Turbulence Measurements in Liquids", Ph.D. Thesis, School of Civil Engr., Purdue University, W. Lafayette, Indiana, 1967.

Longwell, J.P. and Weiss, M. "Mixing and Distribution of Liquid in High Velocity Air Streams," Ind. Engr. Chem., Vol. 45, 1953, pp. 667-677.

MacIntyre, F. "Vibrating Capillary for Production of Uniform Small Bubbles," Review of Sci. Inst., Vol. 38, No. 7, 1967, pp. 969.

Majumdar, H. and Carstens, M.R. "Diffusion of Particles by Turbulence: Effect of Particle Size," Final Report G. R. No. 5, Vol. WP00912-02ESE, C.E., Git., Atlanta, Ga., 1967.

Milne-Thomson, L.M. Theoretical Hydrodynamics, 3rd Edition, London: MacMillan & Co., Ltd., 1955.

Pattle, R.E. "The Aeration of Liquids, Pt. II. Factors in the Production of Small Bubbles," Trans. Inst. Chem. Engr., Vol. 28, 1950, pp. 32-37.

Ramakrishnan, S., Kumar, R. and Kuloor, N.R. "Studies in Bubble Formation-I, Bubble Formation Under Constant Flow Conditions," Chem. Engr. Sci., Vol. 24, 1969, pp. 731-747.

Rennie, J. and Evans F. "The Formation of Froths and Foams above Sieve Plates," Brit. Chem. Engr., Vol. 7, 1962, pp. 498-502.

Roberts, P.H. "On the Application of a Statistical Approach of the Theory of Turbulent Diffusion," J. of Math. and Mech., Vol. 6, 1957, pp. 781-799.

Roberts, P.H. "Analytical Theory of Turbulent Diffusion", N.Y.U., June, 1960, Research Report No. HSN-2.

Rouse, H. "Experiments on the Mechanics of Sediments Suspension, "Proc., Fifth Intern. Cong. of Appl. Mech., Cambridge, Mass., 1938, pp. 550-554.

Sayre, W. W. and Chang, F. M. "A Laboratory Investigation of Open-Channel Dispersion Process for Dissolved, Suspended, and Floating Dispersants," Geological Survey Professional Paper 433-E. 1968.

Schlichting, H. Boundary Layer Theory, McGraw Hill Book Co., 1960.

Shirazi, M. A., Chao, B. T. and Jones, B.G. "On the Motion of Small Particles in a Turbulent Fluid Field," Nuclear Eng. Dept. Univ. of Ill., Urbana, Ill., 1967.

Siemes, W. "Gas Bubbles in Liquids-I, the Formation of Gas Bubbles at Upward Pointing Circular Orifices," Chem. Ing. Techn., Vol. 26, 1954, pp. 479-496.

Singamsetti, S. R. "Diffusion in a Submerged Jet," Proc. ASCE, No. Hy-2, 1966, pp. 153-168.

Smith, F. B. "The Turbulent Spread of a Falling Cluster," Advances in Geophysics, Vol. 6, 1959.

Soo, S. L., Ihrig, H. K. J. and El Kouh, A. F. "Experimental Determination of Statistical Properties of Two Phase Turbulent Motion," J. of Basic Engr., ASME Trans., 9, 1960.

Squire, H. B. and Trouncer, B. A. J. "Round Jets in a General Stream," Great Britain Aero. Res. Council Rept. & Memo. No. 1974, 1944.

Stanisic, M. M. and Groves, R. N. "On the Eddy Viscosity of an Incompressible Turbulent Flow," J. of Applied Math. and Physics, ZAMP, Vol. 16, 1965, pp. 709-712.

Sullivan, S. L. Jr., Hardy, B. W. and Holland, C. D. "Formation of Air Bubbles at Orifices Submerged Beneath Liquids," AIChE Vol. 10, 1964, pp. 848.

Taylor, G. I. "Diffusion by Continuous Movements," Proc. of the London Math. Soc., Ser. 2, Vol. 20, 1921, pp. 196-212.

Tchen, C. M. "Mean Value and Correlation Problems Connected with the Motion of Small Particles Suspended in a Turbulent Fluid," Dissertation, Delft, Martinus Nijhoff, The Hague, Netherlands, 1947.

Tomotika, S., Proc. Roy. Soc. London, 165A, 1938, pp. 65.

Trentacoste, N. and Sforza, P. "Further Experimental Results for Three Dimensional Free Jets," AIAA J. Vol. 5, No. 5, 1967, pp. 885-891.

Valentin, F. H. H. "Absorption in Gas-Liquid Dispersions" Spon's Chemical Engr. Senis, London, 1967.

Vanoni, V. A. "Transportation of Suspended Sediment by Water" Trans. ASCE., Vol. III, 1946, pp. 67-133.

SECTION XIV

PUBLICATIONS

The following is a list of publications which resulted due (in part or fully) to the sponsorship of Grant 16070DEP by The Water Quality Office, EPA. Abstracts are presented in Appendix V.

1. S. C. Chuang and V. W. Goldschmidt "The Response of a Hot Wire Anemometer to a Bubble of Air in Water" Symposium on Turbulence Measurements in Liquids, University of Missouri, Rolla, Missouri, September 1969.

2. S. C. Chuang and V. W. Goldschmidt "Bubble Formation Due to a Submerged Capillary Tube in Quiescent and Co-Flowing Streams" ASME, J. Basic Engineering, Vol. 92, D, No. 4, December 1970, pp 705-711.

3. G. Ahmadi and V. W. Goldschmidt "Dynamic Simulation of The Turbulent Diffusion of Small Particles" Hydrotransport I, First International Conference on The Hydraulic Transport of Solids in Pipes, University of Warwick, Sponsored by The BHRA Cranfield, Bedford, England, September 1-4, 1970.

4. G. Ahmadi and V. W. Goldschmidt "Analytical Prediction of The Turbulent Diffusion of Small Particles," Fluid Dynamics Symposium, McMaster University, Hamilton, Ontario, August 25-27, 1970.

The following articles are currently under the review and pre-publication process:

5. V. W. Goldschmidt and S. C. Chuang "Energy Spectrum and Turbulent Scales in an Axi-Symmetric Water Jet" Submitted to the ASME.

6. V. W. Goldschmidt, M. K. Householder, G. Ahmadi and S. C. Chuang "Turbulent Diffusion of Small Particles Suspended in Turbulent Jets" Submitted for consideration at a forthcoming Symposium on Two Phase Flows.

Preceding page blank

SECTION XV

GLOSSARY OF SYMBOLS

A_1, A_2	numerical constants
A_s	intercepting area of the sensor
a	virtual origin of the jet, defined by equation VI-4 and VI-5
a_1, a_2, a_3	coefficients given in Eq. (VI-15)
b	characteristic jet width; temperature coefficient of the electric resistivity of the sensor
b_u	half width of the velocity profile
b_n	half width of the concentration flux profile
b_γ	half width of the concentration profile
C_D	drag coefficient
C_w	specific heat of the sensor
c	correction factor in pitot tube measurement
c_ω	numerical constant related to the vorticity transport mixing length
c_ℓ	numerical constant related to the scalar quantity transport mixing length
D	jet nozzle diameter
d_b	bubble diameter
d_b^*	d_b/d_i
d_i	inside diameter of the syringe tube
d_o	outside diameter of the syringe tube
d_o^*	d_o/d_i
d_w	sensor diameter
E	mean DC voltage output (measured)
e_p	peak voltage drop in the sensor due to an impacting bubble

Preceding page blank

E_t	mean DC voltage output (true value)
e	fluctuation voltage output due to the turbulent velocity fluctuation
e_f	DC voltage output at a particular frequency f
e_s	voltage drop due to an impacting bubble
F	Froude number = $d_i f \sqrt{gd_i}$
f	bubble generating frequency; frequency of turbulence
h	distance from the center of the sphere to the wall
h_1, h_2	heat transfer coefficients per unit length of the wire exposed to the air and the water phase respectively
K	axial conductivity of a sensor; wave number
K_u	constant in Eq. (VI-17)
k_1, k_2	heat conduction coeff. of the air and of the water at the film temperatures T_{f1} and T_{f2} respectively
k_b	rate of half width spreading in a jet, Eq. VI-4
k_u	decaying rate of the jet center line velocity, Eq. VI-5
k_h	rate of concentration half width spreading, Eq. VI-22
k_γ	center line concentration decaying rate, Eq. VI-23
L_r	length scale in r-direction
L_x	length scale in x-direction
L_θ	length scale in θ-direction
ℓ	mixing length related to the momentum transport; effective length of the sensor
ℓ_ω	mixing length related to the vorticity transport
M	$\rho_w \pi \, d_b^3/6$
N	bubble concentration flux
N_o	bubble concentration flux at the jet mouth
N_{u1}, N_{u2}	Nusselt number for sensor exposed to air and water phase respectively

n	number of bubbles impacting in a time period τ
$\vec{n}_g$	mass flux vector of gas
$\vec{n}_w$	mass flux vector of water
P	mean pressure
P_m	measured static pressure by pitot tube
P_T	true static pressure
P'	instantaneous pressure
p	fluctuation pressure
p_o	static pressure in the outside field of a jet
P_{r2}	Prandtl number of the water
Q	gas flow rate through a syringe tube
R	correlation coeff. of two fluctuating velocity components; total electric resistance of a sensor; Reynolds number
R_e, R_{e1}, R_{e2}	orifice Reynolds number of the jet, Reynolds number of the air and water phases based on the sensor diameter
R_{e_p}	particle Reynolds numbers $\frac{\lvert v_p - v_f \rvert \; d_b}{\nu}$ $\frac{2\sqrt{u^2}\; d_b}{\nu}$ or $\frac{\sqrt{u^2}\; d_b}{\nu}$
r	radial coordinate
r_b	gas bubble radius
r_o	electric resistance at wire temperature T_o
S	area of the stagnation pressure tap of a pitot tube
S_t	turbulent Schmidt number related to the bubble diffusion; sensor sensitivity based on the traverse time, t, of an impacting bubble
S_E	sensor sensitivity to the impacting bubbles based on the voltage drop, e_p
S_u	sensor sensitivity to the velocity of the water stream

s	distance from sphere center to the syringe tube orifice
T	time period measurement
T_e	ambient temperature of a sensor in water
T_{f1}, T_{f2}	film temperature of the sensor in the air and water phases respectively
t	time coordinate;traverse time of a bubble; outside diameter of a pitot tube
U	mean axial velocity
U_{axis}, U_m	mean axial velocity at the jet axis
U'	instantaneous axial velocity
U_o	jet efflux velocity
u	axial fluctuating velocity
u_f	fluctuating velocity scale
u_r	radial fluctuating velocity scale
u_x	axial fluctuating velocity scale
u'	$\sqrt{\overline{u^2}}$
u_θ	tangential fluctuating velocity
V	mean radial velocity; co-flowing velocity for bubble generation; general stream velocity
V_m	general stream velocity measured by pitot tube
$\overline{V}$	mean velocity of the flow field with velocity gradient measured by the pitot tube
V'	instantaneous radial velocity
V_b	bubble velocity
V_w	average impressed velocity due to the wake of the detached bubble
V^*	$V/(d_i f)$
v	radial fluctuating velocity
$\vec{v}$	velocity vector of bubbles and water mixture
$\vec{v}_g$	velocity vector of bubbles

$\vec{v}_w$	velocity vector of water
W	Weber number
W'	instantaneous tangential velocity
w	tangential fluctuating velocity
x	axial coordinate
x_c	potential core distance of the jet
x_t	axial distance between dynamic and static taps of a pitot tube
ρ, ρ_w, ρ_g	fluid density, water density, gas density
ρ'	$\rho_g' + \rho_w'$
ρ_g'	$\rho_g \Gamma v$
ρ_w'	$\rho_w (1 - \Gamma v)$
σ_{xr}	Reynolds stress
$(.)_m$	maximum quantity of (.)
η	$r/(x+a)$
η_*	$(c^2/\omega^2)^{-1/3}\eta$
ξ	$(x+a)/D$
Γ	mean concentration
Γ_o	concentration at efflux of the jet
Γ'	instantaneous concentration
γ	fluctuating component of the concentration
θ	tangential coordinate
ν	kinematic viscosity
$\varepsilon_m, \varepsilon_\gamma, \varepsilon_{\gamma o}$	eddy diffusivity of momentum, bubble and marked fluid particle respectively
$\mathcal{D}$	mass diffusivity (molecular effect)

ε	instantaneous DC voltage output of the total signal
ξ	instantaneous DC voltage output of the turbulent signal
χ	numerical constant related to mixing length
ω	$2\pi f$
ψ_T, ψ_T'	particle parameter, defined in Equation (X-1) and (X-5), respectively
Λ_x	longitudinal macroscale
$E(f)$	energy spectrum in terms of frequency
$F(K)$	energy spectrum in terms of wave number
$F(\eta)$	$\int_o^\eta d\eta f(n)$,
$f(t)$	half length of the wire exposed to the air bubble
$f(\eta)$	U/U_m
$g(\eta)$	V/U_m
$g(\omega)$	Fourier coefficient of $E(f)$
$h(\eta)$	$\sigma_{xr}/\rho U_o^2$
$I(t)$	instantaneous current across the sensor
$K(\eta)$	Γ/Γ_m
$r(y,t)$	electric resistivity per unit length at location y and at time t
$T_b(t)$	instantaneous bubble temperature
$T_w(y,t)$	wire temperature at position y and time t
$v(y)$	velocity in a flow field possessing gradient
$\phi(\xi)$	$D/(x+a)$
$\psi(\xi)$	U_m/U_o
$\mathcal{V}$	volume of one bubble
τ	particle Response time (general)
τ_s	Stokesian Particle Response time

SECTION XVI

APPENDICES

APPENDIX I

Derivation of Equation VI-1

The averaged steady Navier Stokes equation in cylindrical coordinates for an axi-symmetric turbulent jet, assuming $U' = U + u$, $V' = V + v$, $W' = w$, $P' = P + p$, $\frac{\partial\,\overline{\cdot}}{r\partial\theta} = 0$, $\frac{\partial^2\overline{\cdot}}{r^2\partial\theta^2} = 0$, reads,

x-component $$U\frac{\partial U}{\partial x} + V\frac{\partial U}{\partial r} = -\frac{1}{\rho}\frac{\partial p}{\partial x} + \frac{\partial}{\partial x}\left(-\overline{u^2} + \nu\frac{U}{x}\right)$$

$$+ \frac{1}{r}\frac{\partial}{\partial r}\quad r\left(-\overline{uv} + \nu\frac{\partial U}{\partial x}\right) \qquad \text{(A-I-1)}$$

r-component $$U\frac{\partial V}{\partial x} + V\frac{\partial V}{\partial r} = -\frac{1}{\rho}\frac{\partial p}{\partial r} + \frac{\partial}{\partial x}\left(-\overline{uv} + \nu\frac{\partial V}{\partial x}\right)$$

$$+ \frac{1}{r}\frac{\partial}{\partial r}\quad r\left(-\overline{v^2} + \nu\frac{\partial V}{\partial r}\right) - \frac{1}{r}\left(-\overline{w^2} + \nu\frac{V}{r}\right) \qquad \text{(A-I-2)}$$

where U', V', W' are instantaneous velocities in the axial, radial and tangential directions respectively and U, V, and W are respectively the mean velocities and u, v, w are the fluctuation components.

The length scales L_x, L_r and L_θ for the x, r and θ directions respectively may be defined. Then $\frac{L_r}{L_x} \sim \frac{L_\theta}{L_x} << 1$ (since the range of mixing in axial direction is much larger than in the radial direction). Letting u_x, u_r and u_θ be the corresponding velocity scales and assuming that u_r and u_θ have the same order of magnitude, the equation of mass conservation then gives the following relationship

$$\frac{u_x}{L_x} \sim \frac{u_r}{L_r} \sim \frac{u_\theta}{L_\theta}$$

Furthermore, a fluctuation velocity scale u_f such that

$$\overline{u^2} \sim \overline{v^2} \sim \overline{w^2} \sim u_f^2$$

and $\overline{uv} \sim \overline{uw} \sim \overline{vw} \sim R\, u_f^2$

can be defined. R is the correlation coefficient between two fluctuation components and ranges between 0 and 1. The order of magnitude of the various terms in Equations A-I-1 and A-I-2 is then given by

$$U \frac{\partial U}{\partial x} + V \frac{\partial U}{\partial r} = - \frac{1}{\rho} \frac{\partial p}{\partial x} - \frac{\partial \overline{u^2}}{\partial x} - \frac{1}{r} \frac{\partial}{\partial r} (r\, \overline{uv}) \qquad \text{(A-I-3)}$$

$$\begin{array}{llllll}
\text{order} & \dfrac{u_x^2}{L_x} & \dfrac{u_x^2}{L_x} & \dfrac{\Delta p_x}{\rho L_x} & \dfrac{u_f^2}{L_x} & \dfrac{R\, u_f^2}{L_r} \\[2ex]
\text{or} & 1 & 1 & \dfrac{\Delta p_x}{\rho u_x^2} & \dfrac{u_f^2}{u_x^2} & \dfrac{R\, u_f^2\, L_x}{u_x^2\, L_r}
\end{array}$$

$$U \frac{\partial V}{\partial x} + V \frac{\partial V}{\partial r} = - \frac{1}{\rho} \frac{\partial p}{\partial r} - \frac{1}{r} \frac{\partial}{\partial r} (r \overline{v^2}) - \frac{\partial \overline{uv}}{\partial x} + \frac{\overline{w^2}}{r} \qquad \text{(A-I-4)}$$

$$\begin{array}{lllllll}
\text{order} & \dfrac{u_x L_r}{L_x^2} & \dfrac{u_x^2 L_r}{L_x^2} & \dfrac{\Delta p_r}{\rho L_r} & \dfrac{u_f^2}{L_r} & \dfrac{R u_f^2}{L_x} & \dfrac{u_f^2}{L_r} \\[2ex]
\text{or} & 1 & 1 & \dfrac{\Delta p_r L_x^2}{\rho u_x^2} & \dfrac{u_f^2 L_x^2}{u_x^2 L_r^2} & \dfrac{R u_f^2 L_x}{u_x^2\, L_r} & \dfrac{u_f^2 L_x^2}{u_x^2 L_r^2}
\end{array}$$

In the above expressions Δp_x and Δp_r represent the change of pressure in the x and r directions respectively and the viscous terms have been neglected. In reviewing the order of magnitude, it is concluded that in the first equation

$\dfrac{\partial \overline{u^2}}{\partial x}$ is much smaller than $\dfrac{1}{r} \dfrac{\partial}{\partial r}(r\overline{uv})$ and is hence neglected;

in the second equation the terms in the left hand side are at least one order less than the terms in the right hand side and hence are also neglected, moreover in the right hand side of the second equation $\dfrac{\partial \overline{uv}}{\partial x}$ is one order less than the other terms and is also neglected. The final form of the equations simplifies to

$$U \frac{\partial U}{\partial x} + V \frac{\partial U}{\partial r} = - \frac{1}{\rho} \frac{\partial p}{\partial x} - \frac{1}{r} \frac{\partial}{\partial r} (r\overline{uv}) \qquad \text{(A-I-5)}$$

$$\frac{1}{\rho} \frac{\partial p}{\partial r} + \frac{\partial}{\partial r} \overline{v^2} + \frac{\overline{v^2} - \overline{w^2}}{r} = 0 \qquad \text{(A-I-6)}$$

Equation A-I-6 can be integrated with respect to r to give

$$p + \rho\overline{v^2} + \rho \int dr \, \frac{\overline{v^2} - \overline{w^2}}{r} = P_o \qquad \text{(A-I-7)}$$

where P_o is the pressure at the same section but outside the turbulent region. Equation A-I-7 states that the pressure in a jet flow field is only a function of r and is independent of x. With such equation (A-I-5) simplifies to

$$U \frac{\partial U}{\partial x} + V \frac{\partial U}{\partial r} = \frac{1}{\rho r} \frac{\partial}{\partial r} (r \, \sigma_{xr}) \qquad \text{(III-1)}$$

where

$$\sigma_{xr} = - \rho\overline{uv}$$

APPENDIX II

Derivation of Equations (VI-3) to (VI-5)

Dividing Equation (VI-1) by U_o^2 one obtains

$$\frac{U}{U_o} \frac{\partial}{\partial x} \left(\frac{U}{U_o}\right) + \frac{V}{U_o} \frac{\partial}{\partial r} \left(\frac{U}{U_o}\right) = \frac{1}{r} \frac{\partial}{\partial r} \left(\frac{r \, \sigma_{xr}}{\rho U_o^2}\right) \qquad \text{(A-II-1)}$$

where U_o is the jet efflux velocity. The conservation of momentum requires that

$$\int_o^\infty r \, dr \left(\frac{U}{U_o}\right)^2 = \text{Constant} \qquad \text{(A-II-2)}$$

Now denoting

$$\frac{U}{U_m} = f(\eta) \qquad\qquad \frac{\partial \cdot}{\partial r} = \frac{1}{D} \psi \frac{\partial \cdot}{\partial \eta}$$

$$\frac{V}{U_m} = g\ (\eta) \qquad \frac{\partial \cdot}{\partial x} = \frac{\partial \cdot}{\partial \eta} \ \frac{\partial \eta}{\partial \xi} \ \frac{\partial \xi}{\partial x} + \frac{\partial \cdot}{\partial \xi} \ \frac{\partial \xi}{\partial x} \qquad \text{(A-II-}$$

$$\frac{U_m}{U_o} = \psi(\xi) \qquad = \frac{1}{D} \ \frac{\eta}{\phi} \ \frac{d\phi}{d\xi} \ \frac{\partial \cdot}{\partial \eta} + \frac{1}{D} \frac{\partial \cdot}{\partial \xi}$$

$$\frac{\sigma_{xr}}{\rho U_m^2} = h\ (\eta)$$

where $\eta = \frac{r}{D}\,\phi(\xi)$ and $\xi = \frac{x+a}{D}$

then Equations A-II-1 and A-II-2 become

$$f\psi\left(\frac{\psi}{\phi}\ \eta\ \frac{d}{d\xi}\phi\ \frac{df}{d\eta} + f\ \frac{d\psi}{d\xi} \right) + g\psi^2\phi\ \frac{df}{d\eta} = \frac{\phi\psi^2}{\eta}\ \frac{d}{d\eta}\ (\eta h) \qquad \text{(A-II-4}$$

$$\frac{\psi^2}{\phi^2} \int_o^\infty d\ \eta\ \eta\ f^2 = \text{Constant} \qquad \text{(A-II-5}$$

Now consider more closely the term occuring in Equation A-II-5. It appears to consist of the product of two terms, one of which is a function of ξ alone. Hence similarity can be achieved only if these functions of ξ are constant, i.e. $\psi = A_1\phi$ where A_1 is a numerical constant. Substituting this relation into Equation A-II-4 then

$$\phi\ \frac{d\phi}{d\xi}\ (\eta f\ \frac{df}{d\eta} + f^2) + \phi^3 \left[g\ \frac{df}{d\eta} - \frac{1}{\eta}\ \frac{d}{d\eta}\ (\eta h) \right] = 0 \qquad \text{(A-II-6}$$

The terms in the above expression also appear to consist of two parts, one a function of ξ the other a function of η alone. Hence similarity requires that

$\phi \frac{d\phi}{d\xi} = B\ \phi^3$, where B is an arbitrary constant.

A solution of this differential equation reads

$$\phi = \frac{D}{x+a}$$

hence

$$\psi = \frac{A_1}{\xi} = \frac{A_1 D}{x+a}$$

$$\eta = \frac{r}{x+a}$$

In such a manner, Equation A-II-6 becomes

$$f^2 + \eta f f' - g f' + \frac{1}{\eta} \frac{d}{d\eta} (\eta h) = 0 \qquad \text{(A-II-7)}$$

Writing the equation of continuity in terms of $f(\eta)$ and $g(\eta)$, the function $g(\eta)$ in Equation A-II-7 can then be eliminated and Equation A-II-7 simplified to

$$- \frac{FF''}{\eta} - \frac{1}{\eta} (F')^2 + \frac{F}{\eta^2} F' = \frac{d}{d\eta} (\eta h) \qquad \text{(A-II-8)}$$

where

$$F(\eta) = \int_o^\eta \eta \; f(\eta) \quad d\eta$$

Equation A-II-8 after integration yields

$$h(\eta) = -\frac{FF'}{\eta^2} = - \frac{f}{\eta} \int_o^\eta \eta \; f(\eta) \; d\eta \qquad \text{(A-II-9)}$$

where the constant of integration must be zero, since $h(\eta)$ is finite at $\eta=0$. Writing in the original notation, Equation A-II-9 becomes

$$\frac{\sigma_{xr}}{\rho U_m^2} = - \frac{1}{\eta} \frac{U}{U_m} \int_o^\eta d\eta \; \eta (\frac{U}{U_m}) \qquad \text{(VI-3)}$$

Furthermore, the similarity of the flow field requires that $\phi = \frac{D}{r}\eta = \frac{D}{x+a}$, consequentely $\eta = \frac{r}{x+a}$ or $r = \eta(x+a)$. Now letting b_u be the value of r where the velocity is half the maximum at each section and k_b the corresponding value of η, then

$$b_u = k_b \; (x+a)$$

or

$$\frac{b_u}{D} = k_b \left(\frac{x}{D} + \frac{a}{D}\right) \qquad \text{(VI-4)}$$

Equation (VI-4) states that the velocity half width increases linearly along the axial direction

Moreover, $\frac{U_m}{U_o} = \psi(\xi) = \frac{A_1}{\xi} = \frac{A_1 \ D}{x+a}$, and letting $1/A_1 = k_u$, then

$$\frac{U_o}{U_m} = k_u \left(\frac{x}{D} + \frac{a}{D}\right) \qquad \text{(VI-5)}$$

Equation (VI-5) states that the inverse of the center line velocity decay is also linearly proportional to the axial direction.

Equations (VI-4) and (VI-5) are the immediate consequences of the similarity of the jet flow field.

APPENDIX III

Derivation of Equation (VI-11)

Introducing $F(\eta)$ as given in Appendix II into Equation (VI-7)

$$\frac{\varepsilon_m}{U_m \ (x+a)} = - \frac{\frac{F}{\eta} \ \frac{dF}{d\eta}}{\eta \frac{d}{d\eta}\left(\frac{1}{\eta} \ \frac{dF}{d\eta}\right)}$$

or

$$-F \ \frac{dF}{d\eta} = \frac{\varepsilon_m}{U_m \ (x+a)} \ \eta^2 \ \frac{d}{d\eta} \ \left(\frac{1}{\eta} \ \ \frac{dF}{d\eta}\right).$$

This equation can be integrated readily to give

$$\frac{\varepsilon_m}{U_m (x+a)} \ \left(\eta \frac{dF}{d\eta} - 2F\right) = - \frac{1}{2} \ F^2.$$

The constant of integration must be zero, because at $\eta=0$, $F(\eta)$ must be zero. The second integration yields

$$F(\eta) = \frac{2\,C\,\eta^2}{1 + [\,U_m(x+a)/2\varepsilon_m]C\eta^2}$$

The constant of integration C follows from the condition that f(0) = 1. This yields C=1/4. Consequently

$$\frac{U}{U_m} = \left[1 + \frac{U_m(x+a)}{8\,\varepsilon_m}\,\eta^2\right]^{-2} \qquad \text{(VI-11)}$$

APPENDIX IV

Derivation of Equations (VI-19) to (VI-23)

Consider the body of water with bubbles as a "gas-water" mixed solution. Let

$\mathcal{V}$ = volume of one gas bubble

Γ' = number of gas bubbles per unit volume of solution

ρ'_g = mass of gas per unit volume of solution $(=\rho g\Gamma v$, where ρ_g is the gas density)

ρ'_w = mass of water per unit volume of solution $(=\rho_w(1-\Gamma' v)$, where ρ_w is the water density)

ρ' = density of the solution $(= \rho'_g + \rho'_w)$

$\vec{v}_g$ = velocity vector of gas species

$\vec{v}_w$ = velocity vector of water species

$\vec{v}$ = velocity vector of solution $\left(= \dfrac{\rho'_g\,\vec{v}_g + \rho'_w\,\vec{v}_w}{\rho'}\right)$

$\vec{n}_g$ = mass flux vector of gas $(=\rho'_g\,\vec{v}_g)$

$\vec{n}_w$ = mass flux vector of water $(=\rho'_w\,\vec{v}_w)$

D = mass diffusivity (molecular effect)

then Fick's first law gives the following relation (Bird, Stewart and Lightfoot (1960)).

$$\vec{n}_g = \frac{\rho'_g}{\rho'}(\vec{n}_g + \vec{n}_w) - \rho'\,D\,\nabla\left(\frac{\rho'_g}{\rho'}\right) \qquad \text{(A-IV-1)}$$

The above equation states that the diffusion flux of gas species is the resultant of two vectors. The first is the flux of gas resulting from the convection of the fluid motion, and the second is the flux of gas resulting from the diffusion superimposed on the bulk convective flow. The conservation of mass for the gas species reads

$$\frac{\partial \rho'_g}{\partial t} + \nabla \cdot \vec{n}_g = 0 \qquad \text{(A-IV-2)}$$

Substituting Equation A-IV-1 into A-IV-2, and noting that $\vec{n}_g + \vec{n}_w = \rho' \vec{v}$, then

$$\frac{\partial \rho'_g}{\partial t} + \nabla \cdot \rho'_g \vec{v} = \nabla \cdot \left\{ \rho' D \nabla \left(\frac{\rho'_g}{\rho'} \right) \right\} \qquad \text{(A-IV-3)}$$

After changing notation, the above becomes

$$\frac{\partial (\rho_g v \Gamma')}{\partial t} + \nabla \cdot \left[(\rho_g \Gamma' v) \vec{v} \right] = \nabla \cdot \left\{ \left[\rho_g \Gamma' v + \rho_w (1 - \Gamma' v) \right] D \nabla \left[\frac{\rho_g \Gamma' v}{\rho_g \Gamma v + \rho_w (1 - \Gamma v)} \right] \right\}$$

(A-IV-4)

Since the bubble concentration is very low (in the order of 10^{-3} in volume) $\Gamma' v << 1$ and $\rho_g << \rho_w$. Hence $\rho_g \Gamma' v + \rho_w (1 - \Gamma' v) \simeq \rho_w$ or $\rho' \simeq \rho_w$, and Equation A-IV-4 can be approximated by

$$\frac{\partial (\rho_g v \Gamma')}{\partial t} + \nabla \cdot \left[(\rho_g \Gamma' v) \vec{v} \right] = \nabla \cdot \left\{ \rho_w D \nabla \left(\frac{\rho_g \Gamma' v}{\rho_w} \right) \right. \qquad \text{(A-IV-5)}$$

In the present case, the bubble size is relatively small such that the rising bubble velocity due to the buoyancy effect is less than the carrier stream velocity, consequentely $\vec{v}_g$ and $\vec{v}_w$ will be of the same order of magnitude and then $\rho'_g \vec{v}_g << \rho'_w \vec{v}_w$. The following relation is then approximately true

$$\vec{v} = \frac{\rho'_g \vec{v}_g + \rho'_w \vec{v}_w}{\rho'} \simeq \frac{\rho'_w \vec{v}_w}{\rho'} \simeq \vec{v}_w$$

From the above expression, Equation A-IV-5 further simplifies to

$$\frac{\partial (\rho_g \Gamma' v)}{\partial t} + \nabla \cdot \left[(\rho_g \Gamma' v) \vec{v}_w \right] = \nabla \cdot \left\{ D \nabla (\rho_g \Gamma' v) \right\} \qquad \text{(A-IV-6)}$$

In the above ρ_g and v are constant scalars, so they can be cancelled out. Finally Equation A-IV-6 becomes

$$\frac{\partial \Gamma'}{\partial t} + \vec{v}_w \cdot \nabla \Gamma' = \nabla \cdot \left\{ D \nabla \Gamma' \right\} \qquad \text{(A-IV-7)}$$

It is noted that in obtaining the above expression the solenoidality of the flow field has been assumed.

In steady state axi-symmetric turbulent jet flow, letting $\Gamma' = \Gamma + \gamma$, and neglecting the molecular effect, the final form of the governing equation for the bubble diffusion becomes

$$U \frac{\partial \Gamma}{\partial x} + V \frac{\partial \Gamma}{\partial r} = - \frac{1}{r} \frac{\partial}{\partial r} (r\ \overline{v\gamma}) \qquad \text{(VI-19)}$$

Similar to Appendix II the similarity requirement gives

$$\frac{\Gamma_m}{\Gamma_o} = A_2 \frac{D}{x+a}$$

$$\frac{\Gamma}{\Gamma_o} = A_2 \frac{D}{x+a} k(\eta)$$

where $\eta = \frac{r}{x+a}$ and $k(\eta) = \frac{\Gamma}{\Gamma_m}$.

Assuming that the origin of the apparent source for concentration diffusion is the same as that for the momentum diffusion, the combination of Equations (VI-19),(VI-20) and (A-II-3) will give the following relationship

$$-f \frac{d}{d\eta} (\eta k) + g \frac{dk}{d\eta} = \frac{1}{\eta} \frac{d}{d\eta} \left[\eta \frac{\varepsilon_\gamma}{U_m (x+a)} \frac{dk}{d\eta} \right] \qquad \text{(A-IV-8)}$$

After eliminating $g(\eta)$ by using the equation of continuity then

$$- \frac{1}{\eta} \frac{d}{d\eta} (Fk) = \frac{1}{\eta} \frac{d}{d\eta} \left[\eta \frac{\varepsilon_\gamma}{U_m (x+a)} \frac{dk}{d\eta} \right]$$

where $F(\eta)$ is as defined in Appendix II. Integrating the above equation and noticing that the constant of integration is zero

$$F(\eta)\ k(\eta) = - \frac{\varepsilon_\gamma}{U_m (x+a)} \eta \frac{dk}{d\eta}$$

The second integration will give the expression for the concentration profile as

$$\frac{\Gamma}{\Gamma_m} = \exp\left\{ - \int_o^\eta \frac{(x+a)\ U_m}{\varepsilon_\gamma \eta} \left[\int_o^\eta \eta \left(\frac{U}{U_m}\right) d\eta \right] d\eta \right\} \qquad \text{(VI-21)}$$

Let b_γ denote the value of r where the concentration is one half of the maximum, k_h denote the corresponding value of η then

$$\frac{b_\gamma}{D} = k_h \left(\frac{x}{D} + \frac{a}{D}\right) \qquad \text{(VI-22)}$$

The equation (VI-22) states that the concentration half width increases linearly along the axial direction.

Furthermore $\frac{\Gamma_m}{\Gamma_o} = A_2 \frac{D}{x+a}$, and for $1/A_2 = k_\gamma$ then

$$\frac{\Gamma_o}{\Gamma_m} = k_\gamma \left(\frac{x}{D} + \frac{a}{D}\right) \qquad \text{(VI-23)}$$

Equation (VI-23) states that the inverse of the center line decay of the concentration is also linearly proportional to axial distance.

APPENDIX V

ABSTRACTS OF PUBLICATIONS

1. "The Response of a Hot-Wire Anemometer to a Bubble of Air in Water"

The sensitivity of peak voltage and duration of the change in sensor voltages due to the impaction of different size bubbles are computed and measured. Excellent agreement between these is found for bubbles somewhat larger than the sensor diameter and smaller than its effective length in water streams in a range of 1.5 to 9 feet per second. The method suggests a reliable method for sizing bubbles in a water stream. The effects due to nondirect hits are not treated.

2. "Bubble Formation due to a Submerged Capillary Tube in a Quiescent and Co-Flowing Streams"

The case of bubble formation in both quiescent and moving streams due to the injection of a constant gas flow through a small tube is considered. Relationships predicting the expected size and quantity of bubbles generated are proposed. These are compared with measurements taken with stream velocities up to 9 ft/sec, while generating gas bubbles from 40 to 700 microns in diameter.

For the case of generation in a quiescent stream the forces due to the virtual mass, surface tension, viscous drag, buoyancy, and the wake formed by the preceding bubble are accounted for. There still remains some question (only partly answered by a comparison with measurements) as to the proper added mass coefficient and the geometry of the bubble previous to detachment, as well as an adequate estimate of the interaction with a preceding bubble's wake.

The proposed model for generation in a moving stream is in good agreement with actual measurements for co-flowing velocities between 1 and 9 fps and capillary tubes in the order of 10^{-3}cm in dia.

3. "Dynamic Simulation of the Turbulent Diffusion of Small Particles"

The equation of motion of a small spherical nonrotating particle was solved numerically in a two-dimensional homogeneous and isotropic turbulent field. Ensembles of solutions were obtained for particles of different sizes and densities... It was shown that the turbulent transport coefficient increases with particle size and decreases with particle density... The results are in agreement with available measurements.

4. "Analytical Prediction of the Turbulent Diffusion of Small Particles"

A comparison of various measurements has consistently suggested an unexplained increase in the turbulent transport of small suspended particles with size. A comparison with the momentum turbulent transport coefficient suggests an increase of the inverse of the turbulent Schmidt number (or the ratio of mass to momentum transport coefficients) from values close to 1, for zero-size particles, to values as large as 5, for larger particles.

Based on the particle equations of motion, and postulating certain relationships between the statistics of the particle velocity fluctuations and the turbulent carrier phase, a prediction of the particle transport coefficient is made. The analysis predicts the same increasing trend of turbulent transport coefficient with particle size. By limiting the study to a particular range of particle Reynolds number good agreement is noted with the experimental data.

5. "Energy Spectrum and Turbulent Scales in an Axi-Symmetric Water Jet":

The time micro and macroscales are computed from measured energy spectra in the fully developed region of a circular jet. The corresponding longitudinal scales are approximated using Taylor's frozen turbulence hypothesis. The microscale is found essentially constant whereas the macroscale, although increasing linearly along the axis, does not show similarity in the total field.

6. "Turbulent Diffusion of Small Particles Suspended in Turbulent Jet"

The dispersion of liquid droplets in plane two dimensional air jets has been measured and compared with similar results in the literature. From careful measurements of the concentration flux profiles the corresponding turbulent transport coefficient is determined. The results show that within most ranges of interest turbulent transport increases with particle size.

The results are not only compared with each other, but also with an analysis based on the assumption of nonrotating spherical rigid particles acted upon by viscous drag given by Stokes Law. The approximate analysis predicts the same trend as noted in the experiments.

U.S. GOVERNMENT PRINTING OFFICE: 1974— 546-319:391